SANDIA REPORT
SAND2006-7976
Unlimited Release
Printed April 2007

Measurement and Modeling of Transfer Functions for Lightning Coupling into the Sago Mine

Matthew B. Higgins and Marvin E. Morris

Contributing Editors: Michele Caldwell and Larry X. Schneider

Prepared by Sandia National Laboratories
Albuquerque, New Mexico 87185, and Livermore, California 94550

Sandia is a multiprogram laboratory operated by Sandia Corporation,
a Lockheed Martin Company, for the United States Department of Energy's
National Nuclear Security Administration under Contract DE-AC04-94AL85000.

Issued by Sandia National Laboratories, operated for the United States Department of Energy by Sandia Corporation.

Available to DOE and DOE contractors from
U.S. Department of Energy
Office of Scientific and Technical Information
P.O. Box 62
Oak Ridge, TN 37831

Telephone: (865) 576-8401
Facsimile: (865) 576-5728
E-Mail: reports@adonis.osti.gov
Online ordering: http://www.osti.gov/bridge

Available to the public from
U.S. Department of Commerce
National Technical Information Service
5285 Port Royal Rd.
Springfield, VA 22161

Telephone: (800) 553-6847
Facsimile: (703) 605-6900
E-Mail: orders@ntis.fedworld.gov
Online order: http://www.ntis.gov/help/ordermethods.asp?loc=7-4-0#online

SAND2006-7976
Unlimited Release
Printed April 2007

Measurement and Modeling of Transfer Functions for Lightning Coupling into the Sago Mine

Matthew B. Higgins
Electromagnetic Qualification and Engineering Department

Marvin E. Morris
Electromagnetic and Plasma Physics Analysis

Contributing Editors
Michele Caldwell
Larry X. Schneider

Sandia National Laboratories
P.O. Box 5800
Albuquerque, New Mexico 87185-1152

Abstract

This report documents measurements and analytical modeling of electromagnetic transfer functions to quantify the ability of cloud-to-ground lightning strokes (including horizontal arc-channel components) to couple electromagnetic energy into the Sago mine located near Buckhannon, WV. Two coupling mechanisms were measured: direct and indirect drive. These transfer functions are then used to predict electric fields within the mine and induced voltages on conductors that were left abandoned in the sealed area of the Sago mine.

ACKNOWLEDGEMENTS

A complex project of this type could not have been undertaken without the funding, coordination, and hard work of the MSHA staff that were involved. We wish to thank MSHA staff William Helfrich, Richard Gates, Robert Phillips, Harold Newcomb, Russell Dresch, Dean Skorski, Joseph O'Donnell, and Arthur Wooten for their support of this project. Jurgen Brune and Eric Weiss of NIOSH generously provided their Lake Lynn facility for initial trials of the measurement techniques used at the Sago mine. We thank the ICG staff, Chuck Dunbar, Al Schoonover, Johnny Stemple, Larry Dean, Kermit Melvin, and Brittany Bolyard, for their generous help in arranging access and for providing the services we needed to accomplish the measurement tasks. In spite of our obvious interruptions to their operations as well as extensive demands on their time, they generously provided the services we needed in a timely manner. We are grateful for the support of Dr. E. Philip Krider and Dr. Martin Uman, who independently reviewed the lightning database information for this report. We also wish to thank the consultants, Dr. Tom Novak, Dr. E. Philip Krider, Elio Checca, and Dr. Martin Uman for freely sharing their thoughts on this project. Monte Hieb and John Scott of the State of WV Office of Miners' Health, Safety, and Training provided additional useful information and help to accomplish the work. Finally, we would like to thank the property owners of the land above the sealed area, Mrs. Goldie Gooden, Tim and Chris Leggett, Bill Patterson, and George Roessing, for generously allowing us access to their property in order to drive ground rods, string wires, and operate our equipment despite obvious interruptions to their lives. Most importantly, we would like to thank our measurement team, Dawna R. Charley and Leonard Martinez, for their extraordinary work in the field. Without their hard work and long hours the measurements could not have been completed.

TABLE OF CONTENTS

LIST OF FIGURES

LIST OF TABLES

Executive Summary

This report documents measurements and analytical modeling of electromagnetic transfer functions to quantify the ability of cloud-to-ground lightning strokes (including horizontal arc-channel components) to couple electromagnetic energy into the Sago mine located near Buckhannon, WV. These transfer functions, coupled with mathematical representations of lightning strokes, are then used to predict electric fields within the mine and induced voltages on a cable that was left abandoned in the sealed area of the Sago mine. If voltages reach high enough levels, electrical arcing could occur from the abandoned cable. Electrical arcing is known to be an effective ignition source for explosive gas mixtures, and corona discharge has been postulated to be so as well. However, given the time scale of lightning (~100 μs), it is unlikely that corona would develop before an electrical arc. Corona is due to ionization of surrounding air and usually a precursor to arcing, given sufficient voltage.

Two coupling mechanisms were measured: direct and indirect drive. Direct coupling results from the injection or induction of lightning current onto metallic conductors such as the conveyors, rails, trolley communications cable, and AC power shields that connect from the outside of the mine to locations deep within the mine. Indirect coupling results from electromagnetic field propagation through the earth as a result of a cloud-to-ground lightning stroke or a long, low-altitude horizontal current channel from a cloud-to-ground stroke. Unlike direct coupling, indirect coupling does not require metallic conductors in a continuous path from the surface to areas internal to the mine.

Based on the *direct* coupling measurements, lightning currents attenuate rapidly on the conductors as a function of distance into the mine. It is highly unlikely that a worst-case lightning stroke could generate sufficient voltage on a cable within the sealed area to cause concern – even if the lightning stroke directly attached to physical conductors at the entrance to the mine.

Results from the *indirect* coupling measurements and analysis are of great concern. The field measurements and analysis indicate that significant energy can be coupled directly into the sealed area of the mine. Due to the relatively low frequency content of lightning (< 100 kHz), electromagnetic energy can readily propagate through hundreds of feet of earth. Indirect transfer function measurements compare extremely well with analytical models developed for the Sago site which take into account measured soil properties. Lightning stroke data recorded by the National Lightning Detection Network and the United States Precision Lightning Network at the time of the explosion does not support the conclusion that high enough voltage to provide a source of ignition could be generated in the sealed area. However, analyses of credible hypothetical scenarios (an undetected stroke closer to the sealed area or a horizontal arc channel of a recorded stroke above the sealed area) indicate voltages large enough on the abandoned cable in the sealed area to be of concern for electrical arcing. Eyewitness accounts of simultaneous lightning and thunder above the sealed area at the time of the explosion lends further credence to these hypotheses.

This work was sponsored by the Mine Safety and Health Administration. Due to the complexity of lightning interactions with large multi-path structures and the limited duration of this project, it was not possible to address the full intricacies of potential lightning interactions at the Sago mine. However, results cited in this report can be considered as a significant indicator of the potential for lightning to couple energy into underground mining structures. Significant follow-on research would be required to address the complexity of mining structures to an extent to fully characterize these energy coupling mechanisms. Once achieved, it is reasonable to expect that mitigation techniques and safety standards could be developed to secure mining structures from future lightning threats.

ABBREVIATIONS, ACRONYMS AND INITIALIZATIONS

CW	Continuous Wave
dB	deciBel
DOE	Department of Energy
FFT	Fast Fourier Transform
IFFT	Inverse Fast Fourier Transform
NLDN	National Lightning Detection Network
USPLN	United States Precision Lightning Network

Measurement and Modeling of Electrical Transfer Functions for Lightning Coupling into the Sago Mine

1 Introduction

On January 2, 2006, an explosion was initiated in a methane-air mixture within a sealed area at the Sago underground coal mine near Buckhannon, WV that resulted in the deaths of twelve miners. The approximate location of the initiation of the explosion is shown in Figure 1-1.

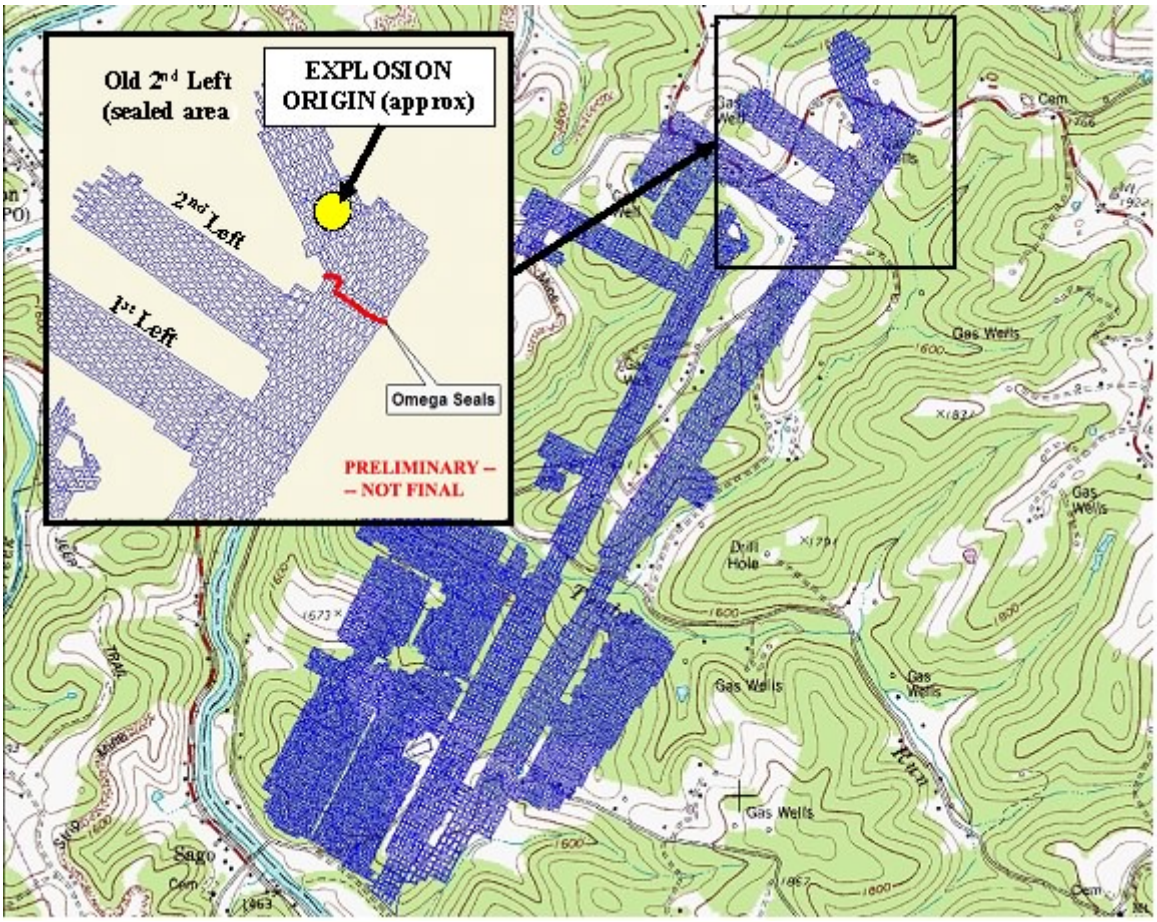

Figure 1-1 Approximate Location of Initiation of Explosion in Sealed Area of Sago Mine.

Because of the fraction of a second simultaneity of the explosion and nearby lightning strokes recorded by the National Lightning Detection Network (NLDN) and the United States Precision Lightning Network (USPLN), lightning is strongly suspected to have caused the explosion. Additional eyewitness reports of other lightning not recorded by NLDN and USPLN further these suspicions [21]. If the timing of the recorded lightning strokes and the underground mine explosion are considered independent statistical events, then the probability that such a combined event would occur at random in a given year is extremely low. When this highly improbable event is coupled with the fact that at least eleven underground coal mine explosions have occurred since 1990 (see Appendix D) in which lightning is suspected of being the cause, it further supports the need to understand the potential role of lightning in the Sago disaster [1-4]. The coupling mechanisms that may have brought lightning energy into the sealed area at Sago were unclear and complicated by the fact that there were no known metallic penetrations into the sealed area of the Sago mine, unlike other sealed area explosions. Prior to 1990, lightning location

and timing data was unavailable, leaving the possibility that many earlier mine explosions would also be correlated to lightning events.

The goal of this project was to perform field measurements at the Sago site and to develop analytical models to quantify potential lightning coupling mechanisms that are capable of delivering significant energy into the sealed area of the Sago mine.

1.1 Motivation for Research and Measurements

Over the last decade, Sandia National Laboratories (Sandia) has developed unique capabilities to characterize and mitigate lightning effects on high value assets within the Department of Energy (DOE) and other agencies as part of a national security mission in nuclear weapons stockpile stewardship. Additionally, the history of potential lightning induced mine explosions suggested that a program using modern electromagnetic measurement techniques and analysis could be valuable during the investigation at the Sago mine. These modern lightning coupling measurement techniques were developed by DOE/NNSA specifically for the evaluation of the performance of lightning protection systems on buried, explosive storage structures, nuclear weapons assembly and dismantlement facilities, and at tunneling systems at the DOE Nevada Test Site. These Sandia developed techniques have been compared and validated using rocket-triggered lightning measurements [5-7] and have undergone significant technical review within the DOE and by the Defense Nuclear Facility Safety Board, an independent federal agency established by Congress in 1988.

1.2 Objectives of Measurements

The principal objectives of this program were to identify, characterize, and quantify the electromagnetic paths of lightning electrical energy into the sealed area of the Sago underground coal mine. These paths include direct coupling through metallic penetrations into the operating area of the mine and indirect coupling through the earth overburden to conductors in the sealed area. Measurement results are compared with basic analytical models to confirm the validity of proposed lightning coupling mechanisms. The measured transfer functions were then used to predict the voltages generated on a cable left abandoned within the sealed area from the lightning stroke locations and amplitudes determined by the NLDN and the USPLN. In addition, the raw lightning event data from the NLDN and USPLN was analyzed to ascertain if there were any instances of data at the correct time that did not meet all of the criteria to be recorded as a lightning stroke.

1.3 Previous Work on Lightning Induced Mine Explosions

Recent previous works by Novak and others [8,9] have utilized commercial, numerical electromagnetic codes to calculate the voltages on metal-cased boreholes connecting the surface with the sealed areas in mines. They have postulated corona discharge as an initiating mechanism based on experimental work by combustion researchers [10,11]. Berger, Geldenhuys, Golledge, Zeh, and others have analyzed the specific situation of lightning-caused explosions in shallow South African underground coal mines [12-16]. The Australian, German, and Chinese literature on lightning initiated underground coal mine explosions has not been thoroughly explored.

1.4 Measurement Method and Analysis

The coupling mechanisms of lightning energy into the Sago mine have been divided into (1) direct coupling via metallic penetrations from the outside of the mine that are terminated immediately outside

the sealed area, and (2) indirect coupling through the soil and rock overburden above the sealed area. The metallic penetrations analyzed and measured were the AC power shields, the coal conveyer system, the transportation rail system, and the mine trolley communication cable. The primary focus of this study was to determine electric fields within the mine and the resulting induced voltage on a cable within the sealed area due to both the direct and indirect coupling mechanisms. Electrical arcing is known to be an effective ignition source for explosive gas mixtures, and corona discharge has been postulated to be so as well. However, given the timescale of lightning (~100 μs) it is unlikely that corona would develop before an electrical arc. Corona is due to ionization of surrounding air and usually a precursor to arcing, given sufficient voltage.

Lightning coupling mechanisms were characterized by driving potential pathways with low-level, continuous sinusoidal signals and measuring the resultant signals at distant locations. The resultant data when divided by the input signal produces a transfer function that can be coupled with a mathematical representation of lightning strokes to calculate a resultant signal at points inside the mine. The advantages of using this technique are as follows:

- Measurements can be made without waiting for a natural or triggered lightning in the vicinity.
- Safety is not compromised due to use of low-level signals and interference with ongoing mine operations is minimized.
- The frequency content of the low-level drive signal can be tailored to that of natural lightning.
- Many data points can be taken with this method which enhances the precision of the transfer functions.

The disadvantage is that the nonlinear effects of high-voltage arcing cannot be taken into account.

1.4.1 Direct Coupling Transfer Function Measurements and Analysis

Because all metallic conductors into the Sago mine were terminated outside the sealed area of the mine, current cannot be injected from outside the sealed area directly into the sealed area. However, currents flowing on conductors inside the mine, but outside of the sealed area, may be able to induce voltage on a cable inside the sealed area through electromagnetic coupling. To determine the amplitude of these currents, attenuation on each conductor entering the mine was measured using transfer function techniques. Low-level direct coupling transfer function measurements were made by injecting current onto metallic penetrations at the entrance to the mine and then measuring the voltage and current levels on these penetrations at various points within the mine, up to immediately outside the sealed area. The voltage induced on conductors inside the sealed area could then be calculated based on the projected current level on conductors outside the sealed area and an analytical estimate of the electromagnetic coupling between this current and the conductors inside the sealed area. The measurements were made over a frequency range from 10 Hz to 100 kHz, corresponding to wavelengths in air of $3x10^7$ meters to 3000 meters respectively. We are able to use very small signals because our instrumentation is very sensitive and has a large dynamic range. We demonstrated that we could measure input currents and at some distance and from the source even with significant attenuation.

Because the direct-drive measurements are taken as a function of frequency, the mathematical representation of a lightning stroke is transformed as a function of frequency. To use the data, the direct-drive transfer functions were multiplied by the frequency representation of a lightning stroke. The product was inverse Fourier transformed to represent the resultant signals inside the mine from a lightning event outside the mine, as a function of time. To represent the worst-case scenario input for the purpose of these calculations, an assumption was made that the lightning stroke attached to the metallic penetrations at the entrance of the mine.

1.4.2 Indirect Coupling Transfer Function Measurements and Analysis

The large currents in a lightning stroke have an associated magnetic field. When a lightning stroke attaches to the earth, this creates a magnetic field tangential to the ground. For a fully developed lightning stroke, it is reasonable to approximate this magnetic field as

$$H(r) = \frac{I}{2\pi r}$$

over a distance of 30 m – 1000 m, where I = lightning current and r = distance from stroke attachment. For distances within 30 m of the attachment, magnetic field calculations are more complex and this approximation is incomplete. To a first order of approximation and as a bound, the magnetic field is calculated above a perfectly conducting ground plane, as above. This approximate tangential magnetic field is used as a drive to generate current in the finitely conducting earth. The calculations in this report do not deal with magnetic fields generated in the immediate vicinity of lightning strokes; therefore, these interactions will not be evaluated here. For distances greater than 1000 m from the attachment, the approximation for the magnetic field at the surface may be an overestimation, but can be considered a reasonable upper bound.

When lightning attaches to the ground, the magnetic field tangential to the ground creates currents not only on the surface, but deeper in the earth as well. It is a fundamental principle of electromagnetics that magnetic fields on the surface of a conductor can generate currents within the conductor of some depth. For frequencies sufficiently low that displacement currents can be neglected, this is called the *skin effect* and is dependent upon the resistivity of the conductor. When displacement currents are neglected, the electromagnetic coupling phenomena are called *diffusion coupling* or, equivalently, *eddy current coupling*. The skin depth characterizes the exponential decay of these currents in planar geometries. Resistivity measurements have shown the soil in the vicinity of the sealed area of the Sago mine to be a fairly good conductor; therefore, it is reasonable to assume that some electromagnetic energy can propagate from the surface of the earth into the sealed area of the mine. This effect is similar to propagating radio waves through seawater, also a fairly good conductor, and communicating with submarines.

The methodology used to measure the electromagnetic coupling through the earth is to simulate magnetic fields in the earth by connecting a frequency variable voltage source via straight wires on the surface between ground rods at either end of the wires. The ground rods are placed a significant distance from each other, approximately 100 m on either side of the region where the electric fields are measured, or where voltage is induced on an insulated wire. The electric field and the voltage on a cable are measured over a frequency range from 10 Hz to 100 kHz. At this point we have the electric field and voltage response on the pump cable in the sealed area from a known linear current distribution on the surface.

Two steps are involved in calculating the response of a lightning stroke attachment at a distance from the sealed area. The first step involves estimating the magnetic field (or surface current) above the sealed area from a lightning attachment to the ground at a distance from the sealed area. The second step involves calculating the electric field in the sealed area of the mine due to the uniform magnetic field (or surface current) on the surface using the parameters determined from the coupling measurements. Once these connections are made with data in the frequency domain, then the Fourier transform of the lightning stroke can be multiplied by the transfer function. The inverse Fourier transform of the product can be taken to determine the peak electric field and peak voltages that would be caused by a lightning attachment of a given amplitude at a given location with respect to the sealed area. If the peak induced voltages are significant, arcing between conductors could occur. A few tenths of a milliJoule of energy in the arc would be a sufficient ignition source for a combustible methane-air mixture [17]. This amount of

energy is readily available from almost any arcing process envisioned in a lightning induced event. Bulk air breakdown in small gaps (several millimeters) occurs at average electric field values of approximately 10 kV/cm with standard lightning waveforms [18]. Surface arcing can occur at electric field values in the 5 kV/cm range.

1.5 Soil and Rock Site Data

The soil and rock resistivity play a major role in determining the amplitude and frequency dependence of indirect coupling into the sealed mine area. Several studies provide resistivities measured with different techniques and equipment. The resistivities determined by the different measurements appear to be somewhat inconsistent. However, resistivities in [19] match the numbers that give us the best fit for our analysis of electromagnetic coupling through the ground. The resistivities in [19], using a best fit to electromagnetic sounding data, are 100 Ohm-m from 0 to 40 feet, 10 Ohm-m from 40 to 120 feet, and 100 Ohm-m from 120 to 350 feet deep, yielding an average of 77.3 Ohm-m above the sealed area at the borehole. In this study an average resistivity of 80 Ohm-m is used to characterize the soil and rock overburden atop the sealed area of the Sago mine.

1.6 Lightning Event Information

Three positive polarity lightning strokes were identified by the NLDN and the USPLN that were coincident with the Sago underground coal mine sealed area explosion. Their location, polarity, and amplitude are shown in Figure 1-2.

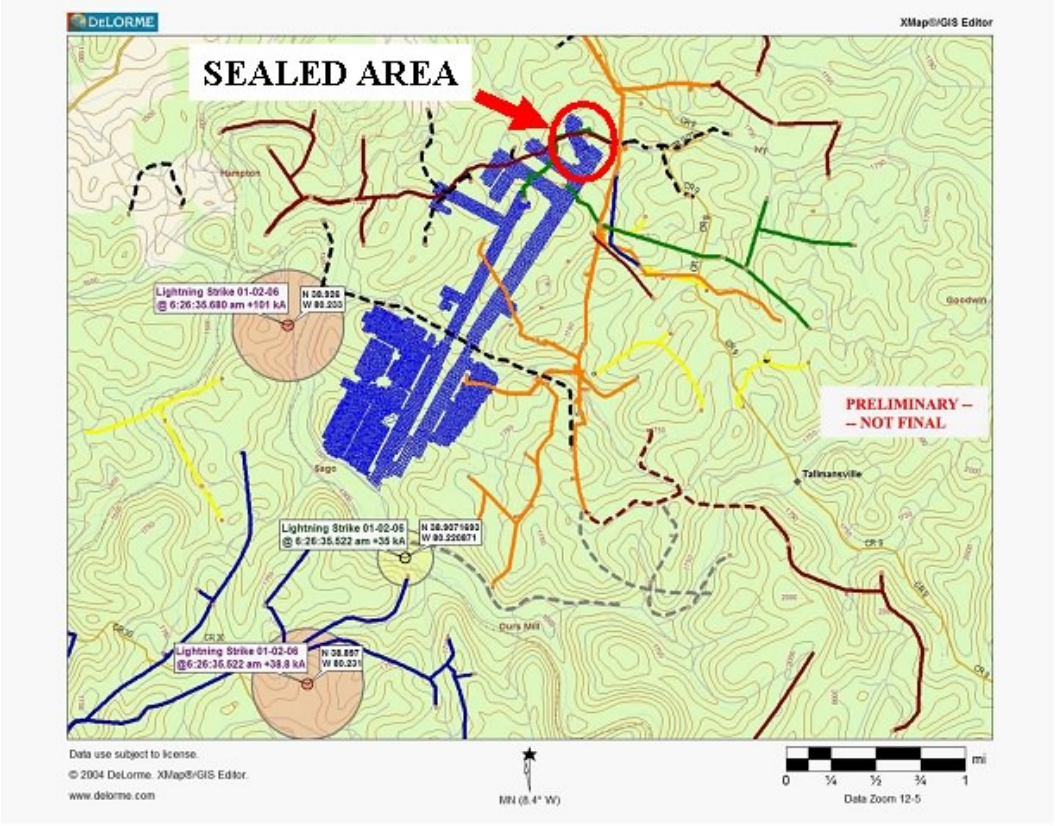

Figure 1-2 Location of Lightning Strokes at Sago Mine Contemporaneous with Sealed Area Explosion.

Table 1-1 gives the location, polarity, and amplitude of the identified strokes. Also provided in the table are the distances from the stroke locations to the sealed area, and the angle that a line between the stroke location and the borehole above the sealed area makes with the pump cable in the sealed area. It should be noted that physical evidence of only stroke number 3 was found after several searches of each attachment area. An analysis of the USPLN and NLDN data strongly suggest that stroke number 1 and 2 in Table 1-1 represent a single stroke, and not two separate events [20,21].

Table 1-1 Lightning Detection Network Data, January 2, 2006

Stroke No.	Time	Longitude/ Latitude	Polarity	Amplitude (kA)	Distance to Borehole (km)	Angle with Cable (Degrees)	Detection System
1	6:26:35.522am	N38.897/ W80.231	Positive	38.8	5.44	52.8	NLDN
2	6:26:35.522am	N38.9071693/ W80.2201	Positive	35	4.02	49.3	USPLN
3	6:26:35.680am	N38.926/ W80.233	Positive	101	2.91	85.5	NLDN

The accuracy of the NLDN is shown in general by the confidence ellipses drawn around the most probable locations. The ellipses give the probability that the lightning is actually inside the ellipse. The estimated 99% location uncertainty for both strokes detected by NLDN was better than 1.1 km (0.7 miles). The fact that the tree was found damaged approximately 197 feet (59 m) from the most probable location of the 101 kA stroke further demonstrates the NLDN location accuracy near the Sago mine [20, 21, 35]. Recent validation experiments on the NLDN have shown stroke detection efficiencies between 70 – 85% and flash detection efficiencies of 90 – 95% [34]. (Lightning flashes are typically comprised of multiple strokes.) It is believed that the two strokes (1 and 3 from Table 1-1) at Sago were part of the same flash [35].

Several other possibilities exist that were not, or could not, be confirmed by the lightning detection network data. Although quite reliable and accurate, the possibility exists of strokes not being detected. Simultaneous thunder and flash were reported by residents living on top of or nearby the sealed area [21]. In addition, the lightning detection networks are designed to locate the ground strike points of cloud-to-ground strokes and do not provide information about the channel geometry above those points, such as if a stroke had a long, low horizontal component that could be important in radiating fields into the mine. Also, upward discharges that are initiated by tall vertical structures will not be detected by the systems unless the initial continuous current phase is followed by at least one leader-return stroke sequence [20, 35]. There were several tall communication towers (the tallest being ~ 200 ft.) within a mile of the sealed area, the closest being approximately 0.5 miles.

1.7 Other Site Information

Measurements discussed in this report were made on the most likely coupling paths into the sealed area. Other potential conduits of lightning energy are mentioned in this section, but were not characterized due to the limited budget and schedule of this project. While they are mentioned here for completeness, the lack of measured data on them does not change the conclusions in this report. If it is desired to develop an overall lightning protection scheme specific to the Sago mine, it would be useful to characterize these potential conduits in the future.

All vertical pipes in the vicinity of the sealed area are shown in Figure 1-3. The vertical pipe closest to the sealed area of the mine is the gas well pointed out in Figure 1-3. It is unlikely that any field enhancements due to the vertical pipes would induce a significant amount of voltage onto the pump cable in the sealed area because the cable is orthogonal to the pipes. However, as potential conduits for lightning energy, they are mentioned here for completeness.

The horizontal gas pipes that are in the vicinity of the sealed area are also shown in Figure 1-3. These pipes are in general buried at a depth of 2 feet from the surface. The response on the pump cable, or electric fields in the sealed area, due to the current drive of the horizontal gas pipes was not characterized because it was not planned for and was not characterized because of liability issues. The gas pipes, if driven locally to the sealed area, would have similar coupling characteristics to the pump cable as that of the indirect drive experimental setup. If the gas pipes were driven remotely, the amount of attenuation from one point on the pipes to another point is mostly dependent upon the resistivity of the soil surrounding the pipes. If the soil surrounding the pipes has low resistivity, a majority of current injected onto the pipes would attenuate in a short distance. However, if the pipes are either not in contact with the soil or the resistivity of the soil is large, then the pipes would act as insulated conductors. Attenuation on the pipes in this case would be much less.

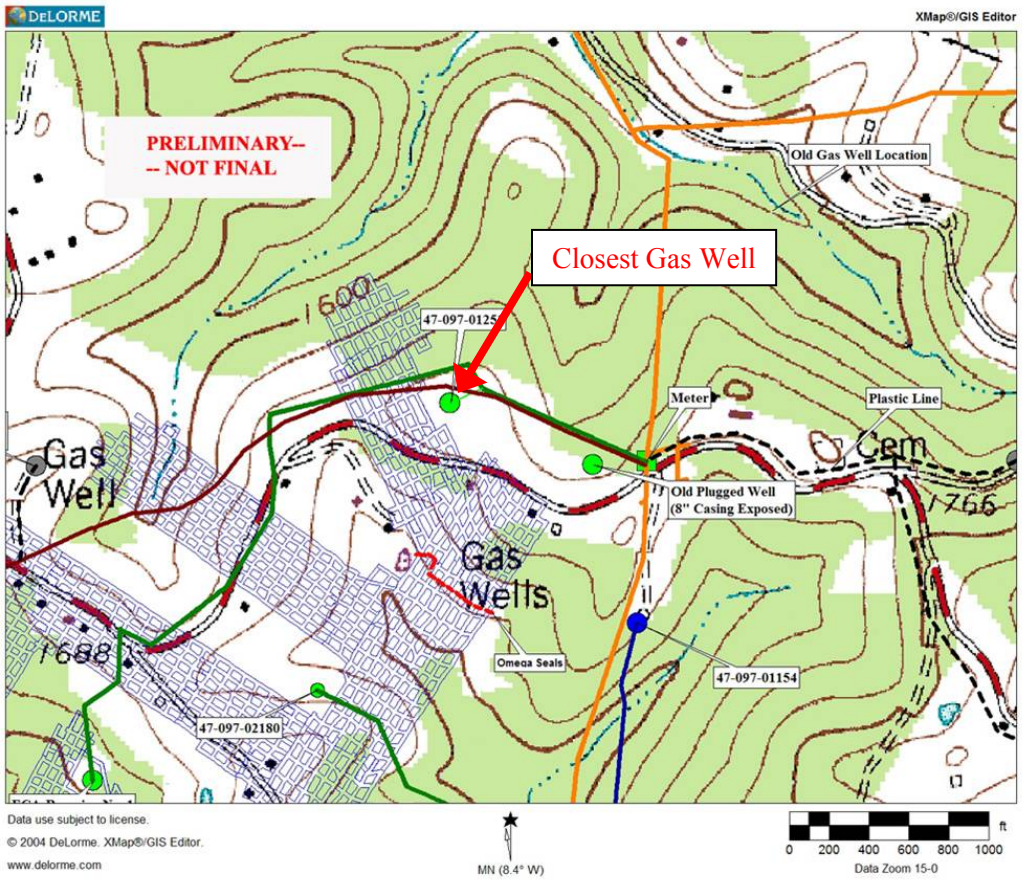

Figure 1-3 Vertical Pipes in Vicinity of Sealed Area of Sago Mine.

Both telephone wires and AC power lines were in the vicinity of the 101 kA positive stroke and could have provided metallic conduction paths into the Sago mine AC power system, or the telephone communication system, or to other metallic penetrations into the mine. The location and routing of this wiring with respect to the stroke are shown in Figure 1-4. The direct-drive measurements discussed in

Section 3.1 lead to the conclusion that even if the power and telephone lines were conduits of the lightning energy, they would not be a plausible source of energy to cause high voltage in the sealed area.

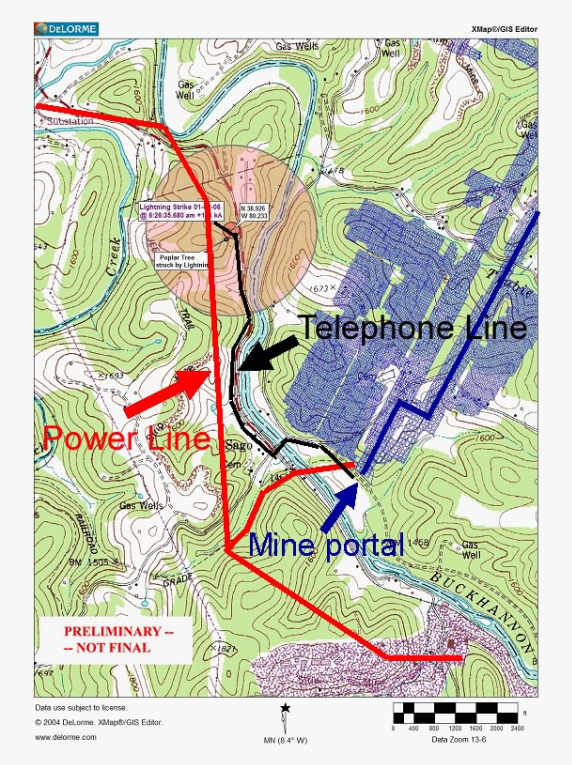

Figure 1-4 AC Power Distribution Lines and Telephone Lines near Positive 101 kA Stroke.

The presence of metallic roof mesh and pump cabling and its relationship to the approximate location of initiation of the explosion are shown in Figure 1-5. The pump cable is shown as the red line and the green shaded area depicts the metallic mesh. The pump cable is noted because indirect coupling measurements are made on it. With these measurements, the voltages induced on the pump cable due to lightning strokes on the surface are calculated in this report.

The metallic mesh is noted because it is used in some of the measurements for grounding purposes. It was not considered a plausible receiver or antenna of the electromagnetic energy that propagates underground because it appears to be well grounded at regular intervals to the roof of the sealed area, and, therefore, would not support a large voltage potential.

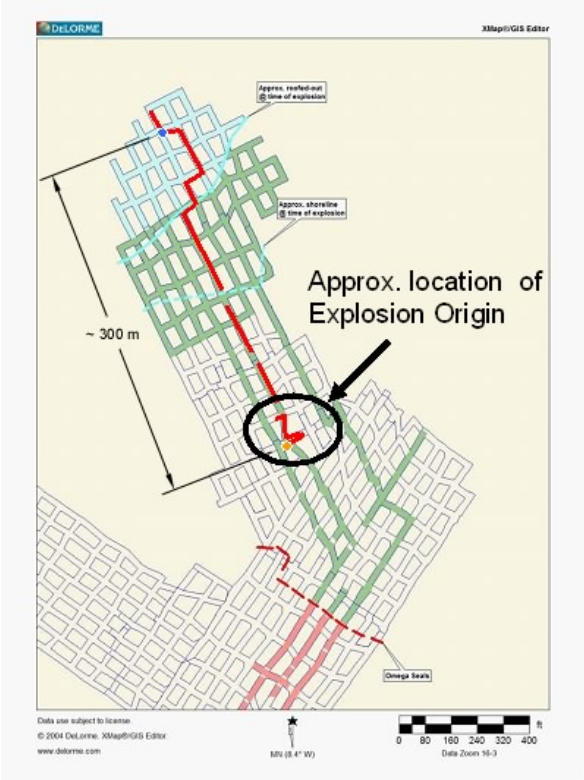

Figure 1-5 Roof Mesh and Cable in Sealed Area Where Explosion Was Initiated. The red line represents a cable from a water pump located at the top of the figure. The green lines represent metallic roof mesh.

1.8 Fidelity Issues of Study

To have confidence in the measured results, several fidelity issues were addressed to ensure that the measurements could be used to calculate a realistic natural lightning response.

1.8.1 Current Flow on the Surface from a Real Lightning Stroke and the Indirect-drive Test Setup

Consideration was given here to two issues that could limit the applicability of the indirect measurements. The first consideration is whether the current flow pattern in the earth is sufficiently similar to lightning. The electric and magnetic fields near rocket-triggered lightning have been measured, and the current flow in the soil out to 30 m distance from the attachment can be inferred [22,23]. Nonlinearities at the lightning attachment point often cause arcing either on the surface of the soil or into the soil that are not duplicated by the low-level drive current measurement method. Because these arcs are limited to the attachment area, they do not affect the overall current flow at large distances to a significant degree. We are not modeling the stroke attachment region, as stated previously.

A second, more significant consideration is that the near-surface current flow pattern produced by these measurement techniques may not accurately represent natural lightning current flow patterns. This is possible because either the current flow at large distances from the attachment point is not duplicated due to the use of ground rods as a return current path during the measurement, or because resistive inhomogeneities in the soil and rock overburden can perturb the flow pattern. However, good correlation between the measured results and the homogeneous earth models suggest these deviations are negligible for this particular project.

1.8.2 Physical Changes to the Sago Site after the Accident

Physical changes were made at the site after the explosion occurred and before Sandia researchers arrived at Sago. These changes do not impact the validity of these measurements, but they are included here for completeness. A three-inch borehole was drilled into the sealed area of the mine immediately above where the explosion is likely to have been initiated. The borehole has only fourteen feet of steel casing from the surface downward, which should not affect the measurements significantly. Also, two eighteen-inch steel casings were added to connect water pumps in the north end of the sealed area to the surface. Because these pipes are a large distance from the region of the sealed area where the explosion originated and are orthogonal to the pump cable, they are not expected to affect the measurements significantly. The pump cable in the sealed area was modified for the indirect drive measurements. The pump cable was spliced with 12-gauge wire to recreate the length of pump cable believed to have been there during the explosion[1]. For the measurements, the pump cable was connected with 12-gauge wire to the ceiling mesh and the exposed conductors were placed underwater approximately four crosscuts from the back of the sealed area. The approximate total length of the recreated cable was 300 m (984 ft).

1.9 Potential Further Areas of Study

The following items are potential areas for further study. Their effects on the coupling mechanisms characterized in this report are unknown, but believed to be of minimal effect. Evaluating these areas will not change the basic conclusions in this report.

1.9.1 Nonlinearities

Surface arcing and arcing through soil and rock are well-known phenomena that can propagate lightning energy over a distance of a hundred feet or less. Because these phenomena occur only at the full amplitudes of natural or triggered lightning strokes, their behavior and effect on coupling could not be studied using the low-amplitude transfer function measurement techniques of this study. There is no evidence an arc can travel a distance of 300 feet through soil and rock, therefore, it is unlikely this would have any effect on this analysis.

1.9.2 Coupling from Vertical Pipes near Sealed Areas

The effect on the coupled electromagnetic field caused by direct drive of the vertical gas well that passed near the sealed area was not measured or modeled in this study. Because we could not guarantee that damage to cathodic protection systems or other instrumentation would not be caused by our drive system, the owners of the system would not allow attachment to the pipe without indemnification. Direct drive of the vertical pipe could have caused some enhancement of the coupled electric fields in the sealed area, but would not change the conclusions of this report.

1.9.3 Distributed Drives for Metallic Penetrations

Although the localized drive at the entrance to the mine of all metallic penetrations to the mine was studied (except pager communication line), the propagation of voltages and currents on these penetrations

[1] As a note, there is some disagreement as to the length and positioning of the pump cable at the time of the explosion. The test team used information provided at the time of the measurements, which was that the pump cable was intact and the cable shield was grounded to the submerged pump.

can be enhanced by current flow on the surface of the earth above the penetrations. Simple considerations indicate that the voltage and current amplitudes are not enhanced significantly. The measurement that could have elucidated this phenomenon was cancelled because of the physical and political impracticality of stringing a wire from the entrance of the mine through dense forests and livestock-occupied pastureland to a location above the sealed area.

1.9.4 Amplification Effects of Wiring Resonances

Several coupling resonances were identified on the mine trolley communication and power wiring that could enhance lightning coupled voltages in sealed and unsealed areas of the mine. The characteristics of the resonances were so small that the enhancement would not be significant; however, the maximum extent to which this factor could amplify voltages in sealed areas was not studied.

1.9.5 Effect of Grounded Roof Meshes

Voltages induced between sections of roof meshes in the sealed area were not measured because the substantial grounding of these meshes via rods driven every three feet or so to provide roof support was thought to prevent buildup of voltages. We found at the site that the use of nonconductive epoxies may prevent good contact between the epoxy bolts and the rock. The voltage buildup between sections of roof mesh and the effect of the roof mesh on electric fields and voltages within the sealed area was not studied in this project. [36]

1.9.6 Coupling Paths Not Present in Sago Mine

Lightning coupling paths into sealed areas that are common in other underground coal mines but are absent from the Sago mine, such as coupling along metal-cased boreholes that extend from the surface into the sealed area and coupling through other metallic penetrations used for monitoring or other instrumentation were not studied in this project.

1.9.7 Geologic Irregularities Affecting Coupling

The extent to which geologic irregularities such as faults and mineral deposits that affect the coupling of lightning energy into underground coals was not quantified in this study.

1.9.8 Lightning Current Return Path Assumptions

The analysis used in this report assumes that lightning current is uniform in the radial direction. The extent to which large-scale inhomogenieties affect the current paths, and the extent to which the variation with depth affects the coupling, were not quantified in this study.

2 Electromagnetic Coupling Phenomenology Models

Modeling was included in this project to compare the measurements with theoretical calculations. The results for mathematical modeling of coupling of electromagnetic energy into the mine by direct coupling and by indirect coupling are now given. The details of the derivations and derivations of more complicated models are given in Appendix A.

2.1 Direct Coupling via Metallic Penetrations into Mine

The conductive penetrations into the mine can be modeled as transmission lines, or lines of distributed impedance (i.e., the combination of resistance, capacitance, and inductance). It is helpful to model the penetrations as transmission lines, because then their behavior over a wide frequency range, such as the measurements made here, can be analyzed. The classic theory of transmission lines is detailed by King in [24]. Useful formulas for calculating the transmission-line parameters in situations similar to those at the Sago mine are given by Warne and Chen in [25].

2.1.1 Localized Drive Transmission-line Theory

Using the differential circuit representation in Figure 2-1, the equations of transmission-line theory can be developed [24].

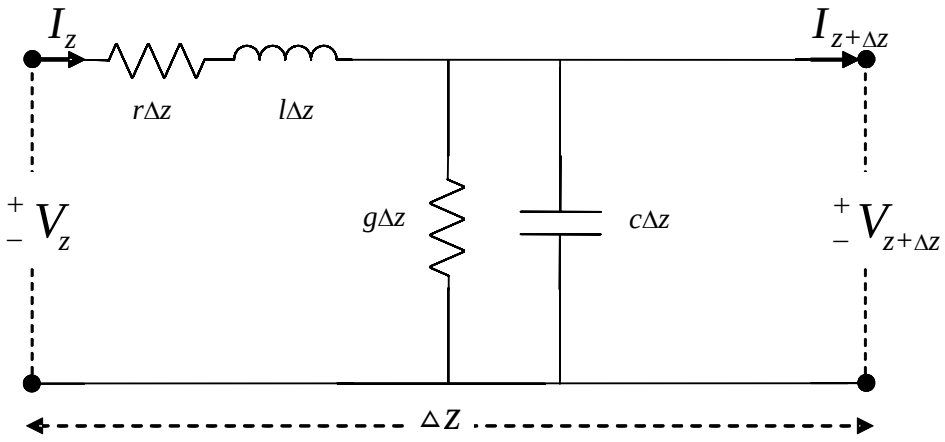

Figure 2-1 Equivalent Circuit of a Section of Transmission Line.

The transmission-line equations are given by

$$\left.\frac{d^2V}{dz^2}\right|_z = yzV$$

$$\left.\frac{d^2I}{dz^2}\right|_z = yzI$$

$$y = g + i\omega c$$

$$z = r + i\omega l$$

The complex propagation constant is given by

$$\gamma^2 = yz = (g + i\omega c)(r + i\omega l)$$

These equations along with current or voltage source terms corresponding to localized current or voltage drives and appropriate loads have been used to develop a formal theory of transmission lines [24], which, along with properly determined transmission line parameters, is appropriate to the study of the propagation of lightning currents along direct coupling paths on metallic conductors into the Sago mine. Note that the variable z is used both as the distance along the transmission line and as the impedance parameter for the transmission line.

2.1.2 Distributed Drive Transmission-line Theory

In many situations the current and voltage sources driving the transmission line of Figure 2-1 are not localized to a small volume but are distributed incremental current and/or voltage sources generated along the length of the transmission-line. An appropriate theory for this type of drive has also been developed in [24]. This type of transmission-line treatment is appropriate if the stroke does not directly attach to or is not conducted via metallic connections to the transmission-line.

2.2 Indirect Electromagnetic Coupling via Soil and Rock

To calculate the electric fields in the earth induced by a current on the surface, the problem is simplified by representing the earth as a homogeneous material with a constant resistivity. Section 2.2.1 calculates the simplest case given a finite-length, DC current drive. The calculations become more complex in Sections 2.2.2 and 2.2.3 as the current drive is assumed to be of infinite length and time-varying, as more appropriate for lightning currents on the surface. These results are used to compare to the indirect measurements of the electric field in the sealed area as a function of the drive current on the surface.

2.2.1 Static Coupling Model for Current Injected into Homogeneous Half-Space

The geometry for the simplest model for DC current coupling is shown in Figure 2-2 and is analyzed in [26].

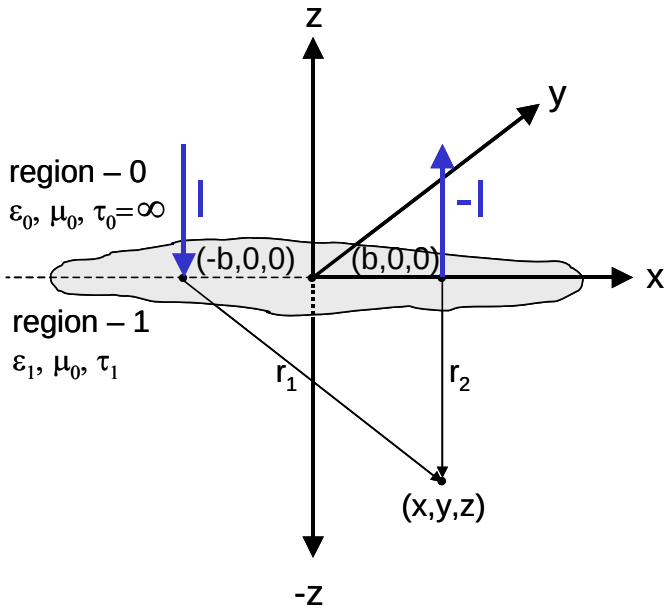

Figure 2-2 DC Current Drive with Homogeneous Conducting Half-Space.

Current I is driven into the conductive half-space at Cartesian coordinate (-b,0,0) and the current is extracted at Cartesian coordinate (b,0,0). The upper half-space, region-0, has infinite resistivity and the lower half-space, region-1 has resistivity, τ_1. From simple considerations, V(x,y,z), the potential at Cartesian coordinate (x,y,z) with respect to infinity is given by

$$V(x,y,z)=\frac{\tau_1 I}{2\pi}\left(\frac{1}{\sqrt{(x+b)^2+y^2+z^2}}-\frac{1}{\sqrt{(x-b)^2+y^2+z^2}}\right)$$

The electric field at point (x,y,z) is easily calculated from

$$\bar{E}(x,y,z)=-\nabla V(x,y,z)$$

And calculating the x-component of interest

$$E_x(x,y,x)=-\frac{\partial}{\partial x}V(x,y,z)$$

$$=\frac{\tau_1 I}{2\pi}\left(\frac{(x+b)}{\left[(x+b)^2+y^2+z^2\right]^{\frac{3}{2}}}-\frac{(x-b)}{\left[(x-b)^2+y^2+z^2\right]^{\frac{3}{2}}}\right)$$

The next coupling models to be considered are generalizations where the current is time varying say as with $e^{i\omega t}$ and the displacement currents are neglected because region-1 is assumed to be a good conductor. This generalization turns out to be more difficult than one might expect because the current in the earth depends on the geometry of the current path above the earth. A simpler model that corresponds to the electromagnetic coupling below an infinitely long, horizontal wire grounded at a large distance away and driven by a voltage source is, however, developed in the next section.

2.2.2 Infinite Line Source above Homogeneous Half-Space

The current drive geometry of an infinitely long, horizontal wire placed a distance, h, above a conductive half-space is shown on the left side of Figure 2-3. A side view is shown on the right side of Figure 2-3. Similar configurations are analyzed in [27-31].

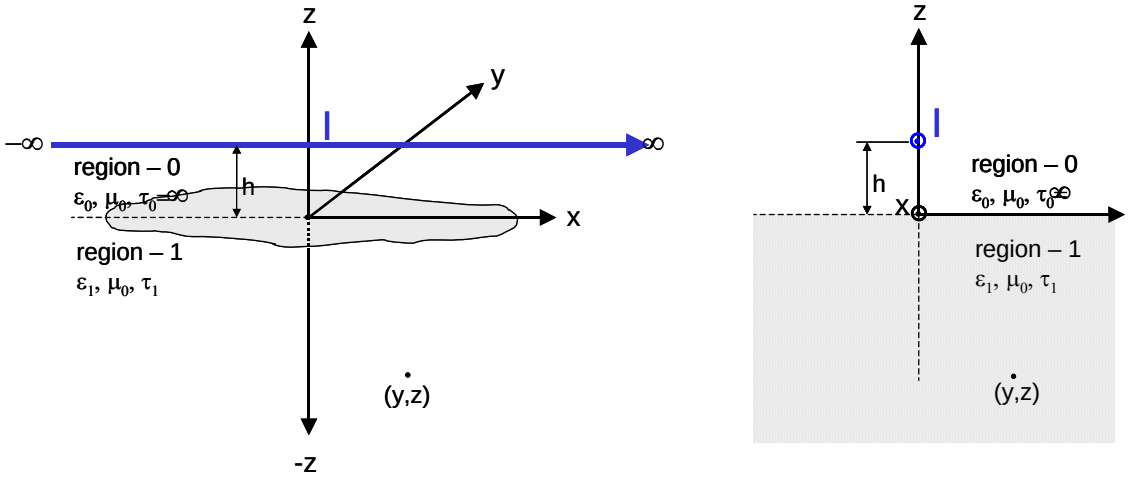

Figure 2-3 Infinite Length, Harmonically Time Varying Horizontal Current Drive over a Conductive Half-Space.

The current drive is harmonically time-varying and is directed along the positive x-axis at height, h, above it. The upper half-space has infinite resistivity and the lower half-space has resistivity, τ_1. If one neglects displacement current and relates current density, $i_x(x,y,z)$ and electric field, $E_x(x,y,z)$, in region-1 through, $E_x(x,y,z)=\tau_1 i_x(x,y,z)$, then the current density in the lower half-space, region-1, can be determined to be

$$E_x(y,z)=\frac{ik\varsigma_0}{\pi}\int_0^\infty \frac{e^{qz}e^{-uh}}{u+q}\cos uydu$$

where

$$k=\omega\sqrt{\mu_0\varepsilon_0}$$

$$q=\sqrt{u^2+ip^2}$$

$$p^2=\frac{\omega\mu_0}{\tau_1}=\frac{2}{\delta_1^2}$$

$$\delta_1=\sqrt{\frac{2\tau_1}{\omega\mu_0}}$$

Numerical calculations of this integral are carried out in Appendix A.

Note that the skin depth, δ, plays an important role as a parameter in all diffusion coupling calculations. For convenience it is plotted for resistivities of 10, 100, and 1000 Ohm-m in Figure 2-4. At a given frequency, the lower the resistivity the smaller the skin depth, meaning a majority of the current is contained closer to the surface. Hence, there will be better coupling deeper underground for ground with resistivity of 100 Ohm-m than for ground with resistivity of 10 Ohm-m.

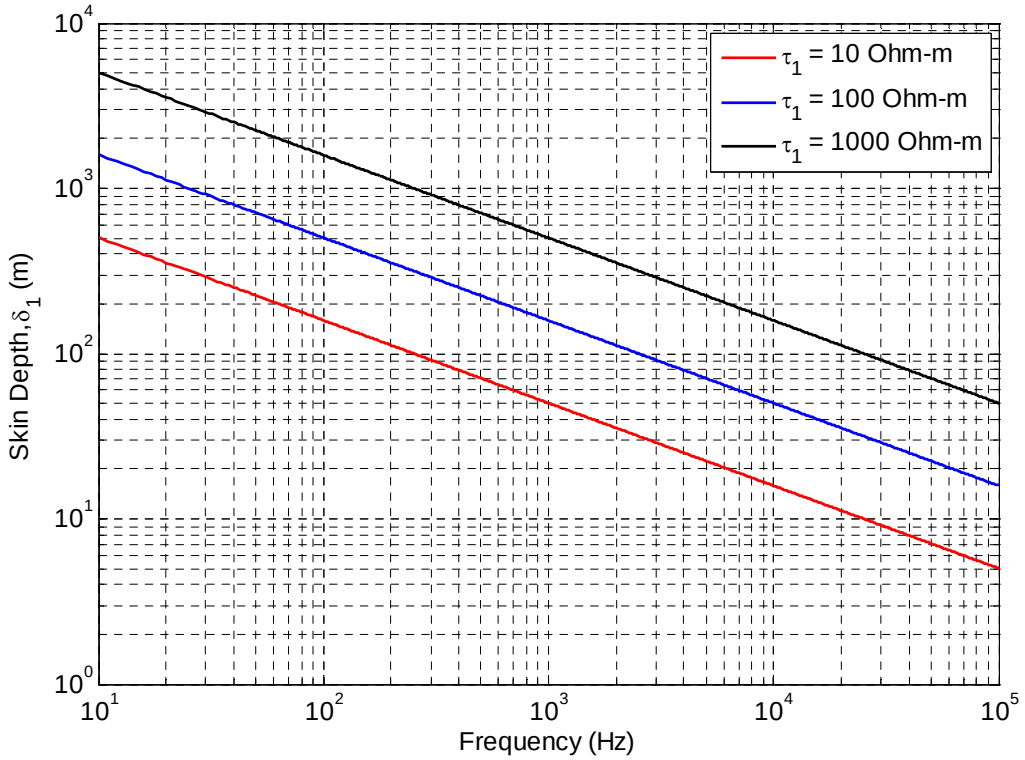

Figure 2-4 Skin Depth, δ_1, as a Function of Frequency for Resistivities of 10, 100, and 1000 Ohm-m.

2.2.3 Infinite Line Source at Surface of Homogeneous Half-Space

If the line current source is brought to the surface of the conducting homogeneous half-space, where h=0, integrating this result for y=0 to get the horizontal electric field immediately below the current source yields

$$E_x(y=0,z)=\frac{\tau_1 I}{\pi}\frac{1}{\delta_1^2}\left\{\left[\left(1+i\right)\frac{1}{\left(\frac{z}{\delta_1}\right)}+\frac{1}{\left(\frac{z}{\delta_1}\right)^2}\right]e^{-(1+i)\frac{z}{\delta_1}}-i2K_0\left[\left(1+i\right)\frac{z}{\delta_1}\right]-\left(1+i\right)\frac{1}{\left(\frac{z}{\delta_1}\right)}K_1\left[\left(1+i\right)\frac{z}{\delta_1}\right]\right\}$$

where K_0 and K_1 are modified Bessel functions. Note that we are now using positive z in the downward direction in the formula. A plot of the electric field at z=100 m depth for resistivities of 10, 100, and 1000 Ohm-m is shown in Figure 2-5.

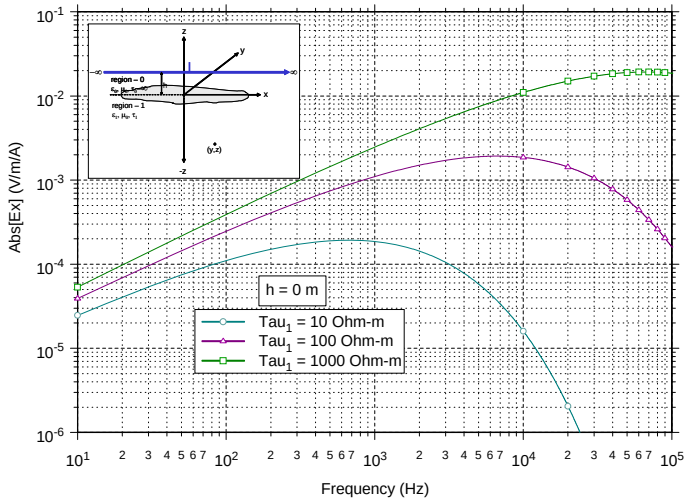

a.) Amplitude of E_x

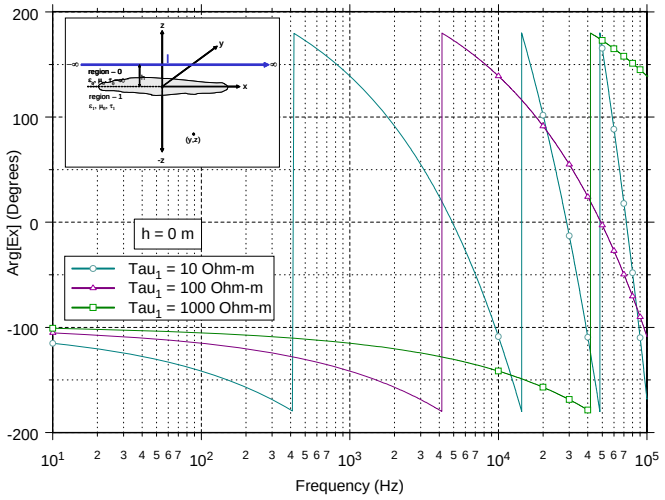

b.) Phase of E_x

Figure 2-5 Amplitude and Phase of Electric Field as a Function of Frequency at Depth of 100m with Resistivities of 10, 100 and 1000 Ohm-m.

2.2.4 Uniform Magnetic Field at Surface above Homogeneous Half-Space

Assume that a uniform y-directed magnetic field of intensity, H_0, is instantaneously applied above a conducting half-space, as shown in Figure 2-6.

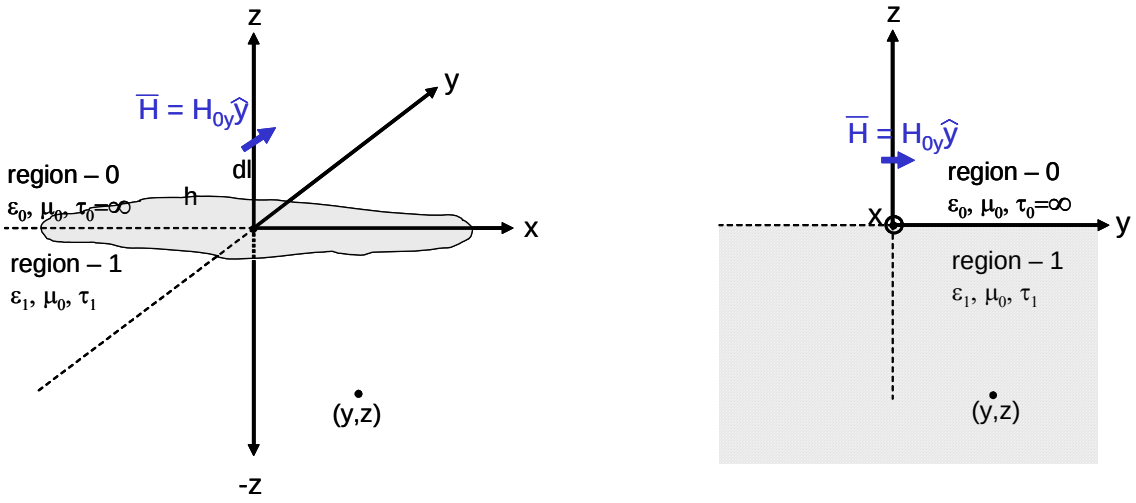

Figure 2-6 Harmonically Time-Varying Magnetic Field Drive over Conductive Half-Space.

If displacement current is neglected, the horizontal electric field below the surface of the conductive half-space is given by

$$E_x(z) = \tau_1 \frac{(1+i)}{\delta_1} H_{0y} e^{-(1+i)\frac{z}{\delta_1}}$$

Note that positive z is used in the downward direction in the formula. Also note that this formulation describes the electric field due to the uniform surface current produced by a cloud-to-ground lightning stroke.

3 Measurement Methods

3.1 Direct Drive

The goal of direct drive is to characterize the attenuation or decrease in signal from the entrance of the mine to various distances into the mine. This is accomplished by directly injecting a current on various conductive lines going into the mine and measuring the current at points further in the mine.

Ideally, the transfer functions of each conductive line going into the mine would be measured in the same configuration as it was during the time of the explosion. However, the grounding at the entrance of the mine was changed following the explosion. Changing back to the old grounding state required the power to the mine be removed, thus stopping all mining operations. A small set of measurements were made while power was disconnected on Sunday, November 5th. It was not possible to conduct all measurements in the one day when the power was disconnected, and stopping mine operations for three days was not feasible. Therefore, the rail, trolley communication line, and conveyor belt structure were measured at six locations at a later time (November 8th and 9th), with the mine grounding system in its current state. The transfer function of the shield on the power cables could not be measured while power was energized.

3.1.1 The Differences and Similarities between Conductive Penetrations

The four conductive penetrations going into the entrance of the mine that were measured were 1) the shield on the power cable, 2) the rail, 3) the trolley communication line, and 4) the metallic structure of the belt conveyor. The conveyor structure and the rail both appeared to be grounded frequently (the rail by surface contact with the ground and periodic bolts), and the conveyor structure by periodic legs bolted to the ground. The shield on the power conductor appeared to be grounded at each power center. The trolley communication cable was an isolated wire running the length of the mine and was only grounded at the entrance. Because of this, at low frequencies the attenuation on the trolley communication line is quite small.

3.1.2 Setup/Equipment Layout with Photos

The principal measurement method used to characterize the coupling through metallic penetrations into the mine is shown in Figure 3-1. Current is driven onto the metallic penetration with an audio amplifier and is returned through either a local ground or a "fence" ground. The local ground consisted of three 18-inch long conductive ground rods driven into the top soil. Each rod was approximately five feet from the other rods and 20 feet away from the driving point. The "fence" ground was long wire attached to the chain link fence that runs along the hillside above the entrance of the mine.

The reasoning for the two grounding techniques was to help show the difference between a local point source drive and a distributed current source drive. A lightning stroke drive could be a distributed current source. The fence drive provided a distributed source for at least several hundred meters. The fence ground also provided a lower ground resistance, which in turn allowed more current to be driven on the lines. By driving more current on the line, the dynamic range of the measurement system was increased. The resistance of the local ground with respect to the rail was 90.2 Ω and the resistance of the fence ground with respect to the rail was 3.68 Ω. It is easy to see from this DC measurement that 20 to 30 times the amount of current could be driven on the fence ground than the local ground. The resistance of the local ground with respect to the conveyor structure was 97.5 Ω, and the resistance of the fence ground

with respect to the conveyor structure was 10.08 Ω. All DC ground measurements were made with a Megger DET 5/2 Earth Tester.

The direct-drive system is broken into two parts, the drive end and the measurement end. The drive end consists of a 12 V marine battery and a 120 VAC inverter to provide isolated power for the measurement equipment, a fiber optic receiver, an audio amplifier driven by a network analyzer, connecting wires to the conductor being driven, and wires to a ground (local or fence). The drive signal produced by the network analyzer is optically coupled to the audio amplifier allowing the signals to be phase-locked to increase the sensitivity of the measurements and allow for phase measurements. The technique of phase-locked detection allows measurement of voltages as low as 10s of nanoVolts. The measurement end consists of a 12 V battery and a 120 VAC inverter for isolated power for the measurement equipment, a fiber optic transmitter, a network analyzer, and current and voltage measurement probes. The voltage measurements on the rail, power, and conveyor were made with respect to the roof mesh. Voltage measurements were not made on the trolley communication line because it was isolated without an exposed conductor.

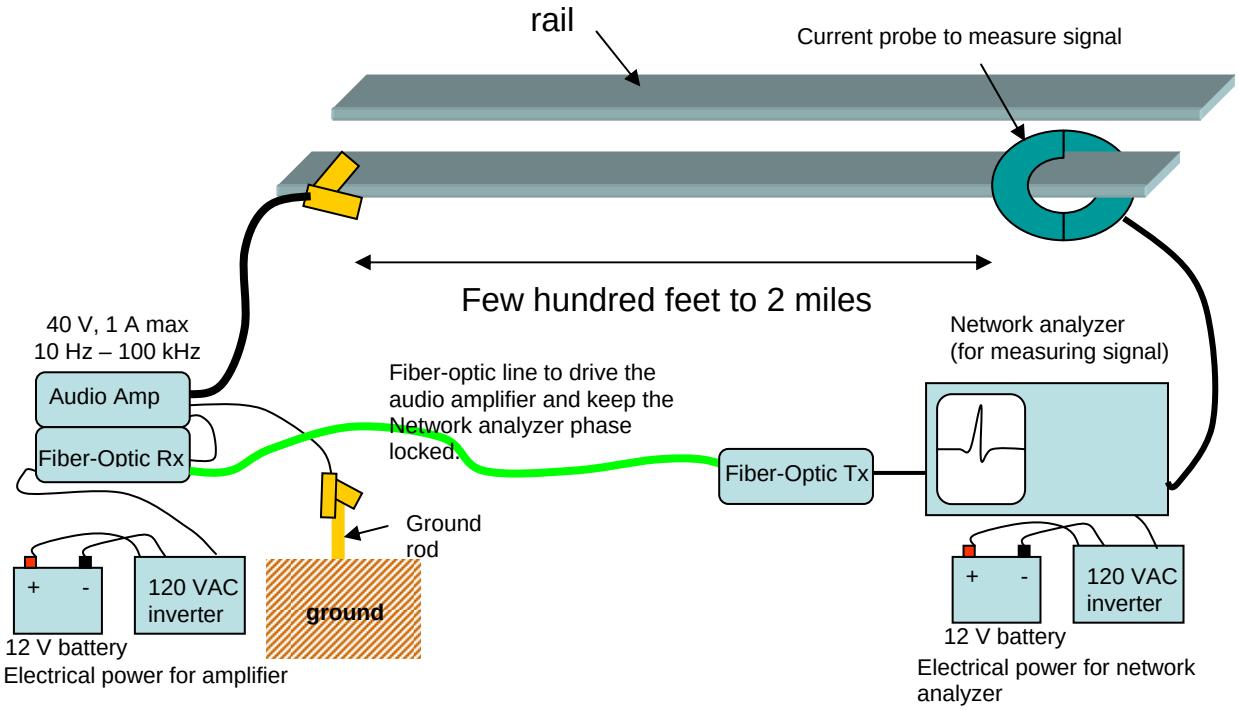

Figure 3-1 Direct Drive Conceptual Drawing.

The measurements were conducted at seven locations along the left rail, trolley communication line, and the conveyor belt structure as they proceeded into the mine. Measurements were conducted at the first three locations for the power cable shield. The power cable shield measurements were completed on Sunday, November 5th while the power was turned off. The power cable shield was not measured during regular mine operation due to safety concerns. Table 3-1 lists mine features at each measurement location, the approximate distance to the entrance (drive location), and the conductors measured. The measurement locations are also shown on the map of the mine in Figure 3-2.

Table 3-1 Direct Drive Measurement Locations

				Conductors Measured: Voltage (V) & Current (I)	
Location	**Mine Feature**	**Break Number**	**Approximate Distance from Entrance**	**Grounding System in Configuration 1[2]**	**Grounding System in Configuration 2[3]**
1	#1 Power Center	Belt 1, Break 1	30 m (98 ft.)	Power Cable Shield (V&I)	Trolley Comm Line (I) Rail (V&I) Conveyor (V&I)
2	#2 Power Center	Belt 2, Break 1	459 m (1506 ft.)	Power Cable Shield (V&I) Trolley Comm Line (I) Rail (V&I)	Trolley Comm Line (I) Rail (V&I) Conveyor (V&I)
3	#3 Power Center	Belt 3, Break 1	669 m (2195 ft.)	Power Cable (V&I) Trolley Comm Line (I) Rail (V&I)	Trolley Comm Line (I) Rail (V&I) Conveyor (V&I)
4	1st Right Spur	Belt 3, Break 16	1076 m (3530 ft.)		Trolley Comm Line (I) Rail (V&I) Conveyor (V&I)
5	2nd Right Spur	Belt 4, Break 11	2178 m (1.35 miles)		Trolley Comm Line (I) Rail (V&I) Conveyor (V&I)
6	1st Left Switch	Belt 4, Break 50	3255 m (2.02 miles)		Trolley Comm Line (I) Rail (V&I) Conveyor (V&I)
7	2nd Left Switch	Belt 4, Break 59	3491 m (2.17 miles)		Trolley Comm Line (I) Rail (V&I) Conveyor (V&I)

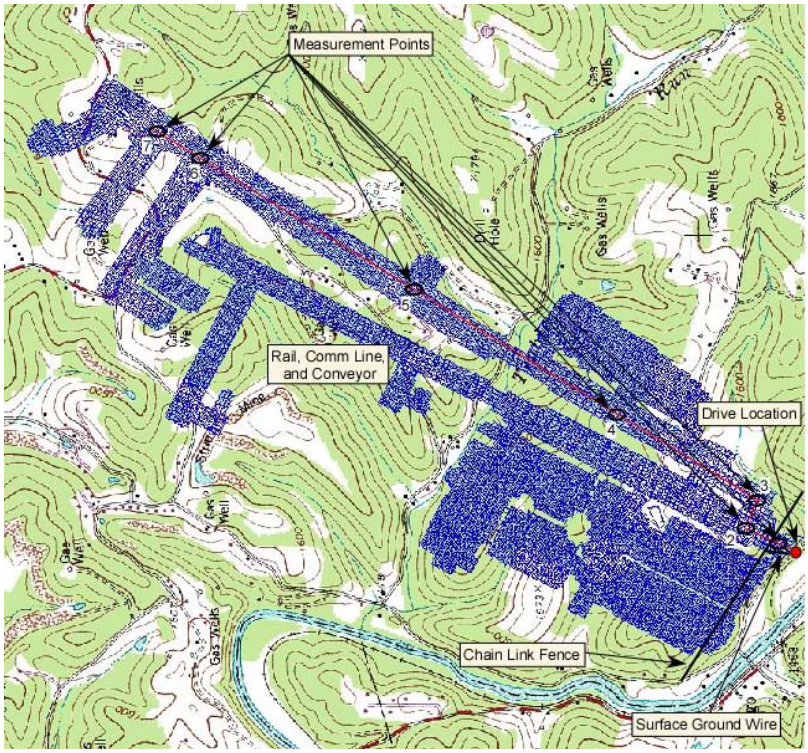

Figure 3-2 Direct Drive Measurement Locations.

[2] Mine grounding system similar to the grounding scheme in place during explosion.
[3] Mine grounding system in current state.

Three current probes were used for the various measurements: a Pearson model 110A; a Pearson model 4688; and a LEM-flex model RR3035 current probe. The voltage was measured with a high-impedance voltage probe model P601 made by Nanofast. The current and voltage probes are shown on the various conductive penetrations in Figure 3-3.The calibration curves for each probe versus frequency are located in Appendix B.

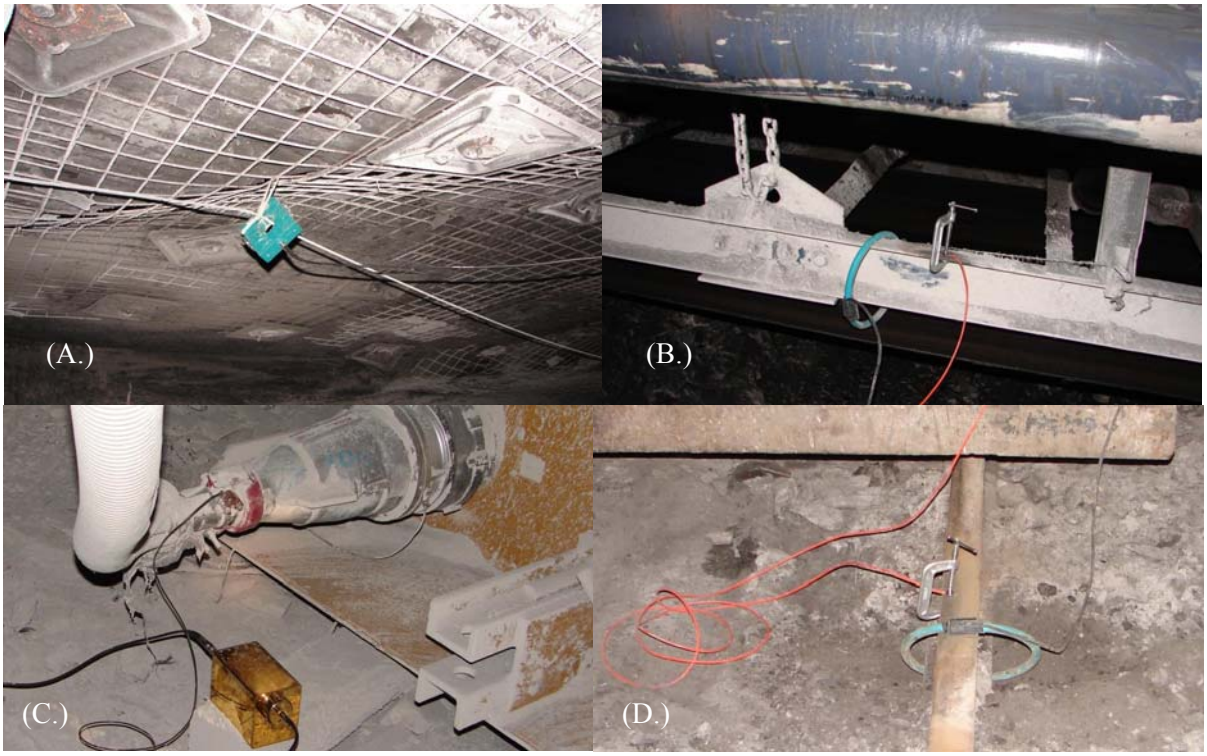

Figure 3-3 (A.) Current probe on trolley communication cable. (B.) Current probe and voltage connection on conveyor belt structure. (C.) Voltage probe on power cable. (D.) Current probe and voltage connection on rail.

3.1.3 Results

The results from the direct drive measurements were consistent with expectations. All of the processed spectral, or frequency-domain, voltage, and current transfer functions for each conductive penetration at each location can be found in Appendix C. For clarity, only a summary of the results is shown here. The summary tables show the attenuation of the peak amplitude of a positive and negative lightning-like pulse attached at the entrance of the mine. This quantity is calculated by multiplying the spectral representation of the current of a positive/negative lightning pulse by the current transfer function measured of a given conductor at a given location (that was measured in the mine). This product is then transformed to the time-domain by an inverse fast Fourier transform (IFFT). The attenuation listed in the tables is then simply the peak output divided by the peak input.

The peak current output to peak current input attenuation, for the various conductors at the measured locations, given a positive lightning waveform, are shown in Table 3-2 and Table 3-3 and, given a negative lightning waveform, are shown in Table 3-4 and Table 3-5. Table 3-2 and Table 3-4 show the attenuation with the mine grounding system in its current state, while Table 3-3 and Table 3-5 show the attenuation with the mine grounding system like it was during the explosion. The darkened cells of the tables indicate no measurements were recorded in the given locations.

Table 3-2 Summary of current transfer functions, using positive lightning waveform, for conductive penetrations with current mine grounding

	Trolley Comm Line		Conveyor		Rail		Power Cable Shield	
Location	Local Gnd	Fence Gnd	Local Gnd	Fence Gnd	Local Gnd	Fence Gnd	Local Gnd	Fence Gnd
1	$1.7x10^{-3}$	$2.9x10^{-3}$	$2.2x10^{-2}$	$2.9x10^{-2}$	$8.9x10^{-2}$	$1.4x10^{-1}$		
2								
3	$1.8x10^{-3}$	$2.8x10^{-3}$	$3.2x10^{-3}$	$4.9x10^{-3}$	$3.6x10^{-4}$	$9.2x10^{-5}$		
4	$1.7x10^{-3}$	$2.8x10^{-3}$	$5.6x10^{-4}$	$1.1x10^{-4}$	$3.8x10^{-4}$	$9.4x10^{-5}$		
5	$1.4x10^{-3}$	$2.2x10^{-3}$	$7.2x10^{-4}$	$2.7x10^{-4}$	$3.9x10^{-4}$	$3.0x10^{-4}$		
6	$1.2x10^{-3}$	$1.9x10^{-3}$	$4.0x10^{-4}$	$1.1x10^{-4}$	$5.5x10^{-4}$	$4.2x10^{-4}$		
7	$1.2x10^{-3}$	$2.0x10^{-3}$	$3.0x10^{-4}$	$9.3x10^{-5}$	$2.3x10^{-4}$	$3.5x10^{-4}$		

Table 3-3 Summary of current transfer functions, using positive lightning waveform, for conductive penetrations with former mine grounding

	Trolley Comm Line		Conveyor		Rail		Power Cable Shield	
Location	Local Gnd	Fence Gnd	Local Gnd	Fence Gnd	Local Gnd	Fence Gnd	Local Gnd	Fence Gnd
1							$4.6x10^{-2}$	$6.2x10^{-2}$
2	$1.3x10^{-3}$	$1.6x10^{-3}$			$2.6x10^{-4}$	$3.7x10^{-4}$	$1.8x10^{-2}$	$2.8x10^{-2}$
3	$1.3x10^{-3}$	$1.5x10^{-3}$			$1.4x10^{-4}$	$1.7x10^{-4}$	$1.6x10^{-2}$	$2.5x10^{-2}$
4								
5								
6								
7								

Table 3-4 Summary of current transfer functions, using negative lightning waveform, for conductive penetrations with current mine grounding

	Trolley Comm Line		Conveyor		Rail		Power Cable Shield	
Location	Local Gnd	Fence Gnd	Local Gnd	Fence Gnd	Local Gnd	Fence Gnd	Local Gnd	Fence Gnd
1	2.4×10^{-3}	4.3×10^{-3}	2.2×10^{-2}	2.9×10^{-2}	8.4×10^{-2}	1.4×10^{-1}		
2								
3	2.7×10^{-3}	4.7×10^{-3}	3.7×10^{-3}	5.2×10^{-3}	3.2×10^{-4}	1.3×10^{-4}		
4	2.4×10^{-3}	4.2×10^{-3}	5.7×10^{-4}	1.4×10^{-4}	3.1×10^{-4}	1.7×10^{-4}		
5	2.0×10^{-3}	3.4×10^{-3}	8.1×10^{-4}	3.1×10^{-4}	4.3×10^{-4}	3.4×10^{-4}		
6	1.8×10^{-3}	3.2×10^{-3}	4.4×10^{-4}	2.9×10^{-4}	5.3×10^{-4}	5.4×10^{-4}		
7	1.7×10^{-3}	3.0×10^{-3}	2.9×10^{-4}	8.7×10^{-5}	2.6×10^{-4}	1.9×10^{-4}		

Table 3-5 Summary of current transfer functions, using negative lightning waveform, for conductive penetrations with former mine grounding

	Trolley Comm Line		Conveyor		Rail		Power Cable Shield	
Location	Local Gnd	Fence Gnd	Local Gnd	Fence Gnd	Local Gnd	Fence Gnd	Local Gnd	Fence Gnd
1							4.7×10^{-2}	6.2×10^{-2}
2	2.2×10^{-3}	3.0×10^{-3}			4.0×10^{-4}	6.0×10^{-4}	1.8×10^{-2}	2.7×10^{-2}
3	2.2×10^{-3}	2.8×10^{-3}			1.6×10^{-4}	2.2×10^{-4}	1.6×10^{-2}	2.4×10^{-2}
4								
5								
6								
7								

3.2 Indirect Drive

3.2.1 Setup/Equipment Layout with Photos

The method used to characterize indirect electromagnetic coupling into the sealed area is shown in Figure 3-4 and Figure 3-5. The current from the audio amplifier (which is driven by the output from the network analyzer) is driven on to a long wire above the ground which is terminated at each end with ground rods. The ground rods are placed so as to produce a current distribution in the ground that simulates a linear current drive.

Two configurations were used for the indirect drive measurements. One configuration was through ground rods placed so as to drive the current parallel to the sealed area of the mine and over the area where the explosion occurred as shown in Figure 3-5A. The surface drive wire was approximately 500 m long. A second configuration was through ground rods placed so as to drive the current perpendicular to the sealed area of the mine and over the area where the explosion occurred as shown in Figure 3-5B. In this case the surface drive wire was only 200 m long.

Two types of measurements were made to characterize the indirect coupling into the sealed area. The more time consuming of the two was the electric field mapping measurements made in the vicinity of the explosion ignition area, where the core hole is located. The other measurement was the induced voltage on a spliced intact pump cable going from the back of the sealed area to the location of the core hole. The pump cable was spliced with 12-gauge wire to recreate the length of pump cable believed to have been there during the explosion[4]. The end of the pump cable at the back of the mine was originally attached to the pump which was submerged underwater and chained to the ceiling mesh. For the measurements, the pump cable was connected with 12-gauge wire to the ceiling mesh and the exposed conductors were placed under water approximately four crosscuts from the back of the sealed area[5]. The approximate total length of the recreated cable was 300 m (984 ft).

The electric field at various locations in the sealed area of the mine was measured with an active dipole antenna connected to a receiver via fiber optics. The fiber-optic receiver is connected to the network analyzer measurement port so that the signals are phase-locked in order to measure very small signals in the microVolt/meter range. The three polarizations of the electric field were measured at a total of 15 locations for both the parallel and perpendicular wire current drives. The three polarizations measured were the vertical, P-directed (parallel to the length of the sealed area), and X-directed (transverse to the length of the sealed area). A photo of the dipole antenna in horizontal and vertical polarization is shown in Figure 3-7. The exact locations of the measured electric field are shown in Figure 3-6 where the distance between locations was approximately 10 m. The figure shows 17 total locations; however, positions P1 and P9 were not measured due to water hazards. Because of the amount of data taken and the spacing between measurement points, the lack of these two points does not impact the results.

The induced voltage measurements were taken on the pump cable with both a parallel and perpendicular surface wire drive. These measurements were also conducted using the instrumentation system shown in Figure 3-4. The induced cable voltage was measured with a Nanofast high-impedance probe in the vicinity of the core hole, and transmitted to the surface with fiber optics.

[4] As a note, there is some disagreement as to the length and positioning of the pump cable at the time of the explosion. The test team used information provided at the time of the measurements, which was that the pump cable was intact and the cable shield was grounded to the submerged pump.

[5] Test team was unable to reach the back of the sealed area where the pump would have been (it was removed after the explosion) due to water.

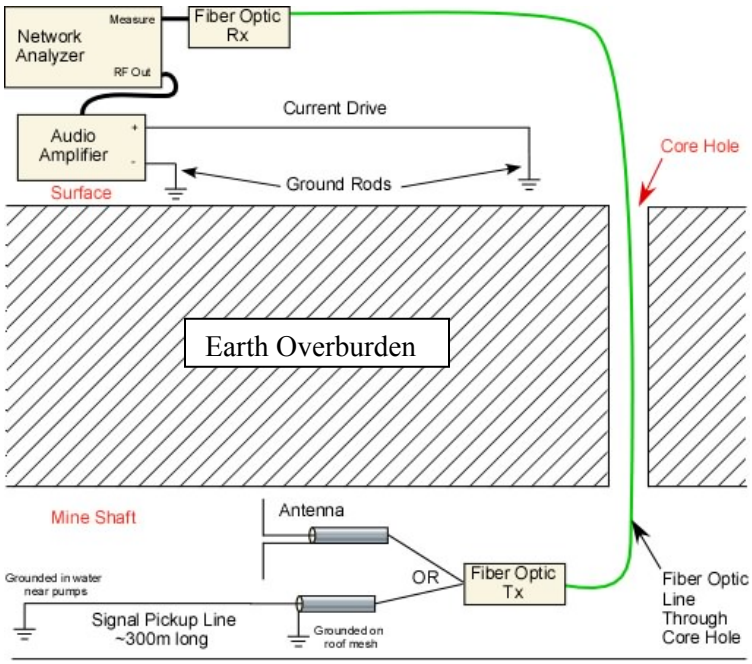

Figure 3-4 Indirect Drive Conceptual Drawing.

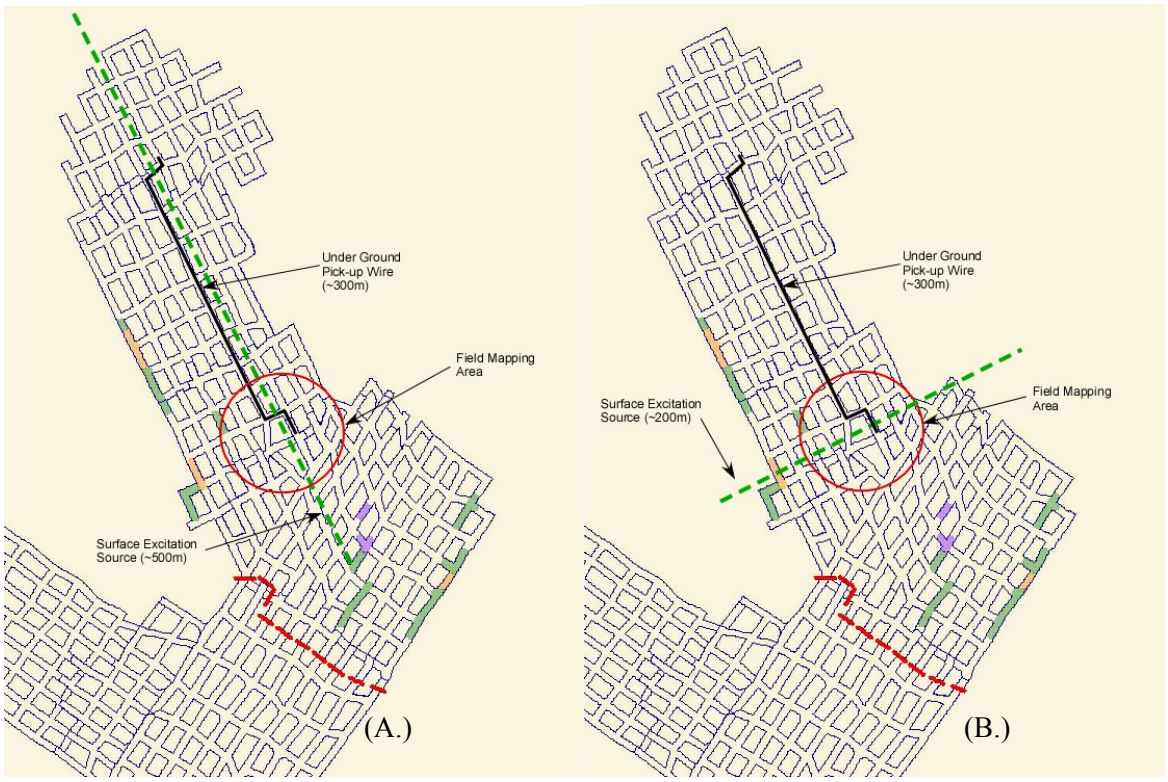

Figure 3-5 Parallel (A.) and perpendicular (B.) surface current drive for indirect drive measurements.

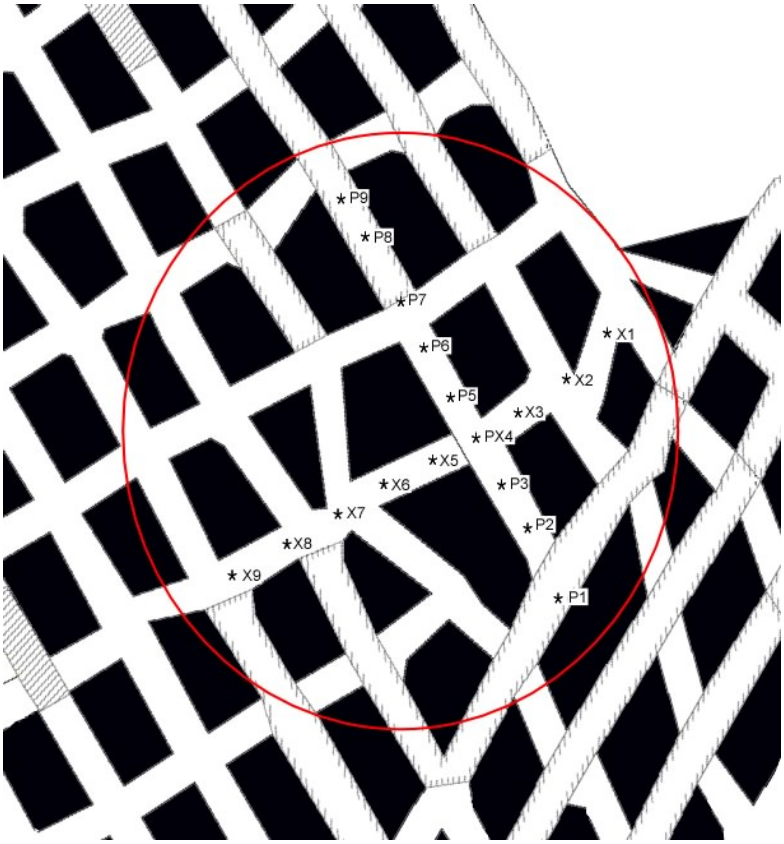

Figure 3-6 Electric field measurement locations.

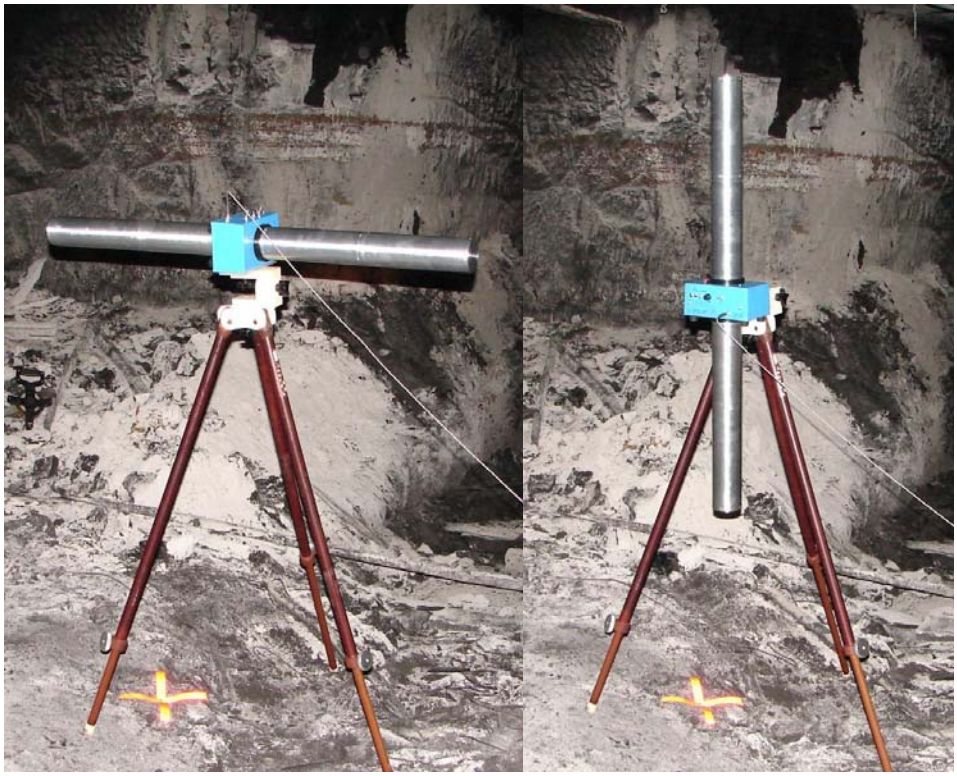

Figure 3-7 Sandia dipole antenna in horizontal and vertical polarizations inside previously sealed area.

3.2.2 Results

The purpose of the electric field mapping of the explosion area was to first look for any field inhomogeneities due to geological features, and second to compare to the analytical model. An added benefit was the ability to verify the induced voltage on the pump cable by integrating the parallel component of the electric field across it. The electric field measurements are shown first and then the induced cable voltage is plotted. The electric field results did show an enhanced electric field at the P5 and the X7 locations (this is noted for general interest,) but do not impact the cable results. The cable integrates or averages the fields over the cable length to build-up a potential difference or voltage.

The data collected for the indirect drive tests from the dipole antenna was only usable above 100 Hz. This was due to a very large 60 Hz clutter signal from surrounding power lines and the high noise level from the network analyzer below 40 Hz. Both of these factors were overcome for the long wire voltage measurement by reducing the IF bandwidth of the network analyzer from 10 Hz to 2 Hz. The reduction of the IF bandwidth lowered the noise floor considerably and reduced the sensitivity of the transfer function to the 60 Hz clutter; however, the time for a single swept measurement increased from ~1.5 minutes to ~10 minutes. With the large number of measurements desired for characterizing the electric field in the sealed area, the higher IF bandwidth was used for the majority of the data collected. The overall effect on the data was minimal. As a result, only data from frequencies above 100 Hz are plotted for the dipole measurements in the body of this report. The full spectrum of the data collected can be found in Appendix C.

The normalized composite electric fields from the dipole antenna at various locations are plotted in this section. The composite electric field is simply the root-sum-square or amplitude of the electric field vector. The measured electric field is normalized by the current in the drive wire on the surface, so that the units are V/m/A.

The normalized electric fields due to the wire current drive parallel to the P-direction, measured at locations P2 through P8 and X1 through X9, are shown in Figure 3-8 and Figure 3-9, respectively. Similarly, the fields due to the wire current drive perpendicular to the P-direction, measured at locations P2 through P8 and X1 through X9, are shown in Figure 3-10 and Figure 3-11, respectively. This information is summarized in Table 3-6.

Table 3-6 Summary of figures for drive configurations

Drive Configuration	Electric Field at P locations	Electric Field at X locations
P-directed Current Drive (Parallel)	Figure 3-8	Figure 3-9
X-directed Current Drive (Perpendicular)	Figure 3-10	Figure 3-11

Referring to Figure 3-8, note that the composite electric fields measured in a path parallel to and immediately below the drive are about the same amplitude. The presence of metal objects near the antenna affects the local fields somewhat. The measurement at P5 was made in the area between unconnected sections of roof mesh. The slight resonance at about 60 kHz in the P5 measurement was probably caused by a resonance of the cable that was attached for the voltage measurements. This cable was not removed for the electric field measurements, and high electric fields may have been induced on the disconnected end of the cable at resonance.

Referring to Figure 3-9, note that the low-frequency amplitude tended to decrease as the electric field antennas were moved away from the center line immediately below the drive line.

Referring to Figure 3-10, the composite electric fields measured in a path perpendicular to the drive cable are reduced significantly from the field due to a parallel drive cable. Again, a slight resonance was seen at P5.

Referring to Figure 3-11, the fields measured parallel to and below the perpendicular drive are comparable in amplitude to those shown in Figure 3-8. Because of the closer spacing of the ground rods on the surface, more variation was shown in the individual measurements.

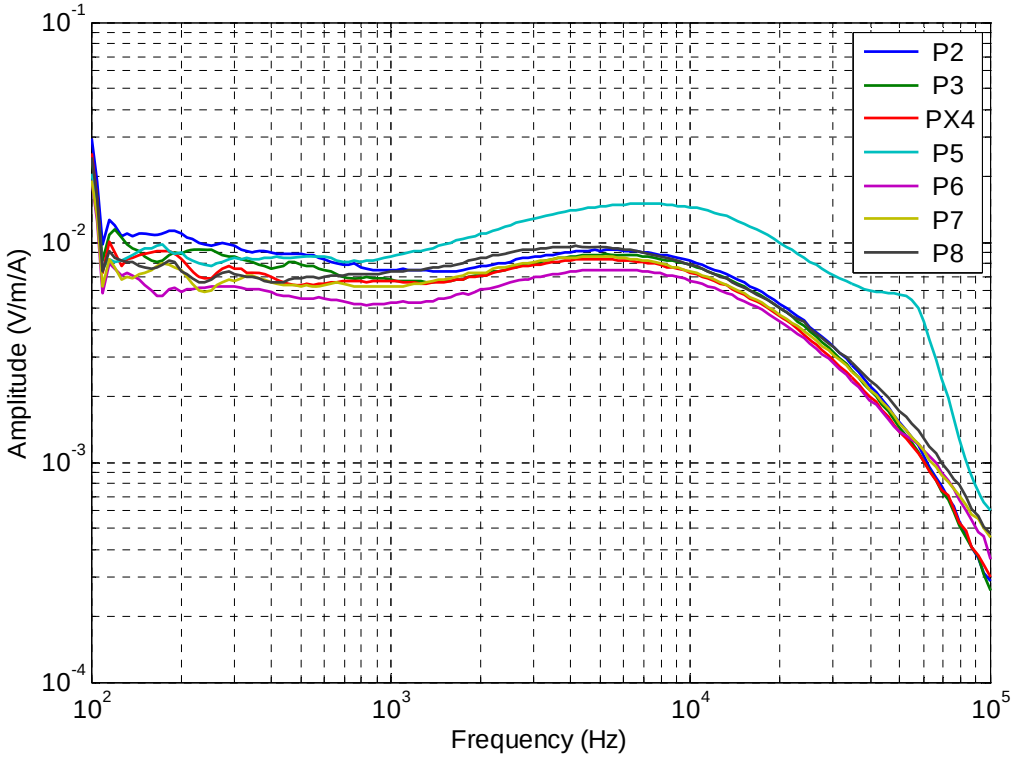

Figure 3-8 Composite Electric Field along P-direction with parallel line drive on surface.

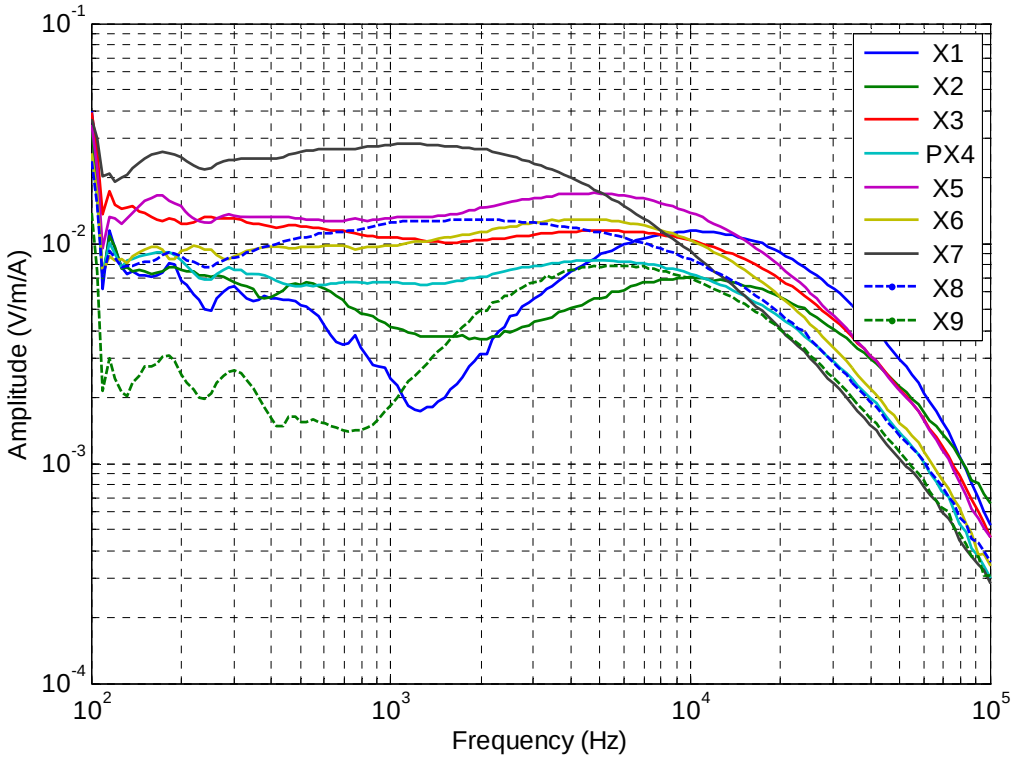

Figure 3-9 Composite Electric Field along X-direction with parallel line drive on surface.

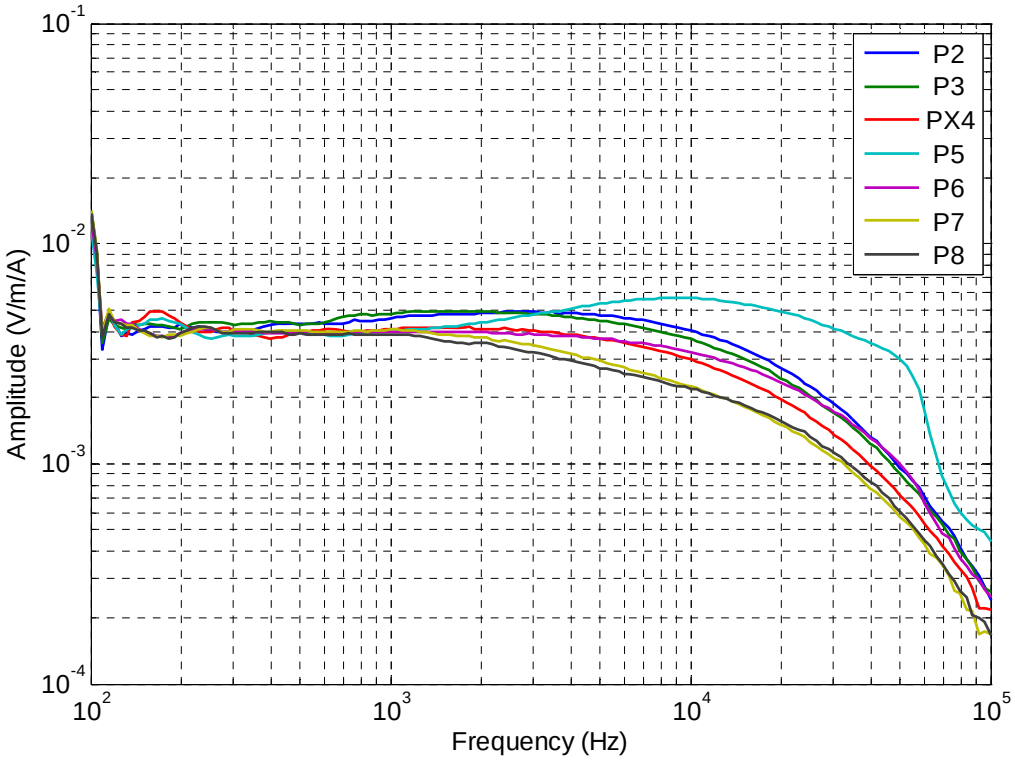

Figure 3-10 Composite Electric Field along P-direction with perpendicular line drive on surface.

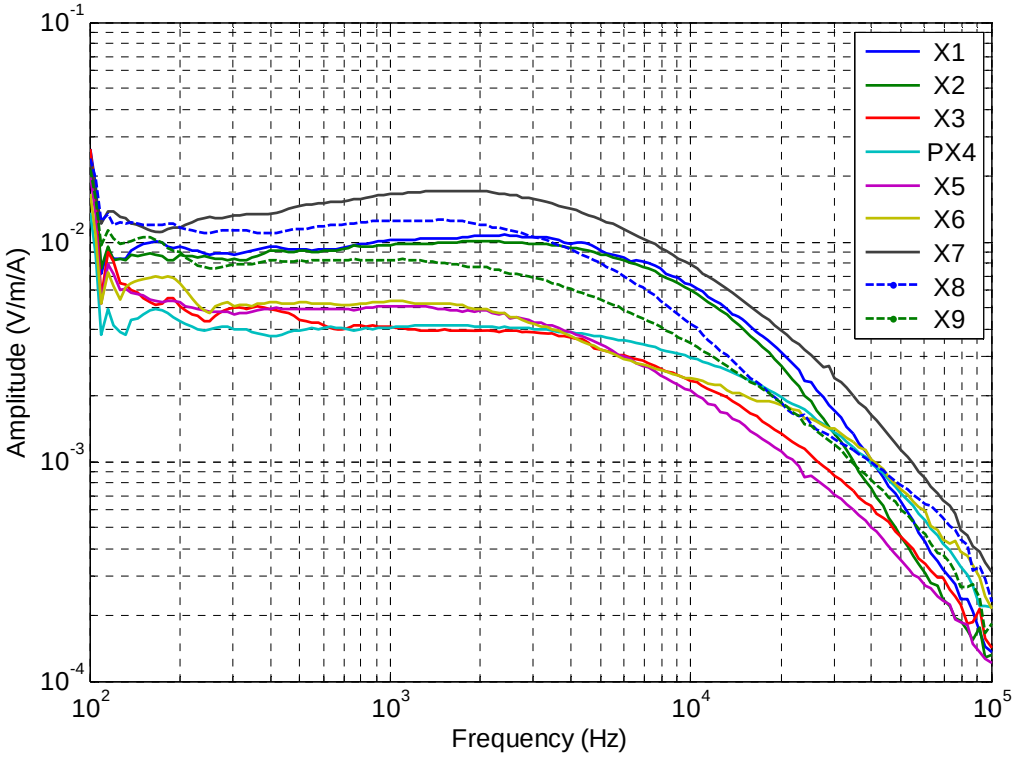

Figure 3-11 Composite Electric Field along X-direction with perpendicular line drive on surface.

The voltage on the pump cable was measured with a high-impedance voltage probe and the network analyzer set to a 2 Hz IF bandwidth. The normalized results of the voltage amplitude plotted relative to the drive current on the surface wire, with units of Volts per Amp (V/A), are shown in Figure 3-12. There is a spike at 60 Hz due to stray signals from power lines. The data is skewed by noise only below 20 Hz.

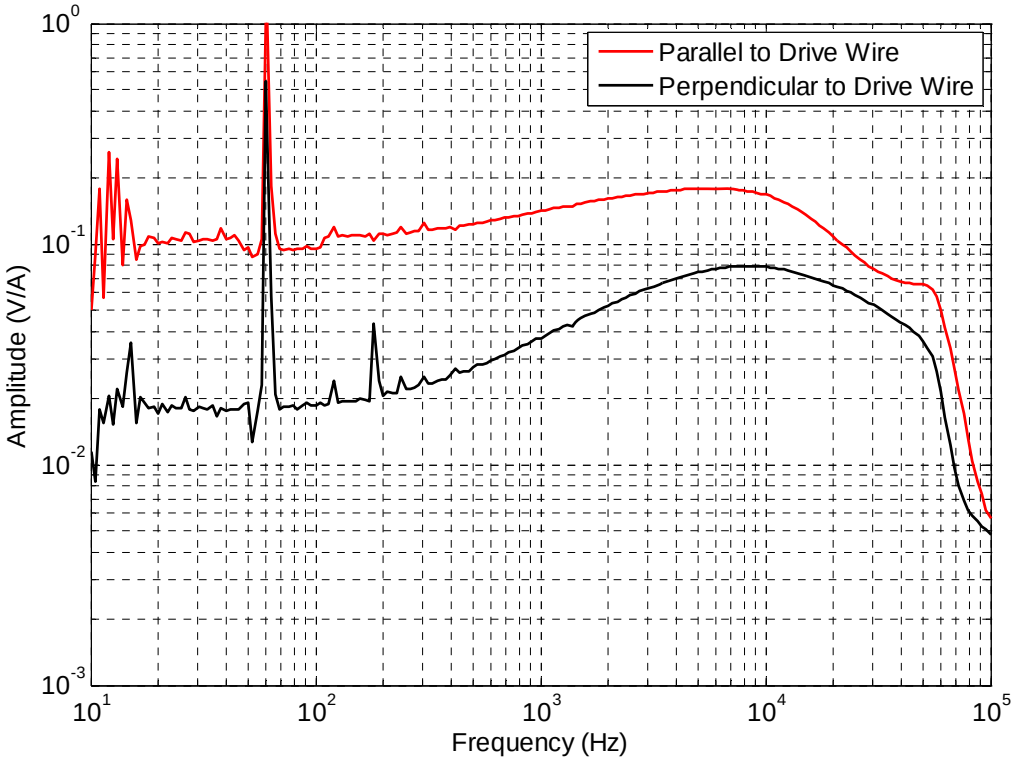

Figure 3-12 Induced voltage on pump cable (~300 m or 984 ft. long) due to wire current drives on surface.

To compare the induced voltage measured on the pump cable with the field measurements, we will look only at the parallel surface drive induced fields from P2 to P8. Furthermore, we will only look at the horizontal polarization directed along the P-axis, parallel to the direction of the drift. The horizontal polarized electric fields are shown in Figure 3-13. The normalized electric fields are in units of Volts per meter per Amp (V/m/A) while the normalized induced voltage on the pump cable are in units of Volts per Amp (V/A). If we integrate the electric fields over the length of the pump cable, we should obtain the induced voltage from Figure 3-12. Assuming a simple uniform distribution we can simply multiply the electric field by a length. The effective length of cable (similar to the effective area of an antenna) needed to match the electric fields measured with the induced voltage measured was found to be approximately 120 m (394 ft). This means that only the 120 m (394 ft) closest to the measurement end of the cable contribute to the induced voltage. The comparison between the measured induced voltage and the electric field multiplied by the effective length of 120 m (394 ft) is shown in Figure 3-14.

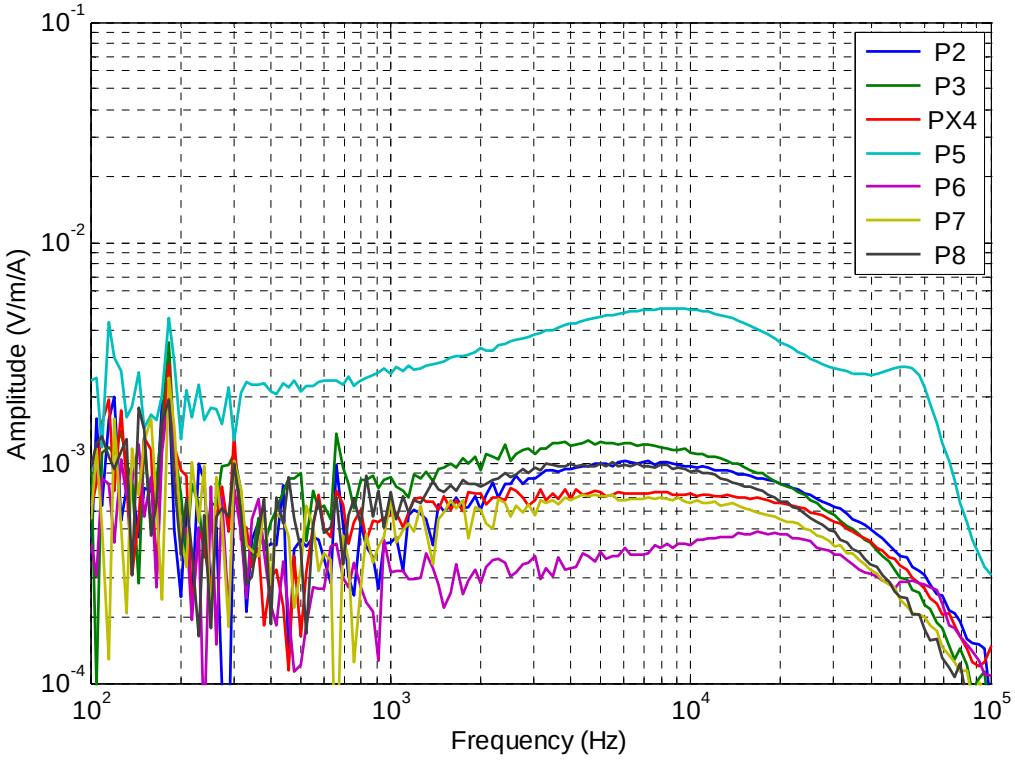

Figure 3-13 P-directed Electric Field along P-direction with parallel line drive on surface.

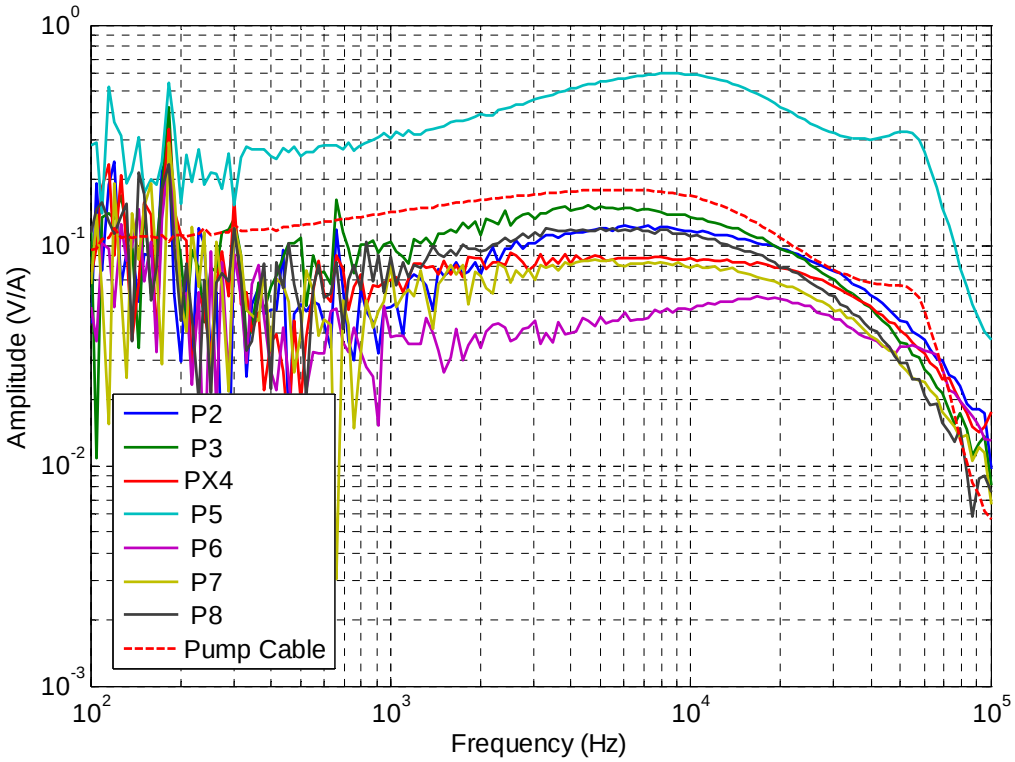

Figure 3-14 P-directed Electric Fields multiplied by an effective cable length of 120 m (394 ft) compared with the induced voltage on the pump cable.

3.2.3 Results Compared with Diffusion Model

The model for diffusion coupling from an infinite current source above a homogeneous half-space was presented in Section 2.2.3. This model is compared with the measured electric field and induced voltage on the pump cable. Using an effective soil resistivity of 80 Ω-m, the analytic model plotted in Figure 3-15 matches very closely the horizontal (P-directed) electric field measured with a parallel current drive. The correlation between model and measured data is extremely good from 10 to 100 kHz. This confirms that the major coupling mechanism from the surface to the sealed area is field diffusion coupling. The measured data is contaminated by 60 Hz resonances and clutter below 1 kHz for this polarization. The data deviates from the model of coupling beneath an infinite line at frequencies below 1 kHz. The measured data stays at a constant level of approximately 0.0006 V/m/A, whereas the analytical model predicts a downward slope. Much of this deviation can be attributed to the field caused by the DC component from the finite spacing of the ground rods. An estimate of this component of the electric field is shown below 1 kHz, where the skin depth is much larger than the depth to the measurement antennas. A comparison of the average of the P-directed electric field measurements from P2 to P8 with the analytic diffusion model is shown in Figure 3-16. The average field is a more meaningful value to compare since it has local variations removed. The amplitude and shape show amazing correlation.

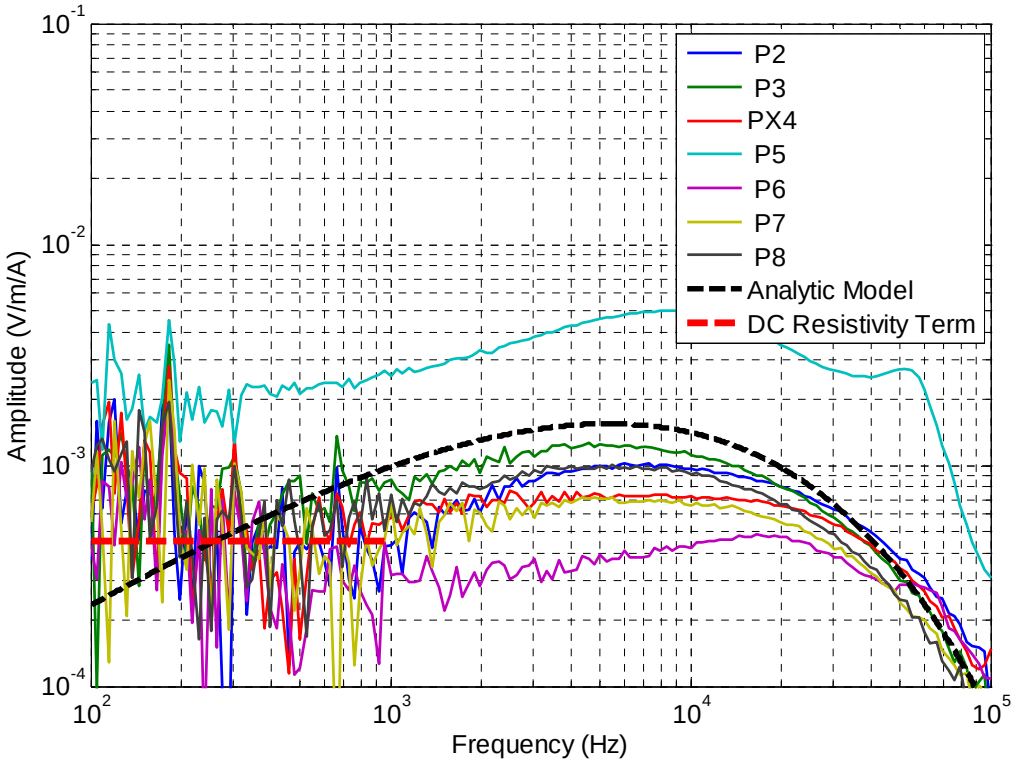

Figure 3-15 P-directed Electric Fields compared with the diffusion model with an effective resistivity of 80 Ω-m.

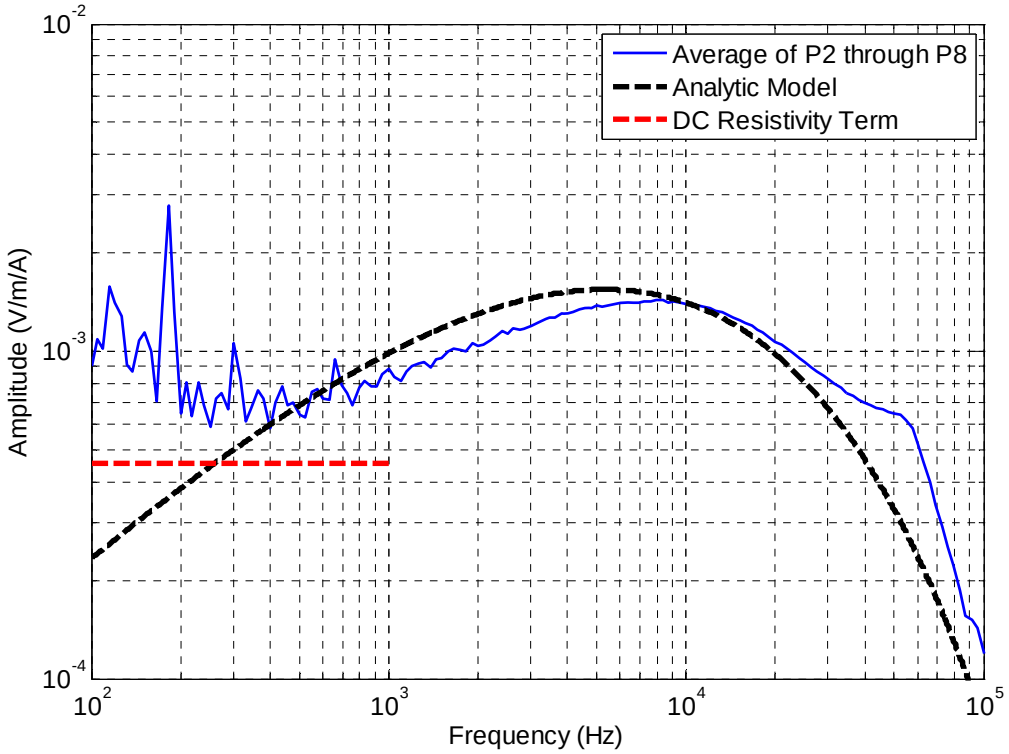

Figure 3-16 Average of P-directed fields from P2 to P8 compared with diffusion model.

To compare the analytic model with the measured induced cable voltage, we simply integrate over the effective length of cable discussed in the previous section, 120 m (394 ft). Again, the model shows excellent agreement with the measured voltage from 1 to 100 kHz. There is a deviation from the model of coupling beneath an infinite line at frequencies below 1 kHz, where the measured data stays at a constant level of approximately 0.1 V/A. Much of this deviation is caused by the field caused by the DC component from the finite spacing of the ground rods. An estimate of this component of the electric field is shown below 1 kHz where the skin depth is much larger than the depth to the cable. The measured data has been processed to remove the 60 Hz clutter signal and its harmonics.

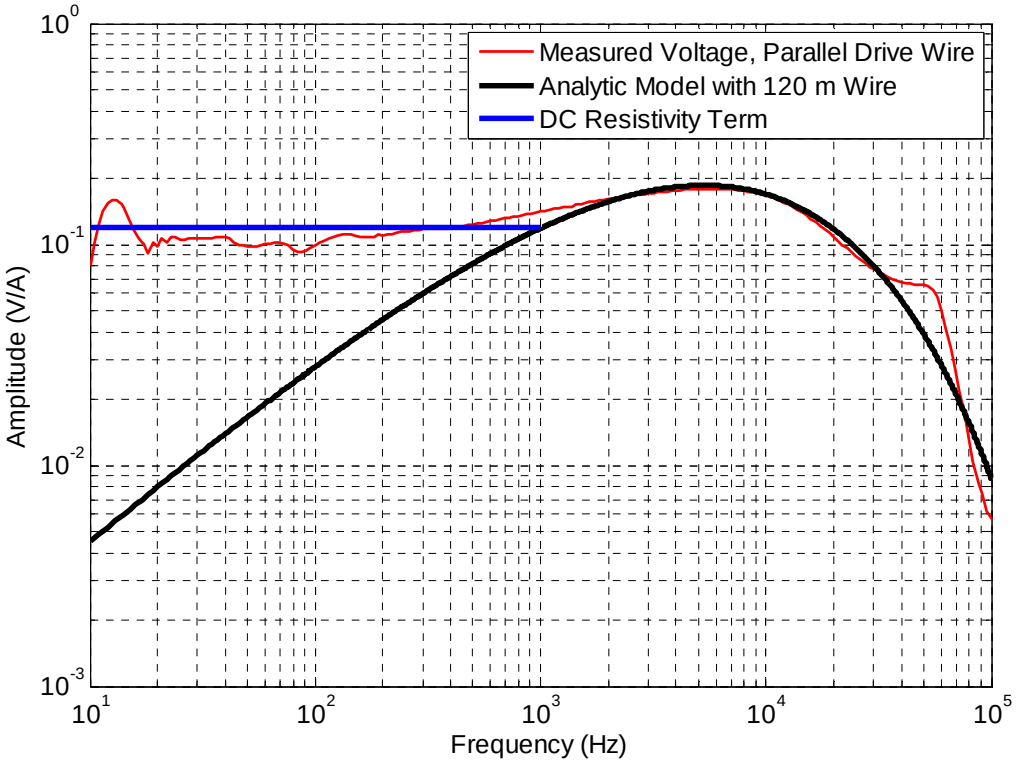

Figure 3-17 Induced voltage on pump cable due to parallel wire current drive on surface (with 60 Hz and harmonics removed) compared with analytic diffusion model of 120 m (394 ft) long cable and an effective soil resistivity of 80 Ω-m and the DC Resistivity term.

4 Results Coupled with Lightning

The results from the direct drive measurements, and the indirect coupling measurements and analysis are coupled with recorded and hypothetical lightning strokes in this section. The analysis performed in this section uses the recorded amplitudes, when appropriate; however, for all other cases, nominal amplitudes of 100 kA were used. The value of 100 kA was used for two reasons: first, there was a cloud-to-ground stroke recorded close in time and distance to the explosion area on the order of 100 kA; and second, the value of 100 kA is easy to scale. It should be noted that the voltages presented in Section 4.2 and 4.3 were calculated using the uniform magnetic field excitation formulation shown in Section 2.2.4. The voltages from a hypothetical long, low altitude horizontal current channel from a cloud-to-ground stroke of Section 4.4 were calculated using infinite line current source above a half-space shown in Section 2.2.2. The basic lightning waveforms used in this section as inputs into the transfer functions are shown in Figure 4-1. The negative lightning waveform was created using a double exponential formula found in [32]. There is no analytic or mathematical model for a positive lightning waveform found in published literature. Hence, a positive lightning waveform was created using a 15th order polynomial of the author's design and appending a 100 ms tail on the backend. The positive lightning waveform characteristics were tailored from values found in [33,20]. Some pertinent waveform characteristics of the modeled lightning waveforms are shown in Table 4-1.

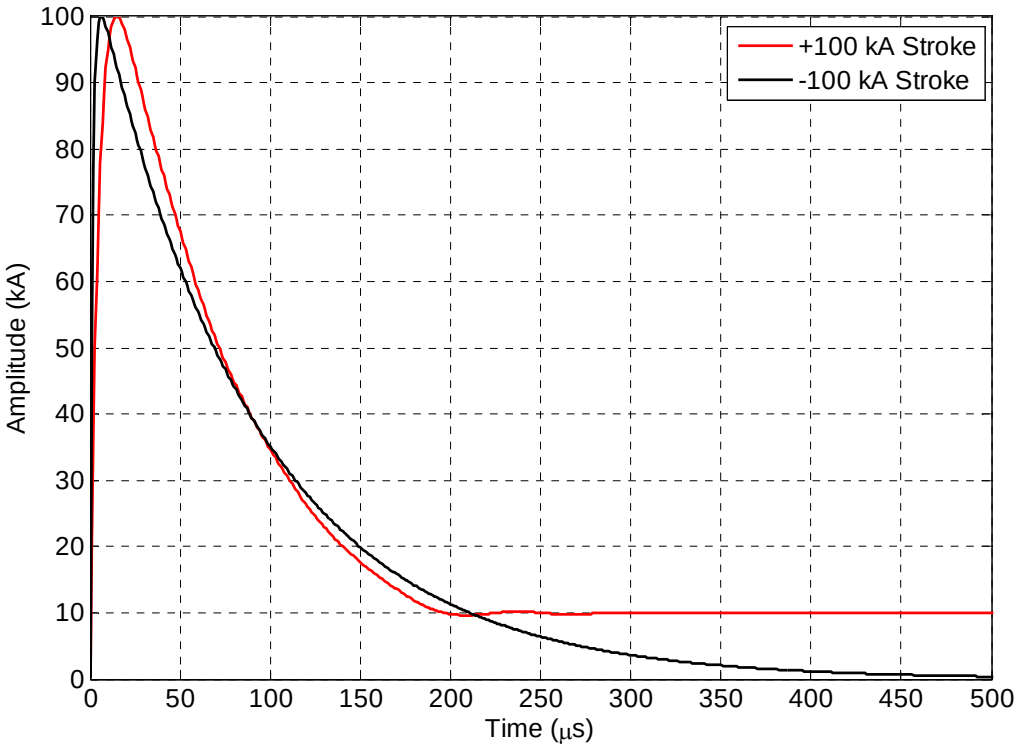

Figure 4-1 Basic positive and negative lightning waveforms used as inputs for analysis.

Table 4-1 Characteristics of positive and negative lightning waveforms used in analysis

Amplitude (kA)	Full Width at Half Maximum, FWHM (μs)	dI/dt (kA/μs)
-100	68	16.7
+100	69	6.5
+30	69	2.0

4.1 Direct Drive Transfer Functions Coupled with Lightning Strokes

If we assume that lightning directly coupled onto the conductive penetrations into the entrance of the Sago mine with either a positive or negative 100 kA stroke, then peak voltages and currents can be calculated. Only the direct drive transfer functions measured with the fence ground are used in this analysis because the fence ground is more representative of a current distribution due to a real lightning stroke.

The peak currents and voltages on the trolley communication line, conveyor, rail, and power cable shield were calculated using the following procedure. First, the lightning waveforms shown in Figure 4-1 were transformed into the frequency domain with a fast Fourier transform (FFT). Then the lightning data was multiplied by the complex transfer function of a given conductor to a given location. The resulting frequency waveform was then transformed back into the time domain with an inverse fast Fourier transform (IFFT). The peak voltage or current was recorded for each waveform. This was then repeated for each conductor at each location measured. Voltage was not measured on the trolley communication line because it was an insulated cable. The measurement locations cross-referenced to break number and approximate distance from the entrance are summarized in Table 4-2 for convenience.

Since the transfer function of the shield of the power cable was only measured out to the #3 power center, an extrapolation was performed to estimate the voltage and current at location 7 (at the 2nd Left Switch). The extrapolated values of voltage and current on the shield of the power cable are shown in the green highlighted cells of the "Power Cable Shield" columns of Table 4-3 and Table 4-5. The voltage was extrapolated using an exponential curve fit, while the current was extrapolated using a simple logarithmic curve fit. These extrapolations were matched with the trend of the first three points, and are a best-guess speculation. The peak current and voltage from a positive 100 kA lightning stroke attached directly to the entrance of the mine for each conductor at each location are shown in Table 4-3 and Table 4-4. The peak currents and voltages due to a negative 100 kA stroke are shown in Table 4-5 and Table 4-6.

Table 4-2 Direct Drive Measurement Locations

Location	Mine Feature	Break Number	Approximate Distance from Entrance
1	#1 Power Center	Belt 1, Break 1	30 m (98 ft.)
2	#2 Power Center	Belt 2, Break 1	459 m (1506 ft.)
3	#3 Power Center	Belt 3, Break 1	669 m (2195 ft.)
4	1st Right Spur	Belt 3, Break 16	1076 m (3530 ft.)
5	2nd Right Spur	Belt 4, Break 11	2178 m (1.35 miles)
6	1st Left Switch	Belt 4, Break 50	3255 m (2.02 miles)
7	2nd Left Switch	Belt 4, Break 59	3491 m (2.17 miles)

Table 4-3 Peak currents and voltages from a positive 100 kA lightning stroke, for conductive penetrations with old mine grounding

	Trolley Comm Line	Conveyor	Conveyor	Rail	Rail	Power Cable Shield	Power Cable Shield
Location	I_{max} (A)	I_{max} (A)	V_{max} (V)	I_{max} (A)	V_{max} (V)	I_{max} (A)	V_{max} (V)
1						6213	8369
2	162			37	643	2841	3229
3	154			17	233	2547	1582
4							
5							
6							
7						480*	1*

* Extrapolated values.

Table 4-4 Peak currents and voltages from a positive 100 kA lightning stroke, for conductive penetrations with current mine grounding

	Trolley Comm Line	Conveyor	Conveyor	Rail	Rail	Power Cable Shield	Power Cable Shield
Location	I_{max} (A)	I_{max} (A)	V_{max} (V)	I_{max} (A)	V_{max} (V)	I_{max} (A)	V_{max} (V)
1	293	2884	10931	14087	136693		
2							
3	279	495	881	9	996		
4	279	11	62	9	436		
5	220	27	11	30	1079		
6	190	11	2	42	321		
7	198	9	1	35	106		

Table 4-5 Peak currents and voltages from a negative 100 kA lightning stroke, for conductive penetrations with old mine grounding

	Trolley Comm Line	Conveyor	Conveyor	Rail	Rail	Power Cable Shield	Power Cable Shield
Location	I_{max} (A)	I_{max} (A)	V_{max} (V)	I_{max} (A)	V_{max} (V)	I_{max} (A)	V_{max} (V)
1						6193	7989
2	295			60	668	2711	3078
3	279			22	218	2417	1438
4							
5							
6							
7						280*	1*

* Extrapolated values.

Table 4-6 Peak currents and voltages from a negative 100 kA lightning stroke, for conductive penetrations with current mine grounding

	Trolley Comm Line	Conveyor	Conveyor	Rail	Rail	Power Cable Shield	Power Cable Shield
Location	I_{max} (A)	I_{max} (A)	V_{max} (V)	I_{max} (A)	V_{max} (V)	I_{max} (A)	V_{max} (V)
1	434	2926	11279	13606	143340		
2							
3	467	515	1052	13	1615		
4	417	14	77	17	934		
5	343	31	13	34	1367		
6	320	29	3	54	650		
7	301	9	1	19	62		

An item of interest is the relatively high current on the shield of the power cable (480 A) at the 2nd left switch (location 7) in Table 4-3. The power cable does not stop at the 2nd left switch, but turns approximately 90 degrees to the left and travels down the 2nd Left Main and onto the 2 Left Power Center. This presents a similar coupling mechanism as the indirect case where a long line current drive on the surface produces electromagnetic fields that propagate through earth. Only in this case, instead of the lightning currents on the surface being the drive, the induced current on the shield of the power cable inside the mine provides the drive mechanism for coupling onto the pump cable. Assuming a direct 100

kA positive stroke onto the shield of the power cable at the entrance to the mine, an analysis of this scenario results in <50 V peak induced on the pump cable, too low to be of concern.

4.2 Indirect Drive from NLDN and USPLN Positive Stroke 1-3

The locations of the three recorded lightning strokes, on the NLDN and USPLN, are shown in Figure 4-2 with the calculated distances and angles. Note that it is highly probable that the 38.8 kA and 35 kA strokes represent a single stroke with a location discrepancy, as discussed in Section 1.6. The angles shown are the angles between the line made up from the lightning stroke to the center of the pump cable, and the line formed by the direction where the pump cable lay. The first stroke analyzed is the 38.8 kA positive lightning stroke, 5.44 km (3.4 miles) away from the sealed area and an angle of 52.8 degrees. The second stroke has an amplitude of 35 kA at a distance of 4.02 km (2.5 miles) away from the sealed area and an angle of 49.3 degrees. The last stroke has an amplitude of 101 kA, a distance of 2.91 km (1.8 miles), and an angle of 85.5 degrees. The resulting induced voltage pulses on the pump cable (at the end of the cable nearest the explosion area) are shown in Figure 4-3, with peak amplitudes of 25.7 V, 33.8 V, and 16.2 V for the three strokes, respectively. The effective length of 120 m (394 ft.) was used for the length of the pump cable in Figure 4-3. Since there is concern about the actual length of intact pump cable present at the time of the explosion, analysis was performed on a pump cable with a length of 61 m (200 ft.) to account for the length of the cable piece found closest to the explosion area. The resulting induced voltage pulses on the 61 m (200 ft.) length of pump cable are shown in Figure 4-4. None of the induced voltages from these recorded strokes have the necessary amplitude to cause an arc inside the sealed area. It should be noted that taking the indirect coupling model approximation out to 3 km and beyond represents an upper bound on the coupling.

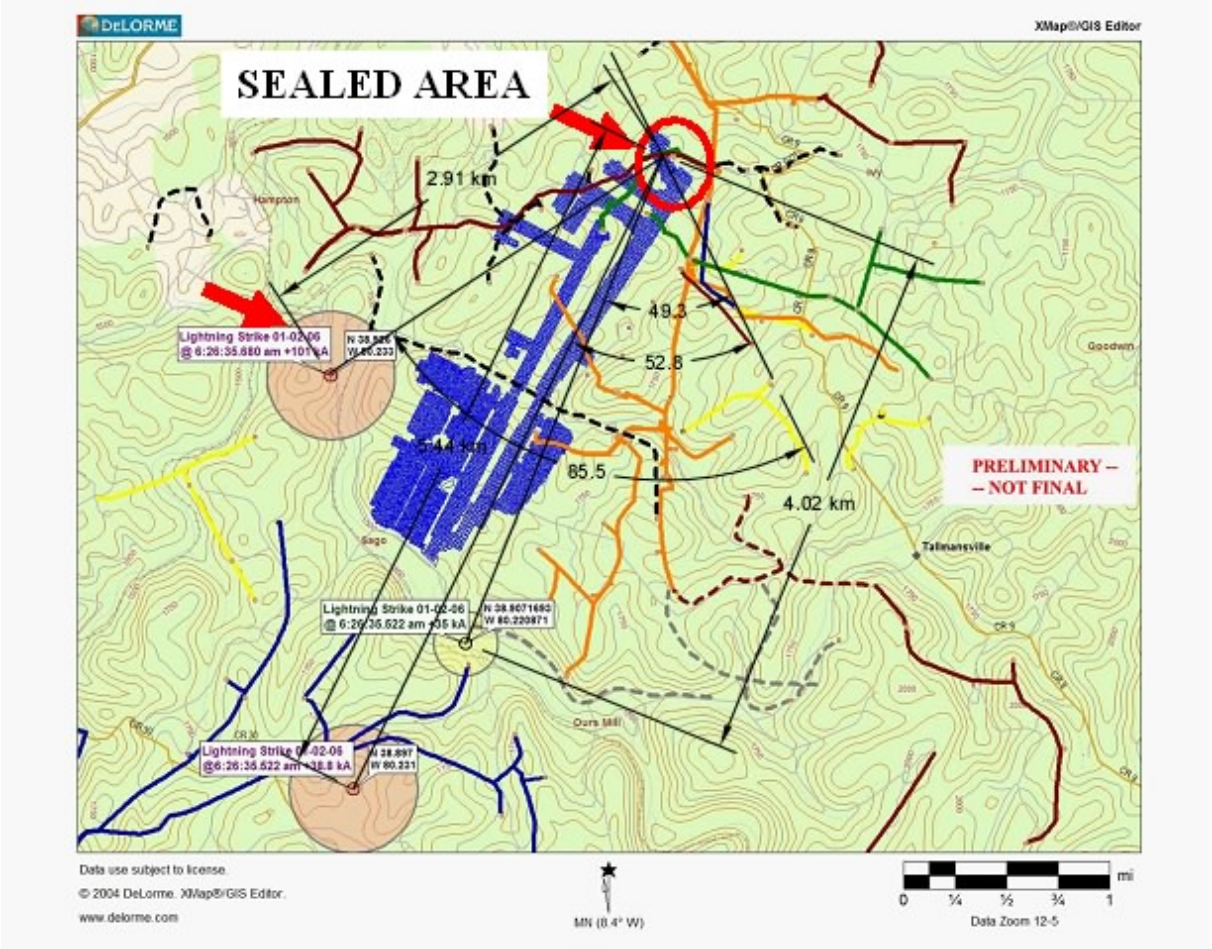

Figure 4-2 Locations of recorded lightning strokes with respect to the sealed area, with distances and angles.

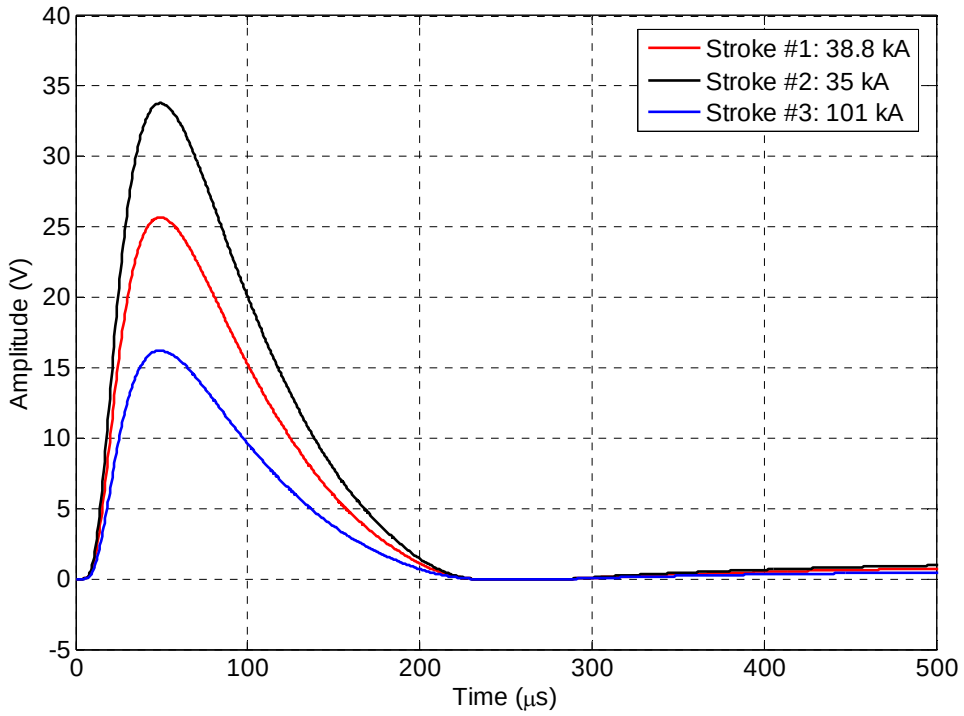

Figure 4-3 Voltage induced on pump cable (using an effective length of 120 m or 394 ft.) due to the three positive lightning strokes recorded on the NLDN and USPLN.

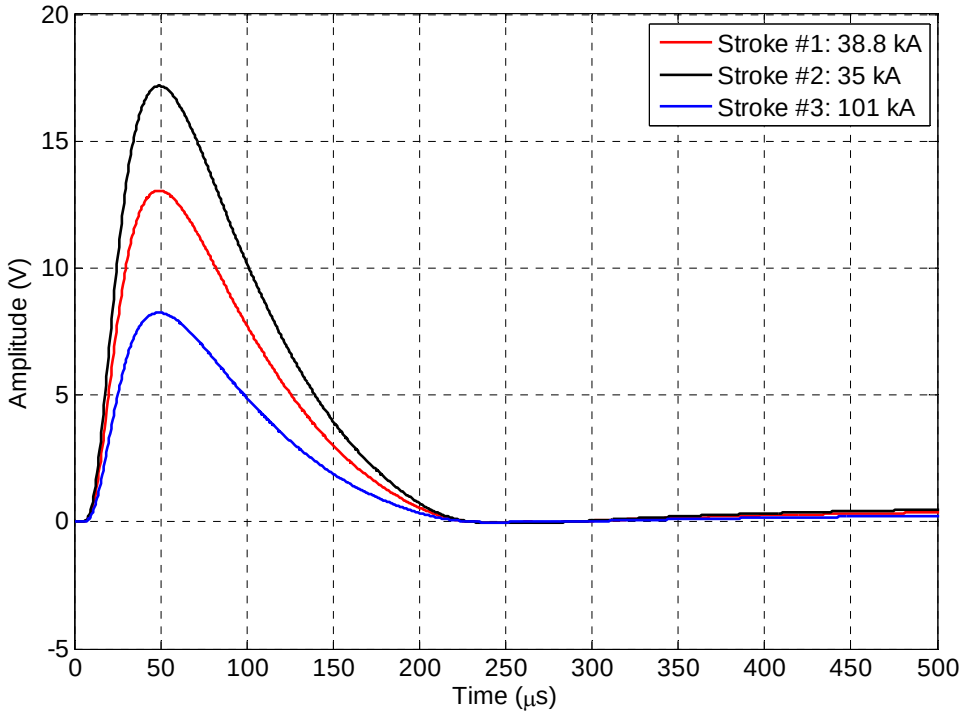

Figure 4-4 Voltage induced on pump cable (length of 61 m or 200 ft.) due to the three positive lightning strokes recorded on the NLDN and USPLN.

4.3 Indirect Drive from Hypothetical Stroke Directly over Sealed Area

If we assume a 100 kA negative or positive lightning stroke attached within 100 m (328 ft.) from directly over the center of the pump cable in the sealed area on the surface, it could induce a sufficiently high voltage in conductors in the sealed area to cause an electrical arc. This effect would be maximized if the stroke were directly inline with the pump cable direction at an angle of zero degrees. The induced voltage on the pump cable (with an effective length of 120 m or 394 ft.) from a 100 kA positive and negative cloud-to-ground stroke is shown in Figure 4-5. The maximum voltages are 23.8 kV from the positive pulse and 22.3 kV from the negative lightning pulse. Again, since there is concern about the actual length of intact pump cable present at the time of the explosion, analysis was performed on a pump cable with a length of 61 m (200 ft.) to account for the cable piece found closest to the explosion area. The resulting induced voltage pulses on the 61 m (200 ft.) length of pump cable are shown in Figure 4-6. The maximum voltages expected on the shorter cable length are 20.5 kV from the positive pulse and 19.1 kV from the negative lightning pulse.

Lightning currents as low as 20 kA (either positive or negative), which is closer to the statistical average peak current of cloud-to-ground lightning strokes, can produce thousands of Volts on the pump cable. This level of voltage is more than capable of initiating an electrical arc under the right conditions. The peak voltage amplitude expected on the pump cable scales linearly with the peak current amplitude of the driving lightning stroke. The results from the 100 kA case shown in Figure 4-5 can be scaled to the 20 kA case by dividing the peak amplitude of the voltage on the cable by a factor of five.

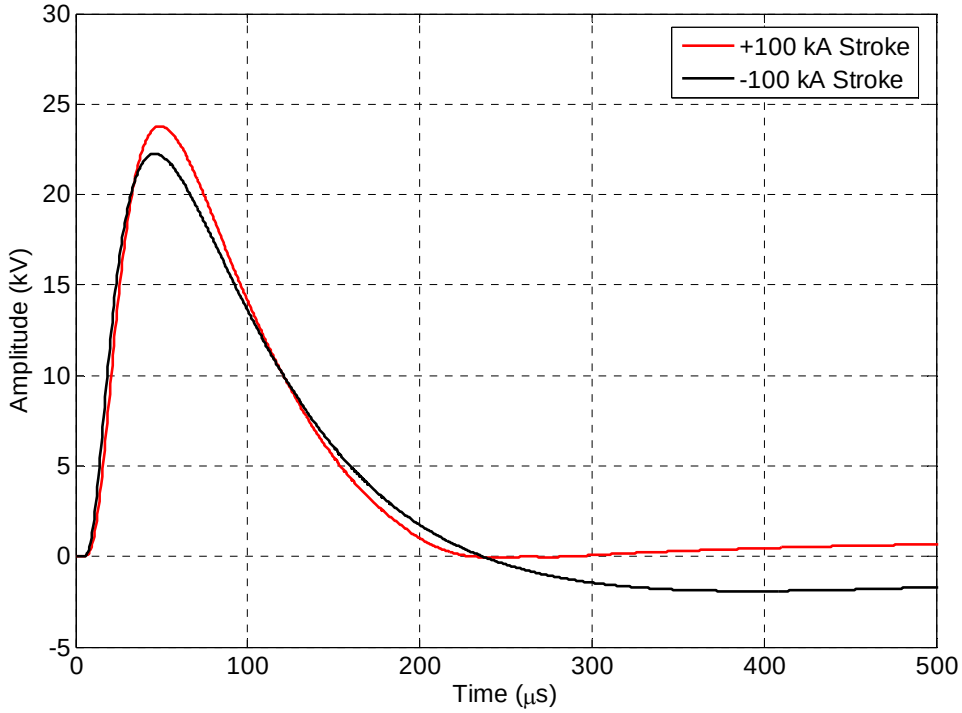

Figure 4-5 Induced voltage pulse on pump cable (using an effective length of 120 m or 394 ft.) due to a hypothetical positive and negative 100 kA cloud-to-ground lightning stroke 100 m from directly above sealed area.

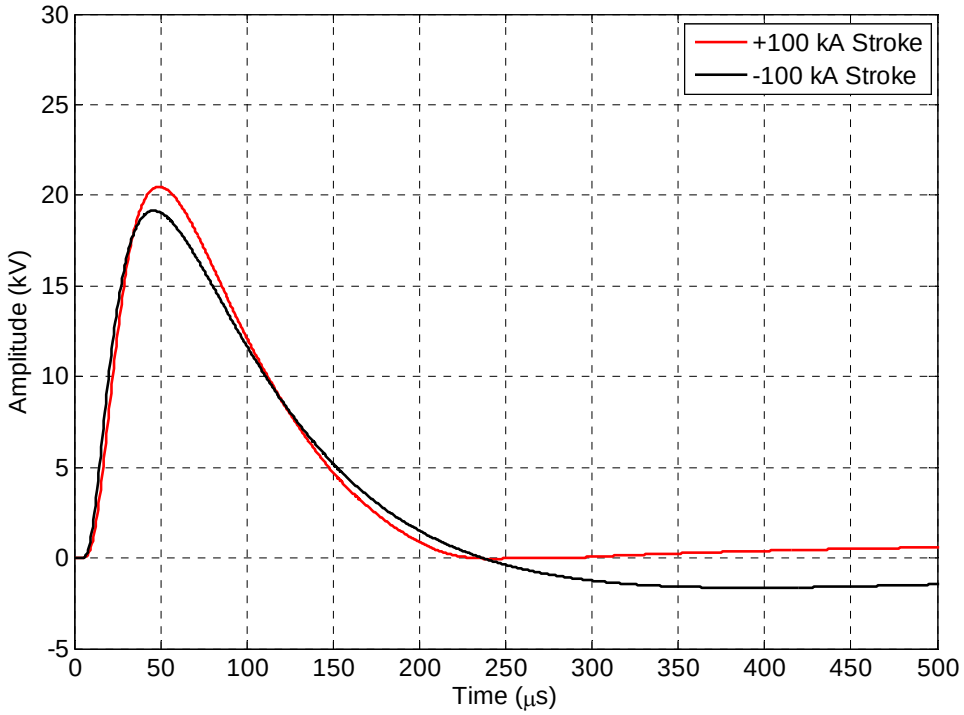

Figure 4-6 Induced voltage pulse on pump cable (length of 61 m or 200 ft.) due to a hypothetical positive and negative 100 kA cloud-to-ground lightning stroke 100 m from directly above sealed area.

4.4 Indirect Drive from a Hypothetical Cloud-to-Ground Stroke with a Current Channel over Sealed Area

If we assume a 100 kA positive cloud-to-ground stroke with a long, low altitude horizontal current channel directly over the sealed area and inline with the pump cable direction at an angle of zero degrees, it could be capable of inducing voltages on the pump cable sufficient to produce electrical arcing. Pump cable (with an effective length of 120 m or 394 ft.) voltages are shown for a positive cloud-to-ground stroke with horizontal current channel at heights (H) of 0, 100 m (328 ft.), 200 m (656 ft.), 500 m (1640 ft.), and 1000 m (3281 ft.) above the surface in Figure 4-7. The maximum voltages from the positive current channel at the heights given are 15.3 kV, 7.2 kV, 4.6 kV, 2.1 kV, and 1.1 kV, respectively. Induced voltages for a negative cloud-to-ground stroke with a current channel directly over the sealed area are shown in Figure 4-9. The maximum voltages from the negative current channel at the heights given are 14.3 kV, 6.7 kV, 4.3 kV, 2 kV, and 1.1 kV, respectively.

Again, since there is concern about the actual length of intact pump cable present at the time of the explosion, analysis was performed on a pump cable with a length of 61 m (200 ft.) to account for the cable piece found closest to the explosion area. The resulting induced voltage pulses on the 61 m (200 ft.) length of pump cable are shown for a positive cloud-to-ground stroke with horizontal current channel at heights (H) of 0, 100 m (328 ft.), 200 m (656 ft.), 500 m (1640 ft.), and 1000 m (3281 ft.) above the surface in Figure 4-8. The maximum voltages from the positive current channel at the heights given are 7.8 kV, 3.7 kV, 2.3 kV, 1.1 kV, and 0.6 kV, respectively. Induced voltages for a negative cloud-to-ground stroke with a current channel directly over the sealed area are shown in Figure 4-10. The maximum voltages from the negative current channel at the heights given are 7.3 kV, 3.4 kV, 2.2 kV, 1 kV, and 0.5 kV, respectively.

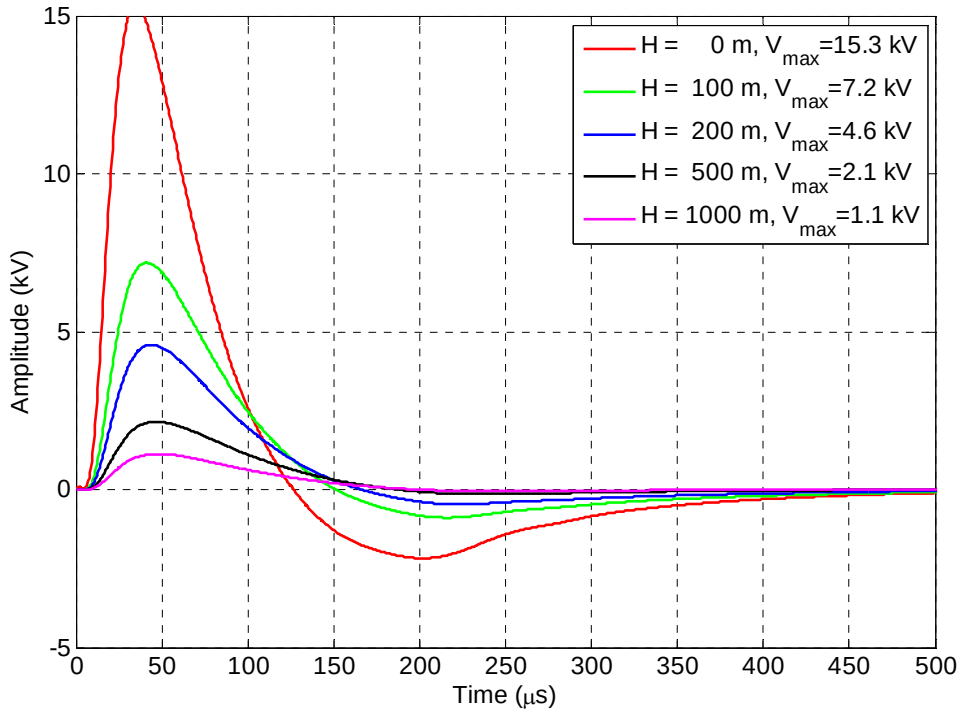

Figure 4-7 Induced Voltage Pulse on Pump Cable (with an effective length of 120 m or 394 ft.) from Hypothetical Horizontal Current Channel from a Cloud-to-Ground +100 kA Stroke, H is distance of the Current Channel above the Ground.

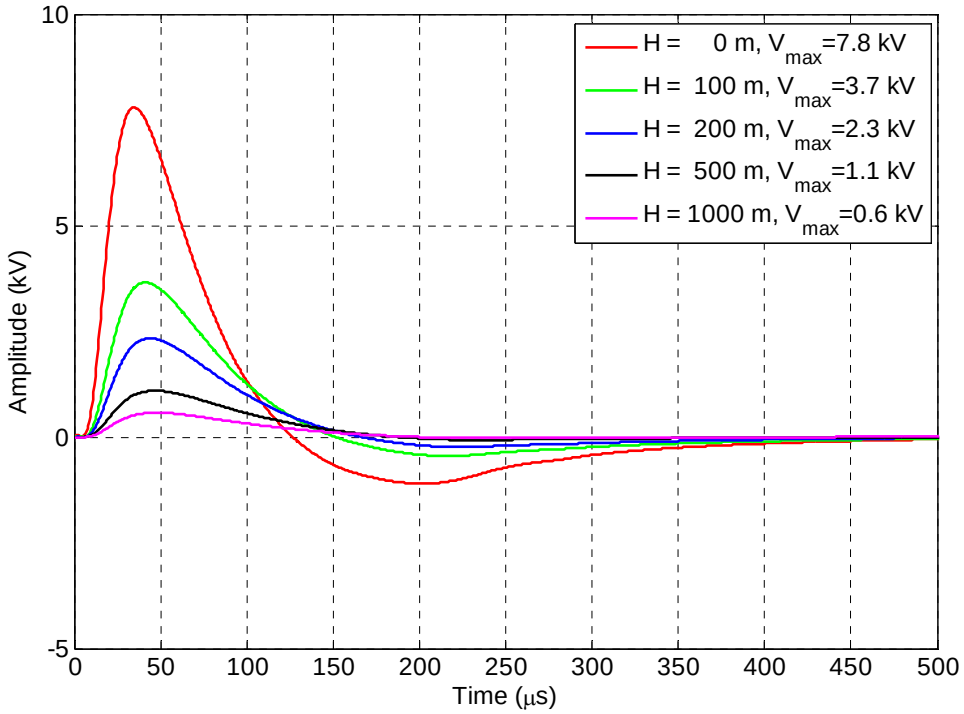

Figure 4-8 Induced Voltage Pulse on Pump Cable (length of 61 m or 200 ft.) from Hypothetical Horizontal Current Channel from a Cloud-to-Ground +100 kA Stroke, H is distance of the Current Channel above the Ground.

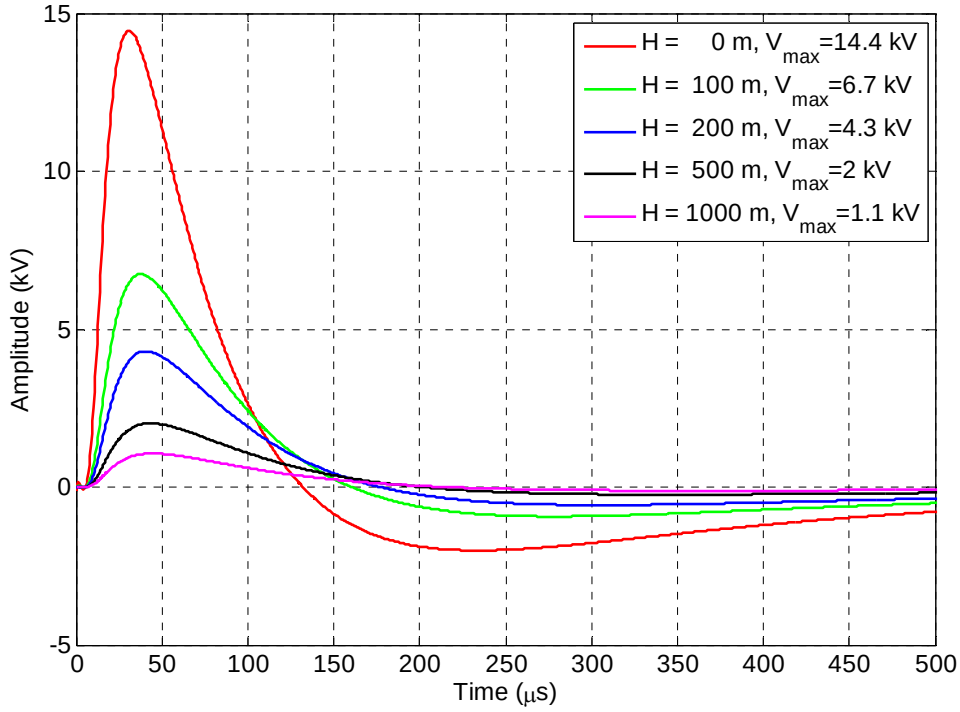

Figure 4-9 Induced Voltage Pulse on Pump Cable (with an effective length of 120 m or 394 ft.) from Hypothetical Horizontal Current Channel from a Cloud-to-Ground -100 kA Stroke, H is distance of the Current Channel above the Ground.

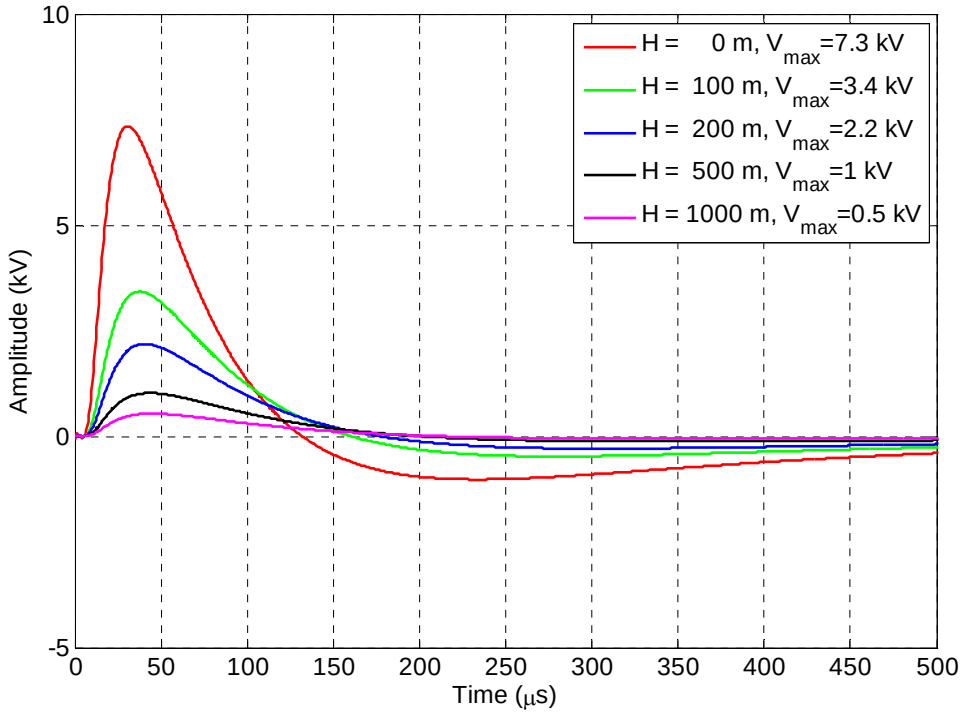

Figure 4-10 Induced Voltage Pulse on Pump Cable (length of 61 m or 200 ft.) from Hypothetical Horizontal Current Channel from a Cloud-to-Ground -100 kA Stroke, H is distance of the Current Channel above the Ground.

5 Conclusions

The conclusions made in this report are specific to the geometry of the Sago mine site where measurements were taken. The results cannot and should not be generalized to any other mining systems.

5.1 Direct Coupling

The current and voltage on metallic penetrations into the mine were calculated given the direct drive transfer functions and a mathematical representation of a positive-polarity, 100 kA peak cloud-to-ground lightning stroke. This calculation assumes that the lightning stroke attaches directly onto the metallic penetration at the entrance to the mine. While there is no evidence that lightning struck the entrance of the mine, this assumption represents the worst-case placement of an attachment for this analysis.

The farthest point into the mine that the direct drive measurements were made was at the entrance to the 2nd Left Parallel, 3,491 m (or 2.17 miles) into the mine, as close to the seal that was breached by the explosion as possible. At this location, the peak currents and voltages calculated at this location given the input of a positive 100 kA peak lightning stroke attaching at the mine entrance are shown in Table 5-1. The voltage was not measured for the trolley communication line because it was insulated and not an exposed conductor.

Table 5-1 Current and voltage at the 2nd Left Switch due to a 100 kA peak, positive cloud-to-ground lightning stroke at the entrance of the mine

Metallic penetration	Current	Voltage
Trolley Communication line	198 A	Not measured
Conveyor Structure	9 A	1 V
Rail	35 A	106 V
Shield of Power Cable[6]	480 A	1 V

The voltages and currents on the conveyor, rail, and shield of the power cable outside the sealed area are incapable of coupling sufficient energy into the sealed area to cause an electrical arc in the sealed area. The voltage on the trolley communication line is not anticipated to be significantly larger than those of the conveyor, rail, and power cable shield.

- *It is highly unlikely that direct drive coupling, even under a worst-case scenario, could have initiated electrical arcing on the cable in the sealed area.*

Because of the substantial initial grounding of metallic penetrations that enter the mine, and because of the multiplicity of grounding points of these systems as they penetrate into the mine, the lightning current is divided sufficiently so that only a relatively small amount of current is injected into the mine near the sealed area. All metallic penetrations were intentionally terminated outside the sealed area. Consequently, the amplitude of current flowing on conductors outside the sealed area is insufficient to generate adequate voltage on the cable inside the sealed area to cause arcing. At low frequencies, the parallel nature of the multiplicity of grounding points is sufficient to divide the lightning current. At higher frequencies, the metallic penetrations can be treated as non-ideal (lossy) transmission lines with periodic grounding that attenuates the high-frequency components of the current even more than lower frequencies. ***Although this coupling mechanism is likely insufficient to cause arcing, the voltage and***

[6] The current and voltage for the shield of the power cable were extrapolated from measurements made at the Power Centers 1, 2, and 3.

current is sufficient to cause electrical shocks to personnel contacting these metallic penetrations, even miles back into the mine.

5.2 Indirect Coupling

Three things are needed to conclude that indirect coupling of lightning energy into the sealed area produced high voltage and an electrical arc that could have been the initiation source of a methane-air explosion in the sealed area of the Sago mine on the morning of January 2, 2006. They are:

- lightning energy propagating from the surface through the overburden into the sealed area;
- an antenna, or receiver (such as a cable), of this energy present in the sealed area; and
- lightning of sufficient magnitude and proximity to the sealed area at the time of the explosion.

The indirect measurements coupled with analytical models discussed in this report confirm that electromagnetic energy with the frequency content of lightning driven on the surface penetrates the ground into the sealed area. Measurements and analyses also confirm that the pump cable acts as a receiver of this energy and is the most likely coupling agent in the sealed area.

Two cloud-to-ground lightning strokes were recorded in the vicinity of the Sago mine within one second of the explosion in the sealed area. Based on the results in this report, these lightning strokes were too far away to have generated enough voltage on the pump cable to create an electrical arc in the sealed area. A thorough, expert analysis of the raw data provided by several lightning detection databases did not uncover evidence to support the detection of another cloud-to-ground stroke in the correct timeframe.

- *It is unlikely that indirect drive from the **vertical components** of the **recorded lightning strokes** (recorded amplitude and location) around the Sago mine could have initiated electrical arcing on the cable present in the sealed area.*

The simultaneous events of recorded lightning strokes and the explosion in the sealed area of the mine; the multiple personal accounts above the sealed area describing simultaneous flash and thunder [21] (indicating extremely close lightning); the lack of data from the lightning detection networks from upward positive lightning initiated from tall structures [20, 35]; the inability of the lightning detection networks to resolve the presence of horizontal lightning arc channels [20, 35]; and the unlikely, but possible, scenario of an undetected cloud-to-ground lightning flash [34] of sufficient magnitude and proximity to the sealed area at the time of the explosion led to the investigation of various hypothetical lightning stroke events. The expected voltage on the abandoned cable was calculated for each scenario using the indirect coupling models developed in this report.

The first hypothetical case explores the possibility of the presence of a horizontal lightning arc channel acting as a source of energy. For this scenario, a 100 kA-peak horizontal arc channel is assumed to be parallel to the pump cable in the sealed area at distances of 100 m (328 ft), 200 m (656 ft), 500 m (1,640 ft), and 1000 m (3,281 ft) above the ground above the sealed area. For a positive-polarity flash, the resultant voltages on the pump cable were 7.2 kV, 4.6 kV, 2.1 kV, and 1.1 kV, respectively. For a negative-polarity flash, the resultant voltages on the pump cable were 6.7 kV, 4.3 kV, 2 kV, and 1.1 kV, respectively. While these calculations use favorable coupling circumstances (high peak arc-channel current and parallel orientation of the arc channel to the pump cable and 120 m cable effective length), this hypothetical scenario presents a reasonable case for high-voltage electrical arcing.

- *It is reasonable to assume that **if** a horizontal, low-altitude arc channel occurred from one of the lightning strokes recorded by the NLDN (or USPLN) or from an unrecorded lightning stroke, it could have initiated electrical arcing on the cable in the sealed area.*

The second hypothetical case explores the possibility of an undetected cloud-to-ground stroke of sufficient magnitude and proximity to the sealed area. Applying a 100 kA-peak, cloud-to-ground stroke of optimum orientation to the pump cable (61 m length) within 100 m (328 ft) of the sealed area, the results are peak voltages on the pump cable of 19.1 kV for a negative-polarity flash, and 20.5 kV for a positive-polarity flash. For the same conditions, the induced voltage decreases as distance of a lightning stroke from the sealed area increases.

- *It is reasonable to assume that **if** an average or above average cloud-to-ground lightning stroke occurred above the sealed area at Sago, that it could initiate electrical arcing on the cable in the sealed area.*

Recent discussions led to a third hypothetical case, which is not examined in detail in the report, of upward-going positive lightning initiating from tall structures. Four tall communication towers (heights of approximately 200 ft or less) are within approximately 1 mile of the sealed area, the closest being about 0.5 miles. If we hypothesize an upward-going positive lightning stroke from the closest tower, (recalling that these type of events are not typically captured by the current lightning detection networks), the induced voltage on the pump cable would be 763 V.

The conclusions of this report are that lightning of sufficient magnitude and proximity to the sealed area would create high voltage on the pump cable to create an electrical arc. The simultaneity in time of recorded lightning strokes and the explosion occurring is very strong evidence of cause and effect. Furthermore, eyewitness accounts of simultaneous lightning and thunder at the time of the explosion, plus the analysis of credible hypothetical scenarios which cannot be confirmed by lightning detection networks, lend credibility to the idea that lightning-induced electrical arcing was not only plausible, but highly likely.

6 Recommendations

The results of this short-term project demonstrate the usefulness of transfer function measurement techniques and analytical modeling to evaluate lightning effects in mining environments. The effects described in this report are significant. A more comprehensive research and development program should be conducted to expand on this work to extend this research for use in other underground coal mining operations. The research program would be conducted using similar transfer function measurement techniques, experiments at other sites with rocket-triggered and natural lightning, and analytical and computational modeling using validated state-of-the-art codes adapted for this application. Once completed, it is reasonable to expect that mitigation techniques and safety standards could be developed to secure coal mining systems from future lightning threats.

7 References

1. Checca, Elio and D. R. Zuchelli, *Lightning Strikes and Mine Explosions*, Proceedings of 7th US Mine Ventilation Symposium, June 5-7, 1995, pp 245-250.
2. Checca, Elio L., *Investigative Report No. C-042094–Oak Grove Mine Methane Gas Ignition*, U. S. Department of Labor, Mine Safety and Health Administration, Pittsburg Safety and Health Technology Center, Pittsburg, PA, April 6-12, 1994.
3. Scott, Doniece S., E. Larry Checca, Clete R. Stephan, and Mark J. Schultz, *Accident Investigation Report (Underground Coal Mine) Non-Injury Methane Explosion, Oak Grove Mine (I.D. No. 01-00851)*, U. S. Department of Labor, Mine Safety and Health Administration, District 11, January 29, 1996.
4. Scott, Doniece S., and Clete R. Stephan, *Accident Investigation Report (Underground Coal Mine) Non-Injury Methane Explosion, Oak Grove Mine (I.D. No. 01-00851)*, U. S. Department of Labor, Mine Safety and Health Administration, District 11, July 11, 1997.
5. Morris, Marvin E., Richard J. Fisher, George H. Schnetzer, Kimball O. Merewether, and Roy E. Jorgenson, *Rocket-Triggered Lightning Studies for the Protection of Critical Assets,* M. E. Morris *et al.*, IEEE Transactions on Industry Applications, Vol. 30, No. 3, pp 791-804, May/June 1994 (1994 Prize Paper Award from IEEE Power Systems Society).
6. Chen, Kenneth C., Kimball O. Merewether, Tom Y. T. Lin, andParris Holmes, Jr., *Final Report: U12g Tunnel Lightning Evaluation*, Sandia National Laboratories Report, SAND2004-1619, Sandia Nationa Laboratories, Albuquerque, NM, April 2004.
7. Dinallo, Michael A., and Roy E. Jorgenson, *Recommended Lightning Protection Practices for Operations Being Conducted in G-Tunnel at the Nevada Test Site*, Sandia National Laboratories Report SAND2006-1049P, Sandia National Laboratories, Albuquerque, NM, February 2006.
8. Novak, Thomas, and Thomas J. Fisher, *Lightning Propagation Through the Earth and Its Potential for Methane Ignitions in Abandoned Areas of Underground Coal Mines*, IEEE Transactions on Industrial Applications, Vol. 37, No. 6, Nov/Dec 2001, pp1555-1562.
9. Sacks, H. K., and Thomas Novak, *Corona Discharge Initiated Mine Explosion*, IEEE Transactions on Industrial Applications, Vol. 41, Sept/Oct 2005.
10. Liu, Jian-Bang, Paul D. Ronney, and Martin A. Gundersen, *Premixed Flame Ignition by Transient Plasma Discharges*,
11. Ronney, Paul D., *Technical Progress Report on Corona Discharge Initiation*, University of Southern Californa, Dept. of Aerospace and Mechanical Engineering, Los Angeles, CA, Sept 12, 2003.
12. Berger, K., *Protection of Underground Blasting* Operations, edited by R. H. Golde, in. *Lightning – Vol 2, Lightning Protection*, Academic Press, New York, NY, 1977, pp633-658.
13. Geldenhuys, H. J., A. J. Eriksson, W. B. Jackson, and J. B. Raath, *Research into Lightning-Related Incidents in Shallow South African Coal Mines*, Proceedings of the 21st Internal Conference on Safety in Mines Research, 1985, pp775-782.
14. Golledge, P., *Sources and Facility of Ignition in Coal Mines*, *in Ignitions, Explosions, and Fires*, 1981, pp2-1–2-12.
15. Geldenhuys, H. J., *The Measurement of Underground Lightning-Induced Surges in a Colliery*, Symposium on Safety in Coal Mining, South Africa National Electrical Engineering Research, Pretoria, South Africa, October 5-8, 1987..
16. Zeh, K. A., *Lightning and Safety in Shallow Coal Mines*, 23rd International Conference of Safety in Mines, 1989, pp691-700.
17. Staff-Mining Research, *Methane Control in Eastern U. S. Coal Mines*, Proceedings of the Symposium of the Bureau of Mines/Industry Technology Transfer Seminar, Morgantown, WV, May 30-31, 1973.

18. Insulating materials for design and engineering practice, John Wiley and Sons, 1962, Library of Congress Catalog Card Number 62-17460.
19. Rucker, Dale, Marc Levitt, Shawn Calendine, John Fleming, and Robert McGill, *Geophysical Survey for the Old 2 Left Section of the Sago Mine, Buckhannon, WV,* hydroGEOPHYSICS, Inc., Tucson, AZ, August 18, 2006.
20. Martin A. Uman, University of Florida (private communication).
21. West Virginia Office of Miners' Health, Safety, and Training, *Report of Investigation into the Sago Mine Explosion which occurred January 2, 2006*, Upshur Co. West Virginia, December 11, 2006.
22. Fisher, R. J., G. H. Schnetzer and M. E. Morris, *Measured Fields and Earth Potentials at 10 And 20 Meters from the Base of Triggered Lightning Channels*, 22nd International Conference on Lightning Protection, Budapest, Hungary, September 19-23, 1994.
23. Schoene, J., M.A. Uman, V.A. Rakov, V. Kodali, K.J. Rambo, G.H. Schnetzer, *Statistical Characteristics of the Electric and Magnetic Fields and Their Time Derivatives 15 m and 30 m from Triggered Lightning*, J. Geophys, Res, Vol. 108, No. D6, 4192, doi:10.1029/2002JD002698, 2003.
24. King, Ronold W. P., *Transmission-line Theory*, Dover, New York, NY, 1965.
25. Warne, Larry K., and Kenneth C. Chen, *Long Line Coupling Models*, SAND2004-0872, Sandia National Laboratories Report, Sandia National Laboratories, Albuquerque, NM, March 2004.
26. Smythe, William R., *Static and Dynamic Electricity*, A Summa Book, Albuquerque, NM, 1989.
27. Wait, James R., *Electromagnetic Waves in Stratified Media*, The Macmillan Company, New York, NY, 1962
28. Tegopoulis, J. A., and E. E. Kriezis, *Eddy Currents in Linear Conducting Media*, Elsevier, New York, NY, 1985.
29. Stoll, Richard L., *The Analysis of Eddy Currents*, Clarendon Press, Oxford, UK, 1974.
30. Krawczyk, A., and J. A. Tegopoulis, *Numerical Modeling of Eddy Currents*, Clarendon Press, Oxford, UK, 1993.
31. Kaufman, A. A., and P. Hoekstra, *Electromagnetic Soundings*, Elsevier, New York, NY, 2001.
32. Cianos, N., and Pierce, E. T., *A Ground-Lightning Environment for Engineering Usage*, Technical Report 1, SRI Project 1834, August 1972.
33. Rakov, Vladimir A., and Martin A. Uman, *Lightning*, Lightning Physics and Effects, Cambridge University Press, New York, NY, 2003.
34. Cummins, Kenneth L., et. al., *The U.S. National Lightning Detection Network: Post-Upgrade Status*, Proceedings of the Second Conference of Meteorological Applications of Lightning Data, 86th AMS Annual Meeting, Atlanta, GA, 29 January - 2 February 2006. American Meteorological Society.
35. E. Philip Krider, University of Arizona (private communication and memorandum, see Appendix E).
36. Phillips, Robert, *Resistivity Measurements*, personal communications from Robert Phillips

8 Appendix A — Analytical and Numerical Models for Voltage and Current Used to Determine Electromagnetic Coupling into the Sago Mine

Marvin E. Morris
Consultant, Sandia National Laboratories, Department 1652

February 11, 2007

Abstract

The purpose of this appendix is to document the relevant analytical models to be used to predict the voltages and currents produced in the Sago mine by current drive sources used to simulate the effects of a lightning stroke attachment near the mine or on the surface of the earth above the mine. Also considered are horizontal arcs above the surface of the mine.

8.1 Introduction

The purpose of this appendix is to document the relevant analytical models to be used to predict the voltages and currents produced in the Sago mine by current drive sources used to simulate the effects of a lightning stroke attachment near the mine or on the surface of the earth above the mine. Subsequent measurements corresponding to these models will be used to identify coupling paths and quantify coupling amplitudes of the lightning energy into the sealed area of the mine where the explosion was thought to have been initiated. The initial section of the appendix documents the DC drive current models for both a homogeneous half-space and for a two layer half-space. The next section of the appendix documents the eddy current models for an infinite length horizontal drive wire over both a homogeneous half-space and a two layer half-space. The next section documents the eddy current coupling into a homogeneous half-space from a uniform magnetic field at the surface. The final section of the appendix references the literature for eddy current models for an infinitesimal length and a finite length horizontal wire over both a homogeneous half-space and a two layer half-space. Computer codes have been implemented in Fortran and Mathematica to calculate the resulting potentials and fields and the resulting voltages generated within the earth.

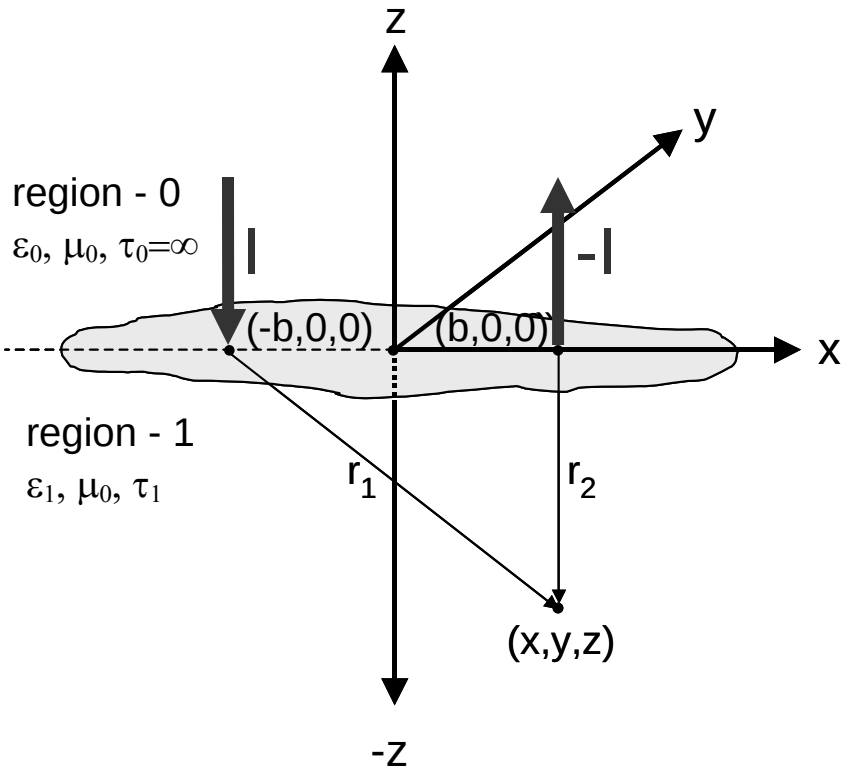

Figure 8-1 DC Current Drive with Homogeneous Half-Space Geometry.

8.2 Static Current Drive Models

The simplest model for current coupling into a conductive earth is the DC conduction of current into a conductive half-space. The models for this are well known.

8.2.1 Homogeneous Half-Space

The DC or very low-frequency situation to be modeled is shown in Figure 8-1.

Current I is driven into the conductive half-space at Cartesian coordinate (-b, 0, 0) and the current is removed at Cartesian coordinate (b, 0, 0). The upper half-space, region-0, has infinite resistivity τ_0 and the lower half-space, region-1, has resistivity τ_1. From simple considerations, *V (x, y, z)*, the potential at Cartesian coordinate (x, y, z) with respect to infinity, is given by

$$V(x,y,z)=\frac{\tau_1 I}{2\pi}\left(\frac{1}{\sqrt{(x+b)^2+y^2+z^2}}-\frac{1}{\sqrt{(x-b)^2+y^2+z^2}}\right)$$

The difference in potential between two points can be calculated by taking the difference of the potentials at the two points calculated with the above formula.

The electric field at point (x, y, z) is easily calculated from

$$\bar{E}(x,y,z) = -\nabla V(x,y,z)$$

and calculating the x-component of interest

$$E_x(x,y,z) = -\frac{\partial}{\partial x}V(x,y,z) = \frac{\tau_1 I}{2\pi}\left(\frac{(x+b)}{\left[(x+b)^2+y^2+z^2\right]^{\frac{3}{2}}} - \frac{(x-b)}{\left[(x-b)^2+y^2+z^2\right]^{\frac{3}{2}}}\right)$$

8.2.2 Two Layer Half-Space

Because there is often a less resistive layer of topsoil above the more resistive layer, which includes the mine, it is necessary to generalize the above homogenous half-space model to a two layer half-space model. The DC or very low-frequency situation to be modeled is shown in Figure 8-2.

Current I is driven into the conductive half-space at Cartesian coordinate (-b, 0, 0) and the current is removed at Cartesian coordinate (b, 0, 0). The upper half-space, region-0 has infinite resistivity τ_0 and region-1, the layer of thickness, a, has resistivity τ_1. The infinitely thick layer region-2 has resistivity τ_2. From more complicated considerations, V (x, y, z), the potential at Cartesian coordinate (x, y, z) with respect to infinity, is given by

$$V(x,y,z) = \frac{I}{2\pi}\left(\frac{2\tau_1\tau_2}{\tau_1+\tau_2}\right)\left(\frac{1}{\sqrt{(x+b)^2+y^2+z^2}} - \frac{1}{\sqrt{(x-b)^2+y^2+z^2}}\right)$$

in region-2.

The difference in potential between two points can be calculated by taking the difference of the potentials at the two points calculated with the above formula.

The electric field at point (x, y, z)is easily calculated from

$$\bar{E}(x,y,z) = -\nabla V(x,y,z)$$

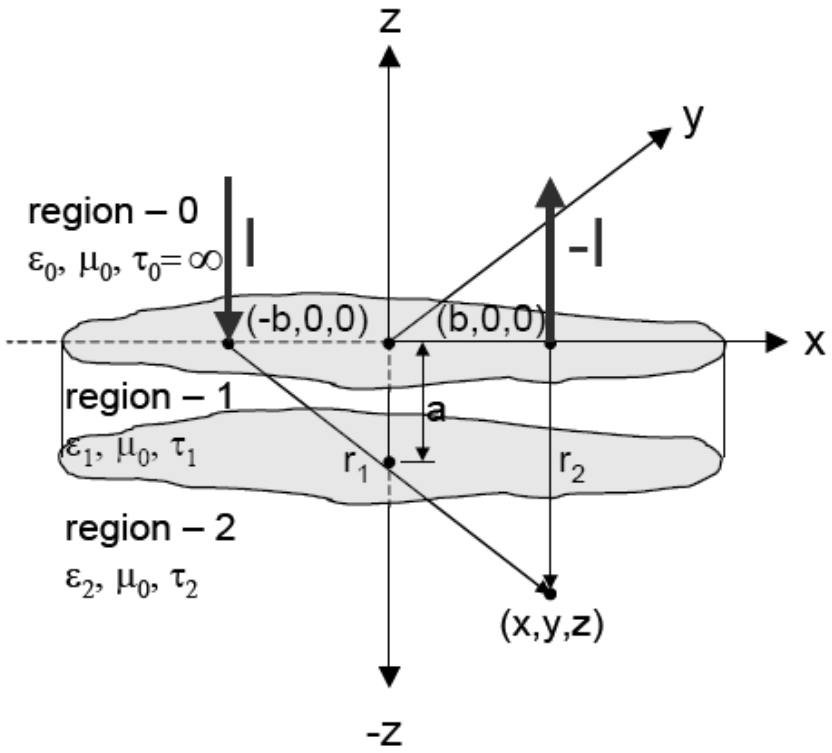

Figure 8-2 DC Current Drive with Two Layer Half-Space Geometry.

and calculating the x-component of interest

$$E_x(x,y,z) = -\frac{\partial}{\partial x}V(x,y,z)$$

$$= \frac{I}{2\pi}\left(\frac{2\tau_1\tau_2}{\tau_1+\tau_2}\right)\left(\frac{(x+b)}{\left[(x+b)^2+y^2+z^2\right]^{\frac{3}{2}}} - \frac{(x-b)}{\left[(x-b)^2+y^2+z^2\right]^{\frac{3}{2}}}\right)$$

8.3 Eddy Current, Infinite Horizontal Drive Wire Models

The next obvious generalization of the above model is to make the current injected into the earth time varying, say $I = I_0 e^{i\omega t}\hat{x}$ and to neglect displacement current. This generalization turns out to be more difficult than one might think because the current in the earth depends on the geometry of the current path above the earth. A simpler model that corresponds the electromagnetic coupling below a long, horizontal wire grounded at both ends and driven by a voltage source can, however, be developed.

8.3.1 Homogeneous Half-Space

The current drive geometry of an infinitely long, horizontal wire placed a distance, h, above a conductive half-space is shown on the left side of Figure 8-3. A side view is shown on the right side of Figure 8-3.

The current drive is harmonically time-varying and directed along the x - axis at height, h, above it. The upper half-space has permittivity $\varepsilon_0$and infinite resistivity and the lower half-space has permittivity ε_1 and resistivity, τ_1. Both regions have free space permeability, μ_0.

If one neglects displacement current and relates current density, $i_x(y, z)$, and electric field, $E_x(y, z)$, in region-1 through, $E_x(y,z) = \tau_1 i_x(y,z)$, then the current density in the lower half-space, region-1, can be determined to be

$$i_x(y,z) = -\frac{i\omega\mu_0 I}{\pi\tau_1}\int_0^\infty \frac{e^{qz}e^{-uh}}{u+q}\cos uydu = \frac{i2}{\pi}\frac{I}{\delta_1^2}\int_0^\infty \frac{e^{qz}e^{-uh}}{u+q}\cos uydu$$

$$E_x(y,z) = \tau_1 i_x(y,z) = \frac{ik\varsigma_0}{\pi}\int_0^\infty \frac{e^{qz}e^{-uh}}{u+q}\cos uydu$$

where

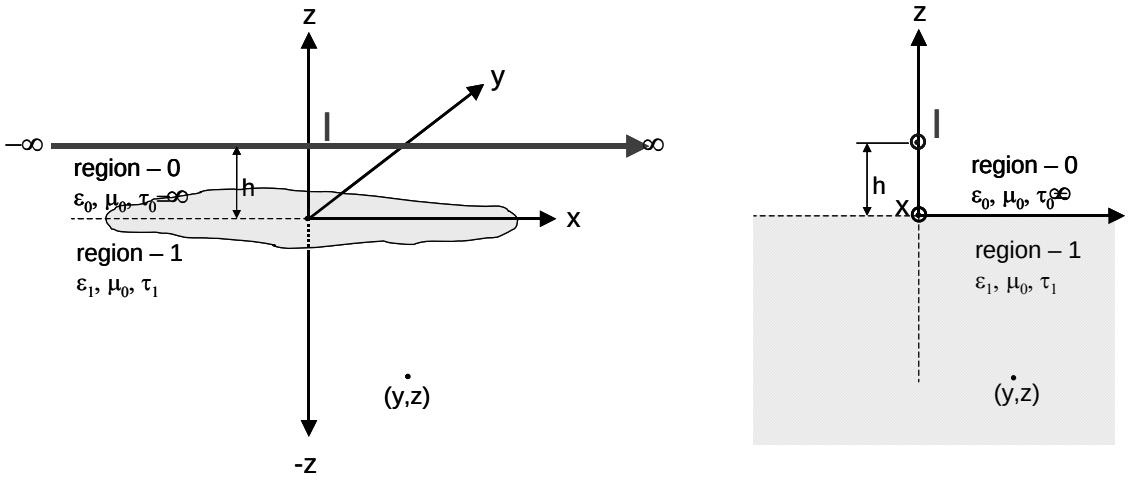

Figure 8-3 Infinite Horizontal Current Drive, Eddy Current Coupling Geometry.

$$k = \omega\sqrt{\mu_0\varepsilon_0}$$

$$q = \sqrt{u^2 + ip^2}$$

$$p^2 = \frac{\omega\mu_0}{\tau_1} = \frac{2}{\delta_1^2}$$

$$\delta_1 = \sqrt{\frac{2\tau_1}{\omega\mu_0}}$$

This or similar expressions are given in [A1-A3].

Note that the skin depth, $\delta_1 = \sqrt{\frac{2\tau_1}{\omega\mu_0}}$, plays an important role as a parameter in all diffusion coupling calculations. For convenience it is plotted for various values of resistivity.

Integrating this result for y =0 and for h =0 yields the closed form result:

$$E_x(y=0,z) = i_x(y,z) = \frac{\tau_1 I}{\pi}\frac{1}{\delta_1^2}\left\{\left[(1+i)\frac{1}{\left(\frac{z}{\delta_1}\right)} + \frac{1}{\left(\frac{z}{\delta_1}\right)^2}\right] e^{-(1+i)\frac{z}{\delta_1}} - i2K_0\left((1+i)\frac{z}{\delta_1}\right) - (1+i)\frac{1}{\left(\frac{z}{\delta_1}\right)}K_1\left((1+i)\frac{z}{\delta_1}\right)\right\}$$

where K_0 and K_1 are modified Bessel Functions.

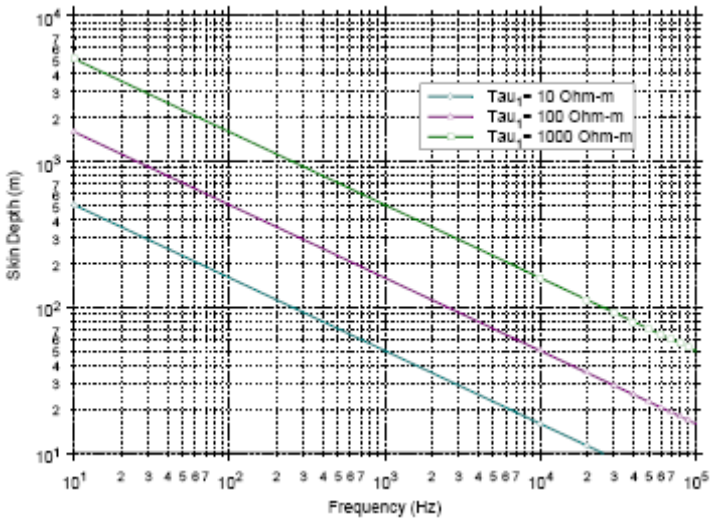

Figure 8-4 Skin Depth as a Function of Frequency for Resisitivities, τ_1 = 10, 100, 1000 Ω-m.

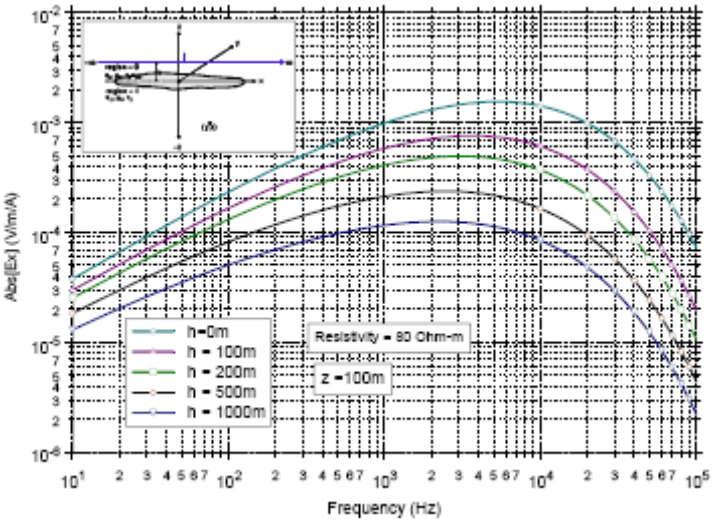

Figure 8-5 Amplitude of Electric Field from a Line Source Placed at Heights, h = 0m, 100m, 200m, 500m, and 1000m, at z = 100m with τ_1 = 80 Ω-m.

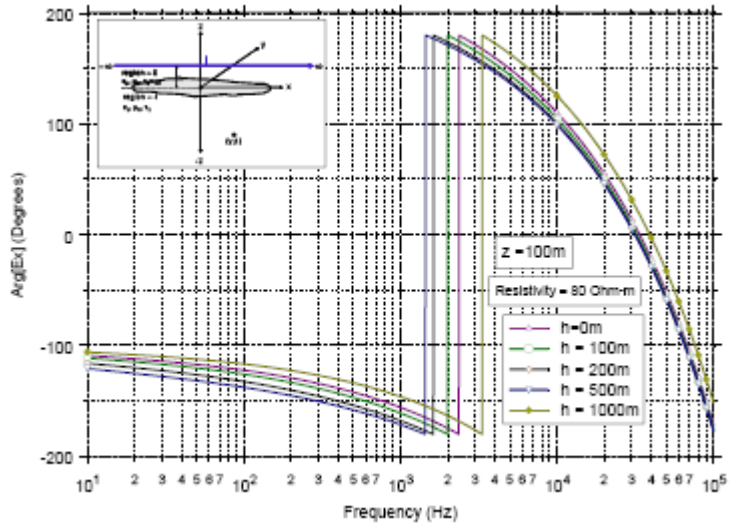

Figure 8-6 Phase of Electric Field from a Line Source Placed at Heights, h = 0m, 100m, 200m, 500m, and 1000m, at z = 100m with τ_1 = 80 Ω-m.

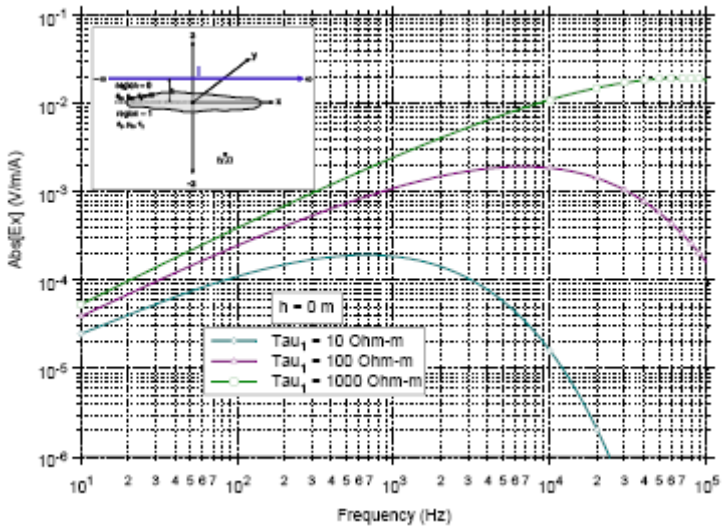

Figure 8-7 Amplitude of the Electric Field at z = 100m from a Line Source Placed the Surface of a Homogeneous Half-Space with τ_1 = 10, 100, 1000 Ω-m.

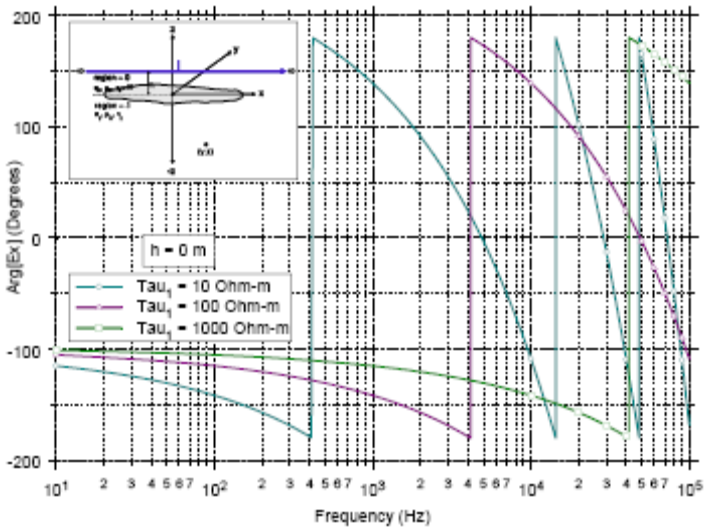

Figure 8-8 Phase of the Electric Field at z = 100m from a Line Source Placed the Surface of a Homogeneous Half-Space with τ_1 =10, 100, 1000 Ω-m

8.3.2 Two Layer Half-Space

The current drive geometry of an infinitely long, horizontal wire placed a distance, h, above a conductive half-space is shown on the left side of Figure 8-9. A side view is shown on the right side of Figure 8-9.

The current drive is harmonically time varying and directed along the x - axis at height, h, above it. The upper half-space has permittivity $\varepsilon_0$and infinite resistivity, the layer of thickness h_1 has permittivity $\varepsilon_1$and resistivity, τ_1, and the lower region has permittivity $\varepsilon_2$and resistivity, τ_2. All regions have free space permeability, μ_0.

If one neglects displacement current and relates current density, $i_x(y, z)$, and electric field, $E_x(y, z)$, in region-2 through, $E_x(y, z) = \tau_2 i_x(y, z)$, then the current density in the lower half-space, region-2, then for h =0 and y =0 can be determined to be

$$E_x(y=0,z) = -\frac{i4\tau_2 I}{\pi}\frac{1}{\delta_2^2}\int_0^\infty \frac{u_1 e^{u_2 h_1}}{(u+u_1)(u_1+u_2)e^{u_1 h_1}+(u-u_1)(u_1-u_2)e^{-u_1 h_1}} e^{-u_2 z}\,du$$

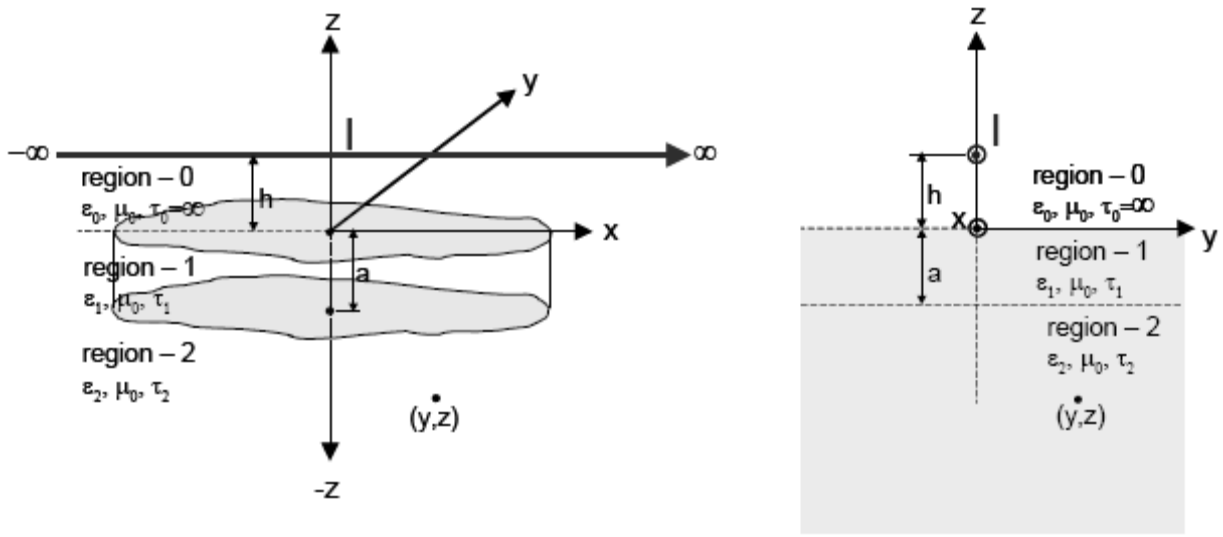

Figure 8-9 Infinite Horizontal Current Drive, Two-Layered, Eddy Current Coupling Geometry.

$$u_1 = \sqrt{u^2 + ip_1^2}$$

$$p_1^2 = \frac{\omega\mu_0}{\tau_1} = \frac{2}{\delta_1^2}$$

$$\delta_1 = \sqrt{\frac{2\tau_1}{\omega\mu_0}}$$

$$u_2 = \sqrt{u^2 + ip_2^2}$$

$$p_2^2 = \frac{\omega\mu_0}{\tau_2} = \frac{2}{\delta_2^2}$$

$$\delta_2 = \sqrt{\frac{2\tau_2}{\omega\mu_0}}$$

Similar expressions are developed in [A1-A3], but I am aware of no closed form expression for the above integral. The formula must be integrated numerically to obtain results. Note that the variable of integration is on the positive real axis and that no singularities are present on the positive real axis. As the skin depths get longer and longer, the branch cuts get closer to the real axis. If we consider the asymptotic behavior of the integrand as u→∞, then

$$E_x(y,z) = -\frac{i4\tau_2 I}{\pi}\frac{1}{\delta_2^2}\left[\begin{array}{l}\displaystyle\int_0^c \frac{u_1 e^{u_2 h_1}}{(u+u_1)(u_1+u_2)e^{u_1 h_1} + (u-u_1)(u_1-u_2)e^{-u_1 h_1}} e^{-u_2 z}\,du \\ \displaystyle +\frac{1}{4}E_1(cz) + \frac{i}{4\delta_1^2}(2h_1 - z)\frac{1}{c}E_2(cz)\end{array}\right]$$

to the first two terms in $\frac{e^{-uz}}{u}$ and $\frac{e^{-uz}}{u^2}$ where c » max[δ_1, δ_2].

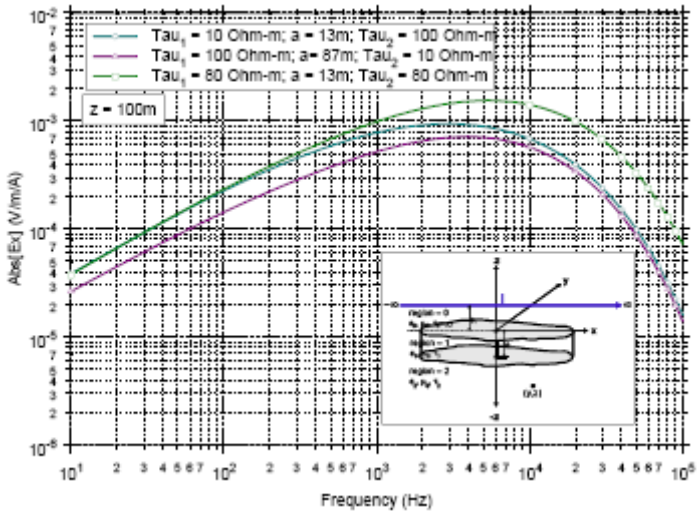

Figure 8-10 Amplitude of the Electric Field at z = 100m from a Line Source at the Surface of a Two-Layered Half-Space.

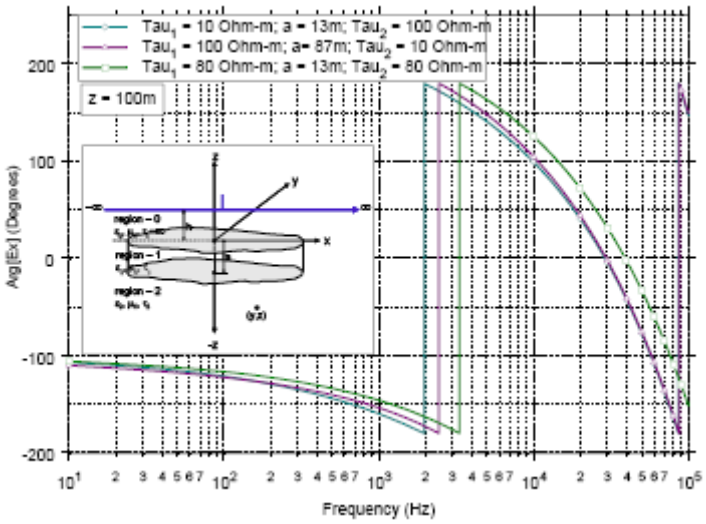

Figure 8-11 Phase of the Electric Field at z = 100m from a Line Source at the Surface of a Two-Layered Half-Space.

8.4 Eddy Current Coupling into Homogeneous Half-Space from Uniform Magnetic Field at Surface

If we consider the geometry shown in Figure 8-12,

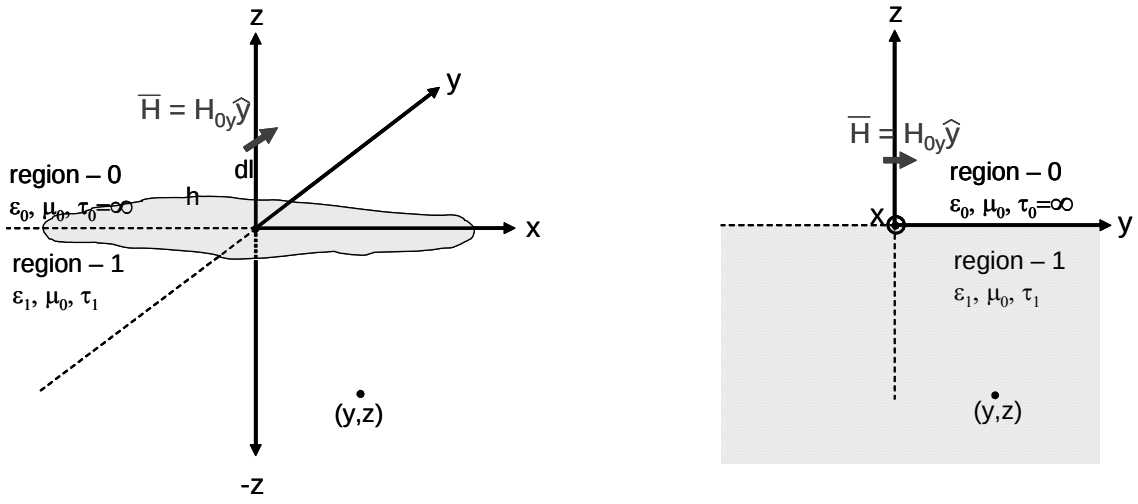

Figure 8-12 Geometry for Eddy Current Field Calculations in Homogenous Half-Space Driven by Uniform Magnetic Field at the Surface.

with uniform harmonic magnetic field with time harmonic variation $e^{i\omega t}, \bar{H} = H_{0y}\hat{y}$, in the y-direction, then the electromagnetic field equations, neglecting displacement current can be developed directly from Maxwell's equations.

$$\frac{\partial j_x(z)}{\partial y} = i\omega\sigma_1\mu_0 H_y(z)$$

where $j_x(z)$ is the current density in region-1 and $H_y(z)$ is the magnetic field in region-1. The second equation is given by

$$\frac{\partial H_y(z)}{\partial y} = j_x(z)$$

Substituting one equation into the other yields

$$\frac{\partial^2 H_y(z)}{\partial y^2} = \alpha^2 H_y(z)$$

where

$$\alpha = \frac{(1+i)}{\delta_1}$$

$$\delta_1 = \sqrt{\frac{2}{\omega \mu_0 \sigma_1}}$$

where δ_1 is the skin depth in region-1. The general solution of the above equation is

$$H_y(z) = K_1 e^{\alpha z} + K_2 e^{-\alpha z}$$

Choosing the properly decaying solution as z → -∞, and using the boundary condition at the surface of $H_y(0)=H_{0y}$

$$H_y(z) = H_{0y} e^{\alpha z}$$

$$j_x(z) = \frac{\partial H_y(z)}{\partial y}$$

$$= \alpha H_{0y} e^{\alpha z}$$

Because

$$E_x(z) = \tau_1 j_x(z)$$

where

$$\tau_1 = \frac{1}{\sigma_1}$$

$$E_x(z) = \tau_1 \alpha H_{0y} e^{\alpha z}$$

is the only component of the electric field in region-1.

Because a surface current density is related to the magnetic field immediately below a perfect conductor by the relationship

$$j_{0x} = -2\hat{n} \times H_{0y}$$

the above solution could also be considered to be the electric field of a homogeneous half-space excited by a uniform x-directed current flowing on the bottom surface of a perfectly conducting sheet on the surface of the homogeneous half-space, but electrically isolated from it. The exciting current on the sheet to produce the field in the equations would be

$$j_{0x} = -2H_{0y}$$

in the x-direction, or alternatively

$$H_{0y} = -\frac{1}{2} j_{0x}$$

in the above formulas.

8.5 Eddy Current, Infinitesimal and Finite Length Horizontal Drive Wire Models

Eddy current models for infinitesimal and finite length horizontal drive wires over a homogeneous half-space have been developed in [A4-A7]. The x-directed electric field immediately below the wire can be expressed in closed form for the infinitesimal length dipole [A7]. Expressions for the electric field in a two-layer half-space excited by an infinitesimal horizontal drive wire have been developed in [A8]. These models are quite complicated and were not further developed for this program because of lack of time and resources.

8.6 References for Appendix A

A1. Wait, James R., *Electromagnetic Waves in Stratified Media*, The Macmillan Company, New York, NY, 1962.

A2. Tegopoulis, J. A., and E. E. Kriezis, *Eddy Currents in Linear Conducting Media*, Elsevier, New York, NY, 1985.

A3. Kaufman, A. A., and P. Hoekstra, *Electromagnetic Soundings*, Elsevier, New York, NY, 2001.

A4. Goldstein, A. A., and D. W. Strangway, *Audio-frequency Magnetotellurics with a Grounded Electric Dipole Source*, Geophics, Vol. 40, December 18, 1974, pp669-683.

A5. Sommerfeld, Arnold, *Electromagnetic Waves Near Wires*, Wied. Annalen, Vol 67, 1899, pp233-290.

A6. Sommerfeld, Arnold, *Partial Differential Equations in Physics, Lectures on Theoretical Physics, Vol. VI*, Academic Press, New York, NY, 1964.

A7. King, Ronold W. P., Margaret Owens, and Tai Tsun Wu, *Lateral Electromagnetic Waves*, Springer-Verlag, New York, NY, 1992.

A8. Riordan, John, and Erling D. Sunde, *Mutual Impedance of Grounded Wires for Horizontally Stratified Two-Layer Earth*, Bell System Technical Journal, Vol 12, pp162-177, 1933.

9 Appendix B –Calibration Documentation of Measurement Equipment

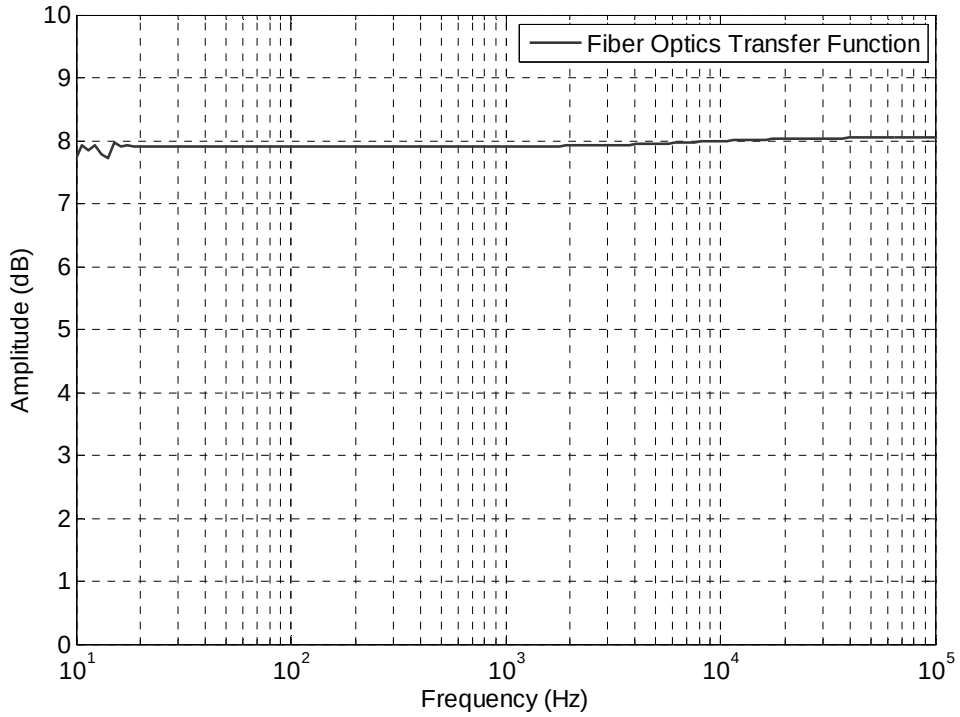

Figure 9-1 Calibration Frequency Response of Fiber-optic Transmitter/Receiver Pair.

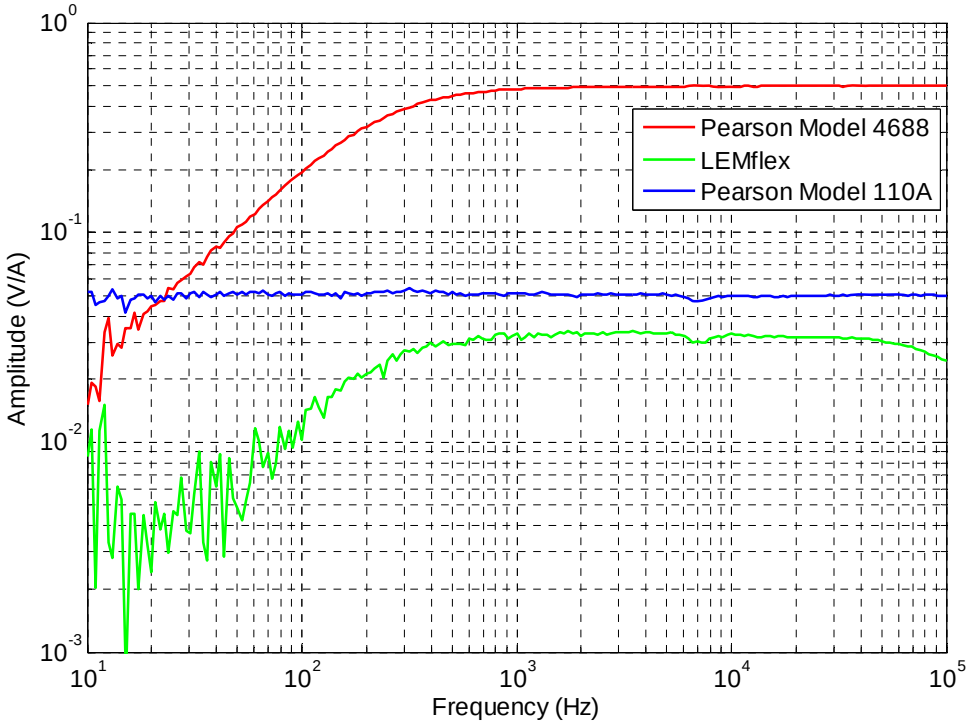

Figure 9-2 Calibration Frequency Response of Current Probes used.

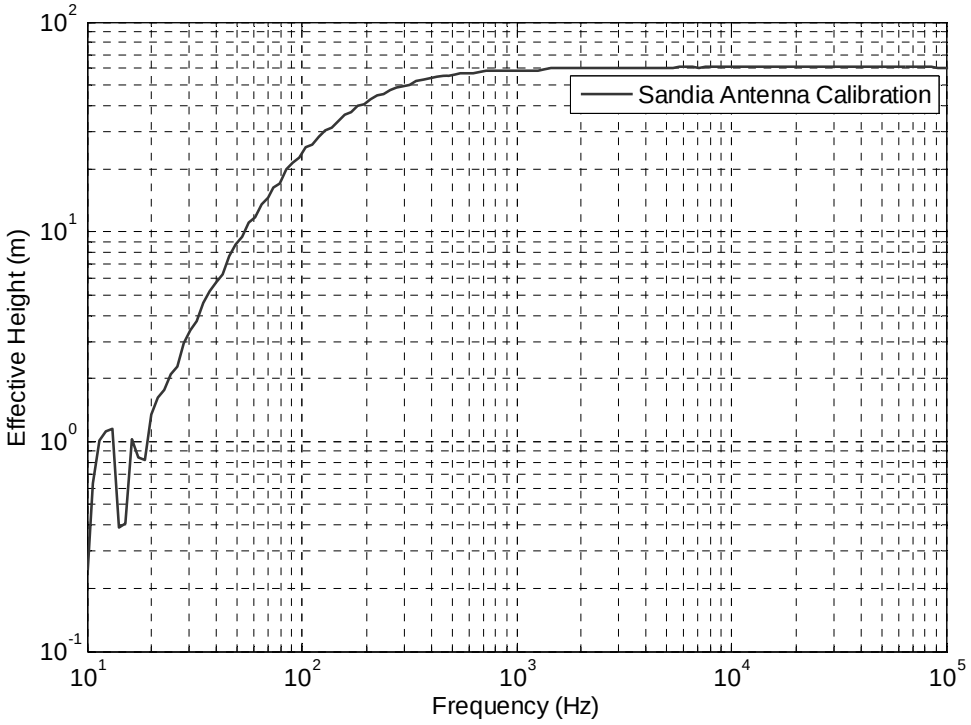

Figure 9-3 Calibration Frequency Response of Sandia Dipole Antenna.

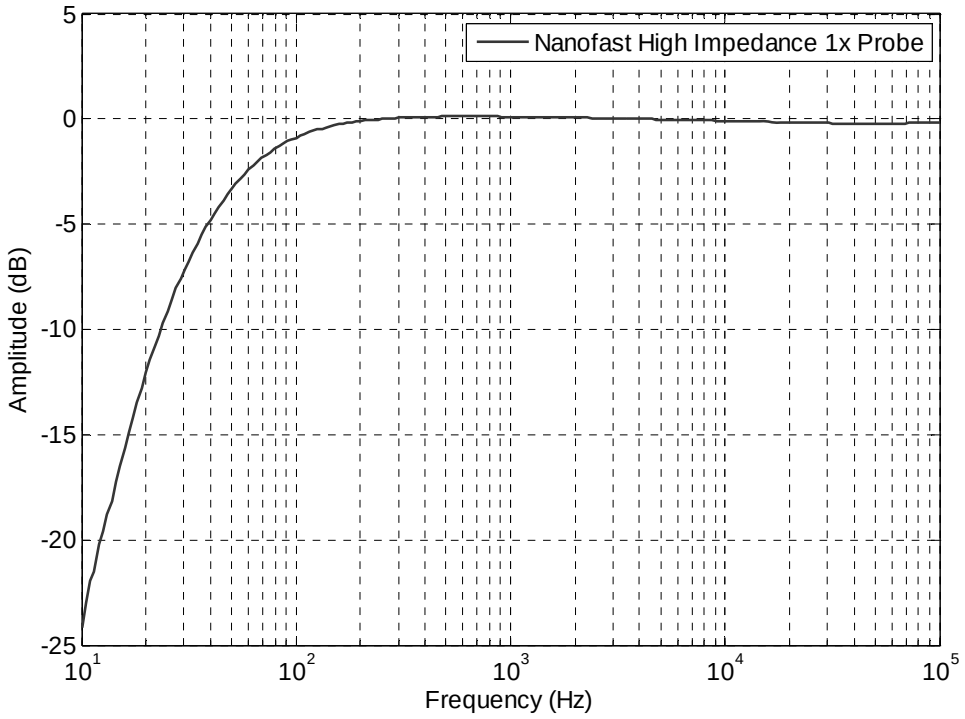

Figure 9-4 Calibration Frequency Response of Nanofast High-Impedance Probe.

PRIMARY STANDARDS LABORATORY
Sandia National Laboratories, Albuquerque, New Mexico 87185

NVLAP
Accredited by the National Voluntary Laboratory Accreditation Program for the scope of accreditation under Lab Code 105002

CERTIFICATE

File No. 51649

PRIMARY STANDARDS LABORATORY
Sandia National Laboratories
CALIBRATION
File No. 51649
Certified: 08/07/06
Expires: 08/07/07
NETWORK/SPECTRUM/IMPEDA
Hewlett Packard Co.
Model:4395A
Serial:SG41100394
See Certificate
By: JAW

NETWORK ANALYZER (Type N)

Manufacturer: Agilent
Model: 4395A
Serial Number: SG41100394
Property Number: S853091

Test Set Model No.: 87511A
Test Set Serial No.: 3026J00604

Cal. Kit Model No.: 85054A
Cal. Kit Serial No.: 2345A00121

Submitted by: 01653
P.O. Box 5800 M/S 1152
Albuquerque, NM 87185-1152

Certification performed on August 7, 2006.
Certified: August 7, 2006
Expires: August 7, 2007

The attached data sheets tabulate uncertainties expected from the Network Analyzer system defined above and in the data sheets; the uncertainties do not apply to any other configuration or system. The uncertainties and errors of the complex S-parameters derive from an assumed mathematical model based on measurements of suitably chosen standards. These standards - air line(s), 10 dB fixed attenuator, and when applicable, mismatches - are directly traceable to NIST. The frequency reference for the Network Analyzer synthesizer during calibration was the internal 10 MHz frequency reference of the 4395A. The certification was performed at 23 ± 2°C and 40 ± 10% RH.

4395A File 51649 Frequency TimeBase Error is 0.288 +/- 0.191 ppm.

Program: CERTVANA.B12 Version date is April 3, 2006

Metrologist: J. A. Woods - 2542
Approved by Project Leader: R. D. Moyer - 2542

Copy to:
01653 (2)
2542 File <<<<<<

Page 1 of 12

Figure 9-5 Certificate of Calibration for 4395A Network Analyzer.

10 Appendix C – Compilation of Measured Data

Direct Drive Transfer Function Data:

The following transfer functions were measured with the mine grounding system in current state.

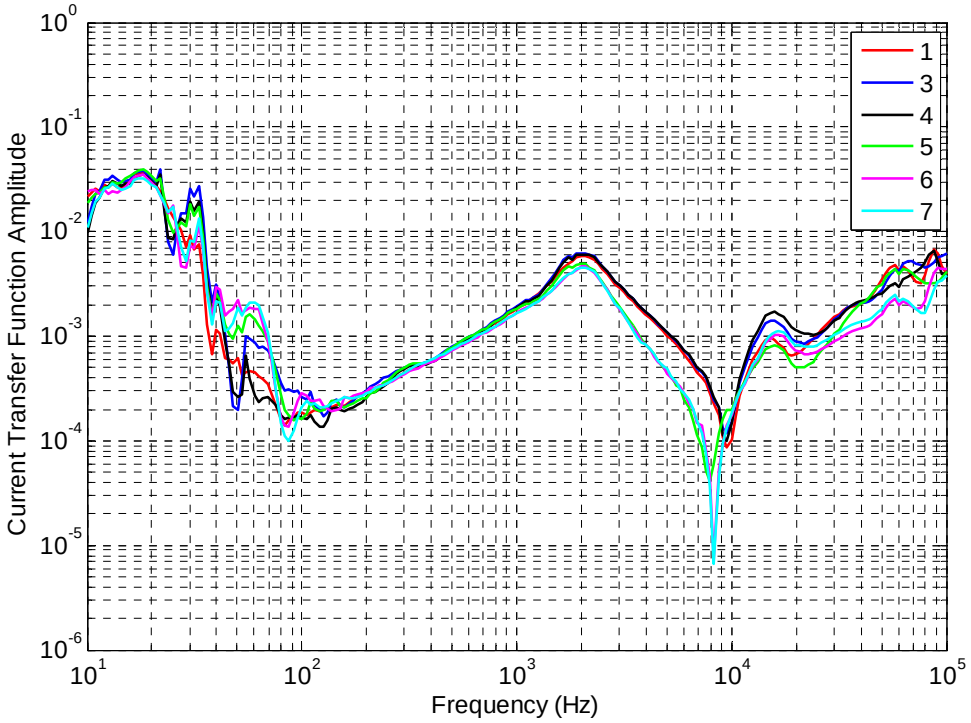

Figure 10-1 Direct Drive Current Transfer Function of Trolley Communication Line with a Local Ground.

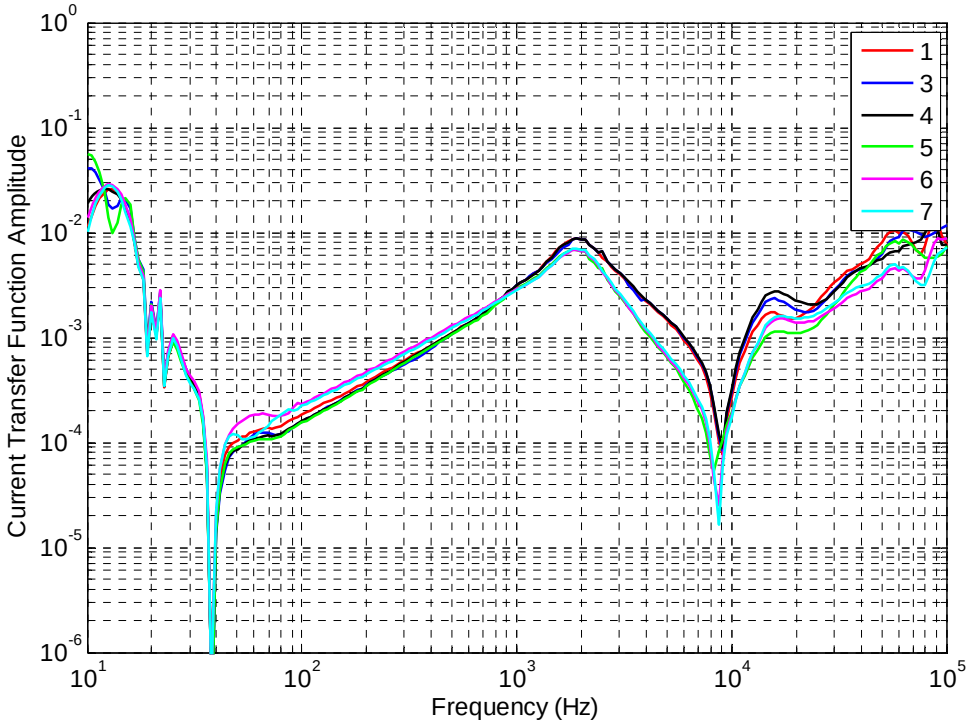

Figure 10-2 Direct Drive Current Transfer Function of Trolley Communication Line with a Fence Ground.

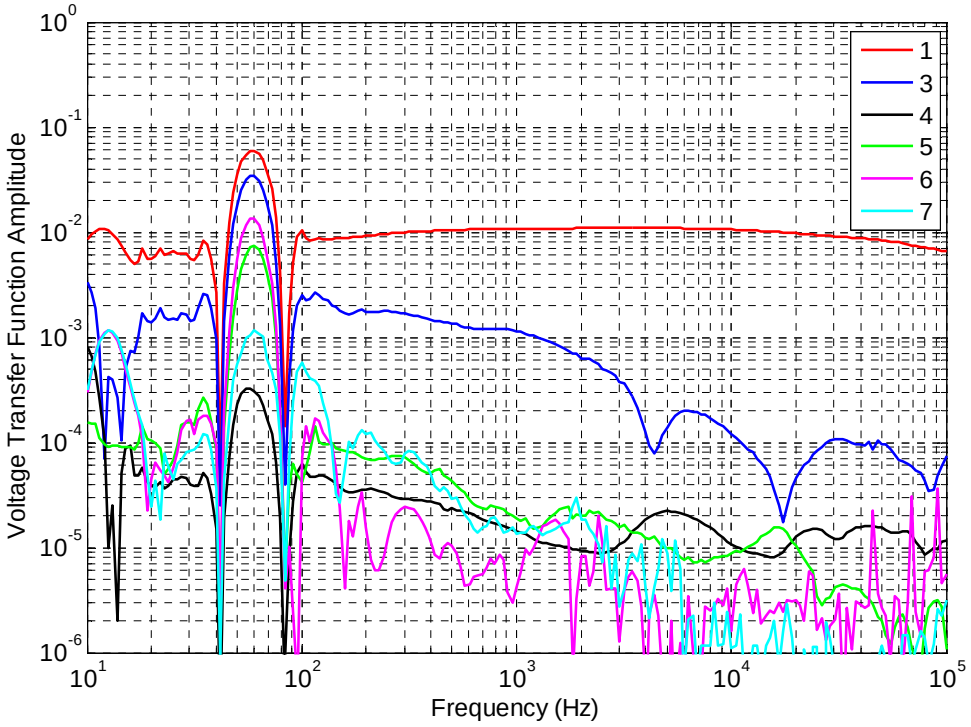

Figure 10-3 Direct Drive Voltage Transfer Function of Conveyor Structure with a Local Ground.

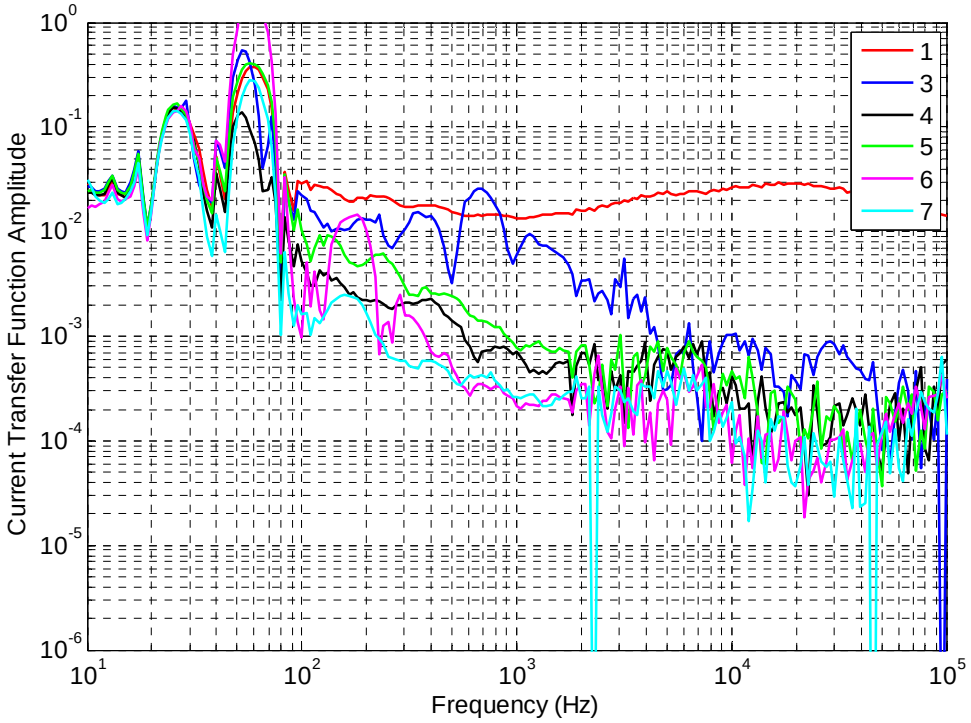

Figure 10-4 Direct Drive Current Transfer Function of Conveyor Structure with a Local Ground.

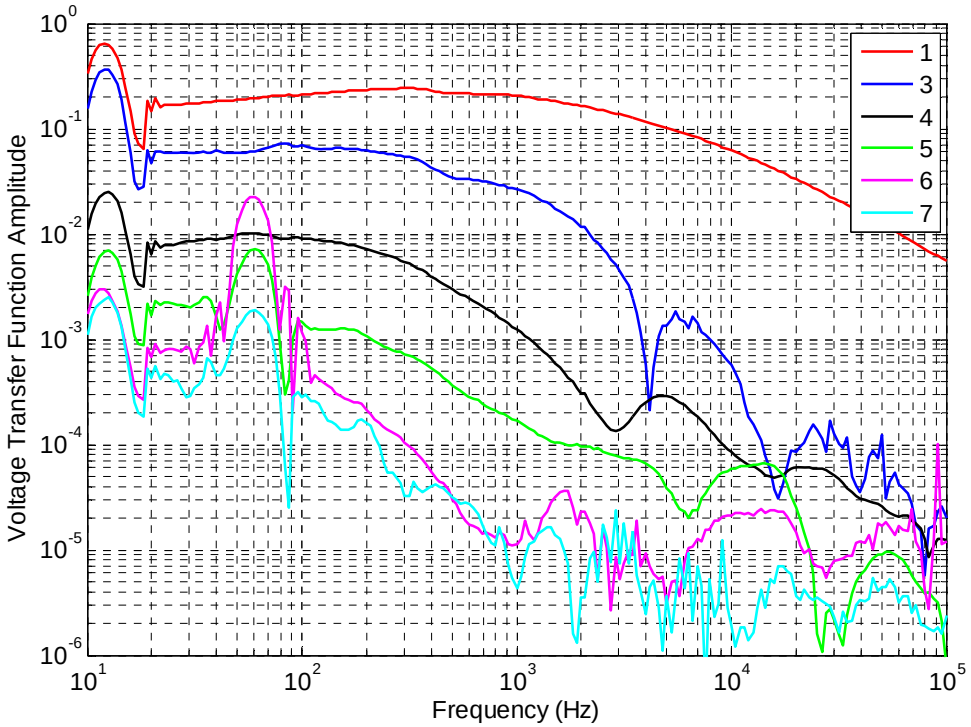

Figure 10-5 Direct Drive Voltage Transfer Function of Conveyor Structure with a Fence Ground.

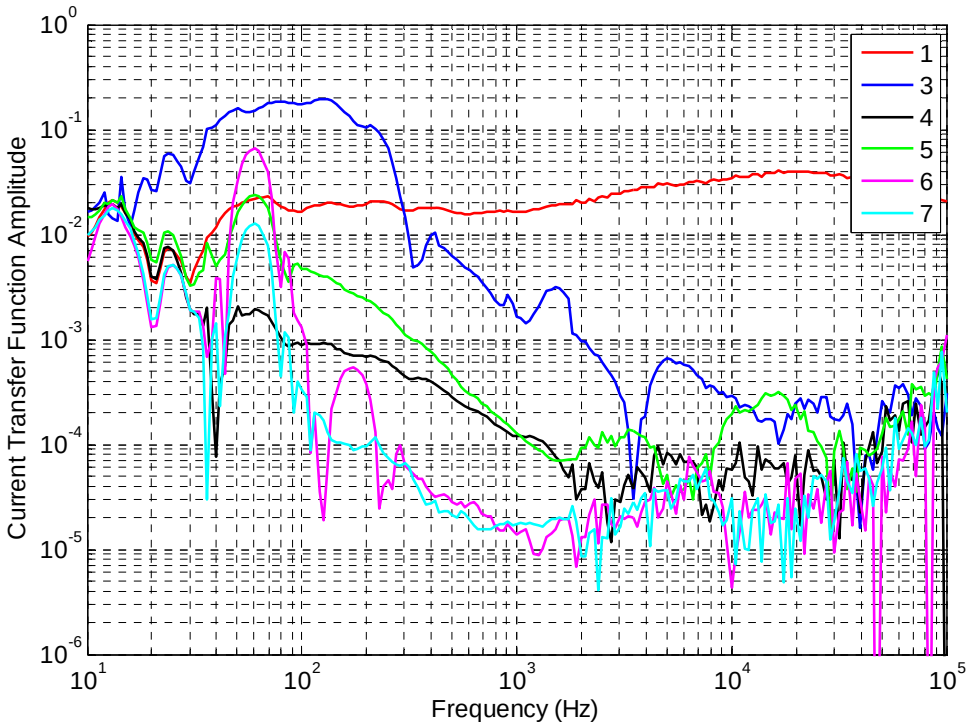

Figure 10-6 Direct Drive Current Transfer Function of Conveyor Structure with a Fence Ground.

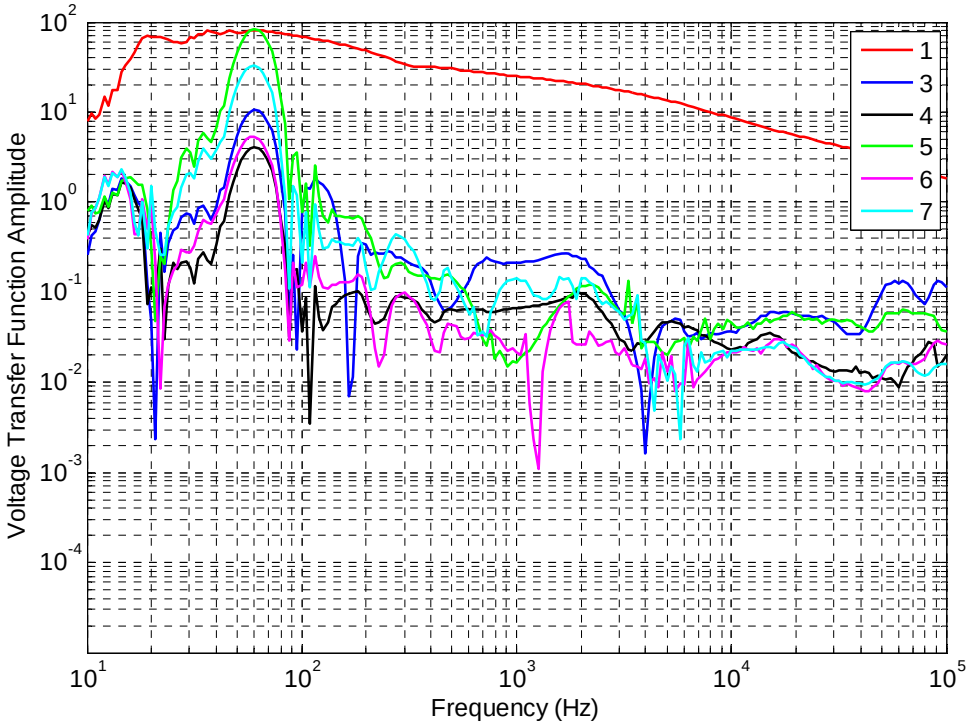

Figure 10-7 Direct Drive Voltage Transfer Function of Rail Structure with a Local Ground.

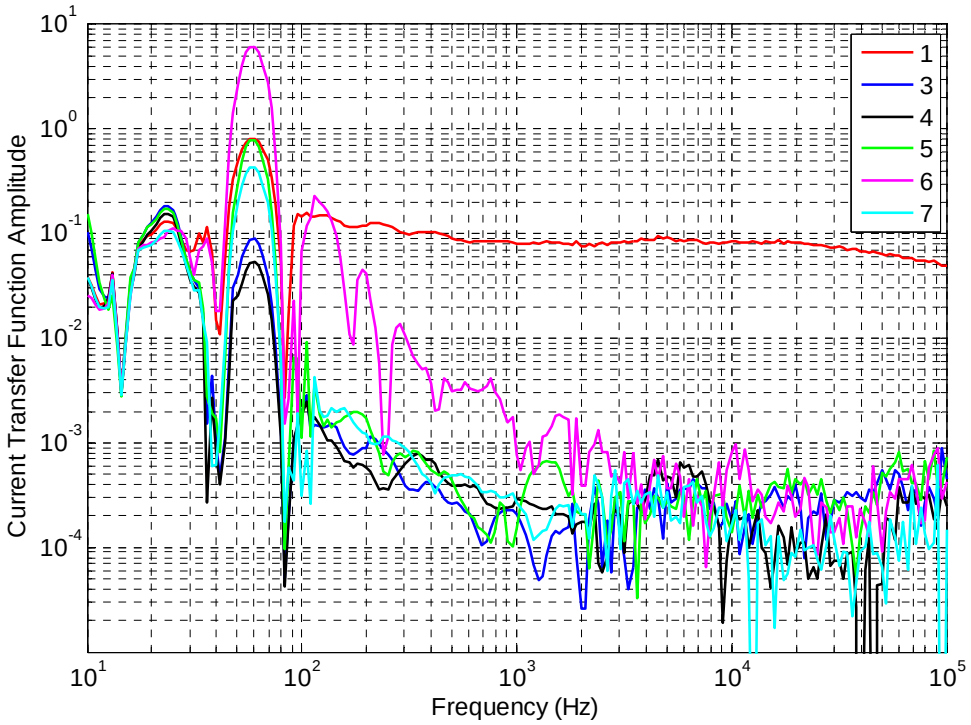

Figure 10-8 Direct Drive Current Transfer Function of Rail Structure with a Local Ground.

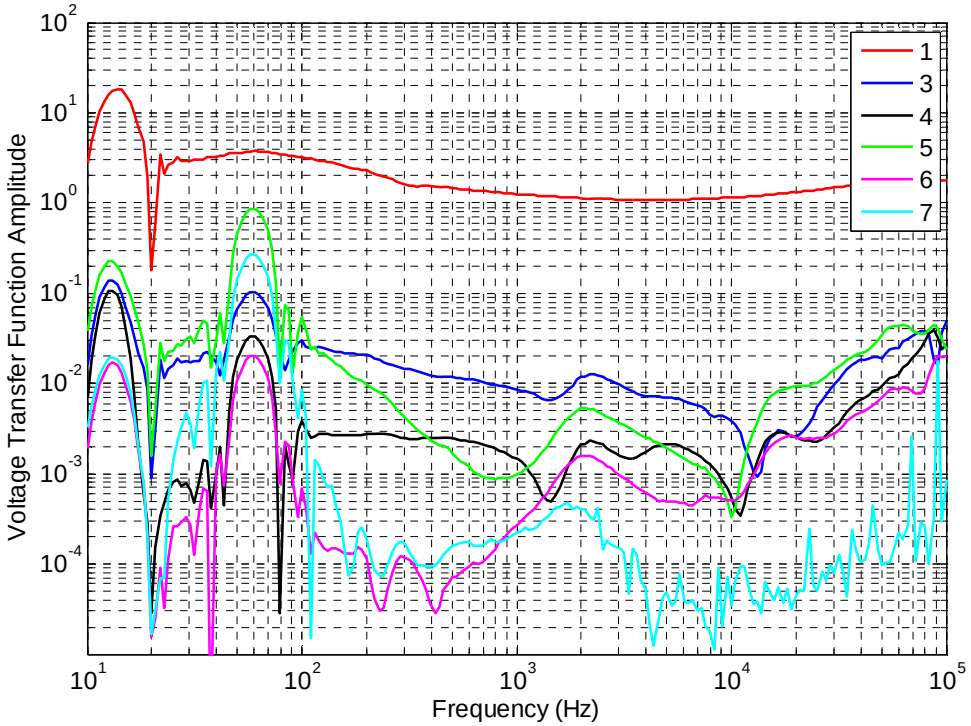

Figure 10-9 Direct Drive Voltage Transfer Function of Rail Structure with a Fence Ground.

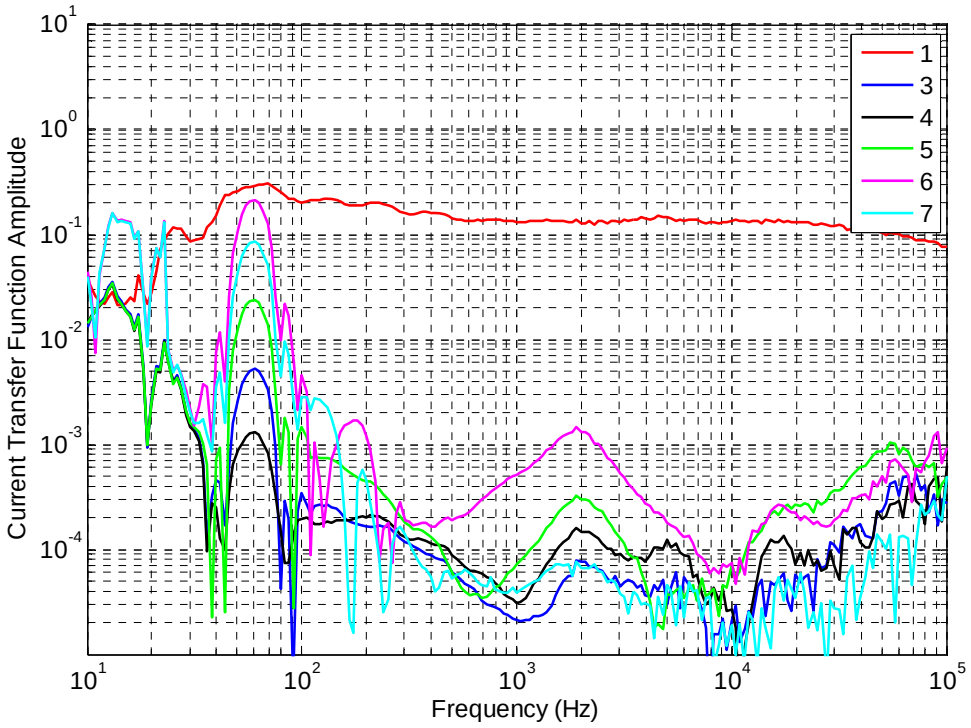

Figure 10-10 Direct Drive Current Transfer Function of Rail Structure with a Fence Ground.

The following transfer functions were measured with the mine grounding system similar to the grounding scheme in place during explosion.

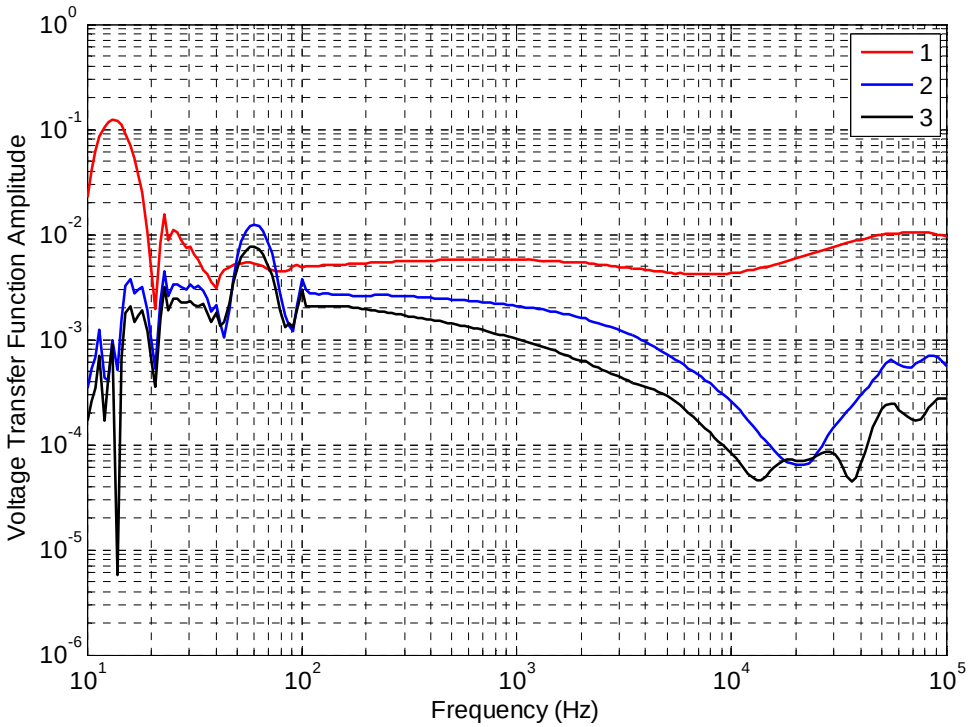

Figure 10-11 Direct Drive Voltage Transfer Function of Power Cable Shield with a Local Ground.

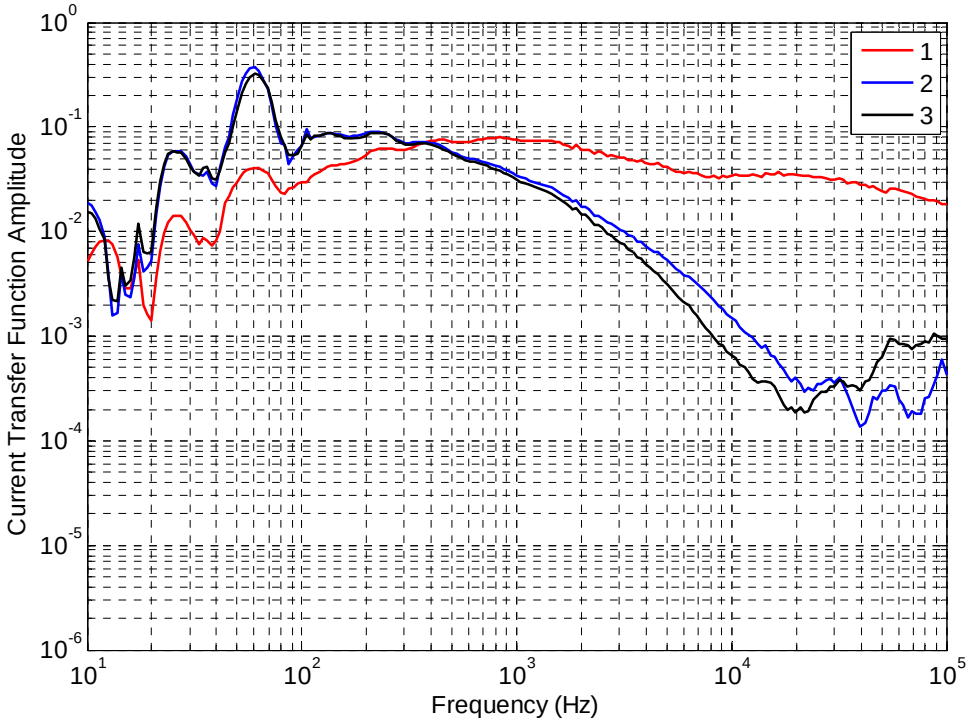

Figure 10-12 Direct Drive Current Transfer Function of Power Cable Shield with a Local Ground.

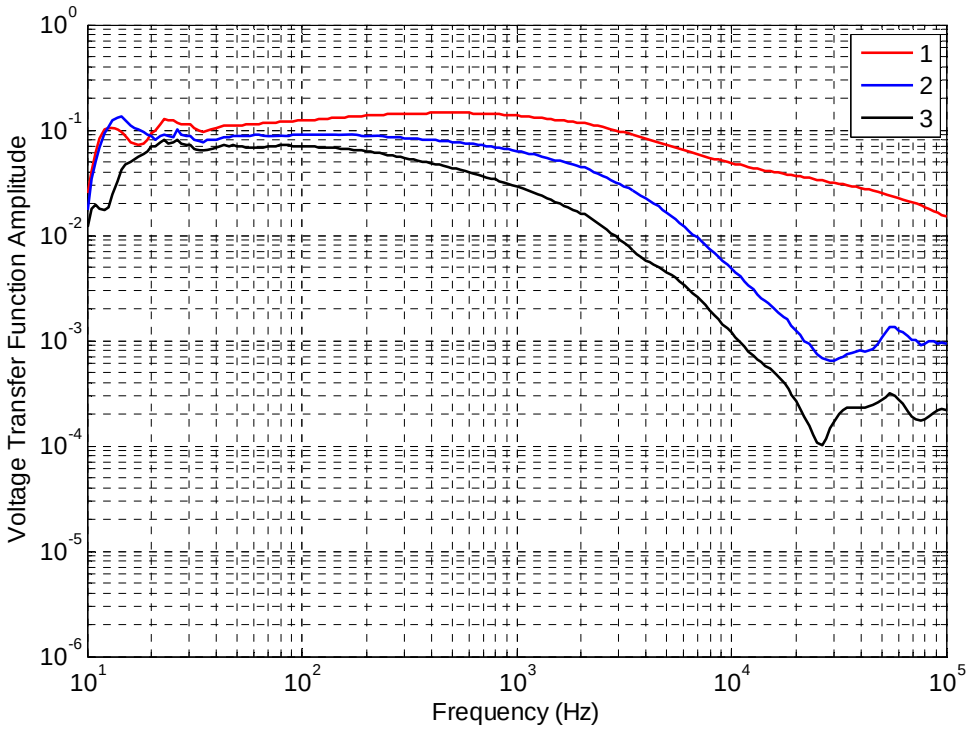

Figure 10-13 Direct Drive Voltage Transfer Function of Power Cable Shield with a Fence Ground.

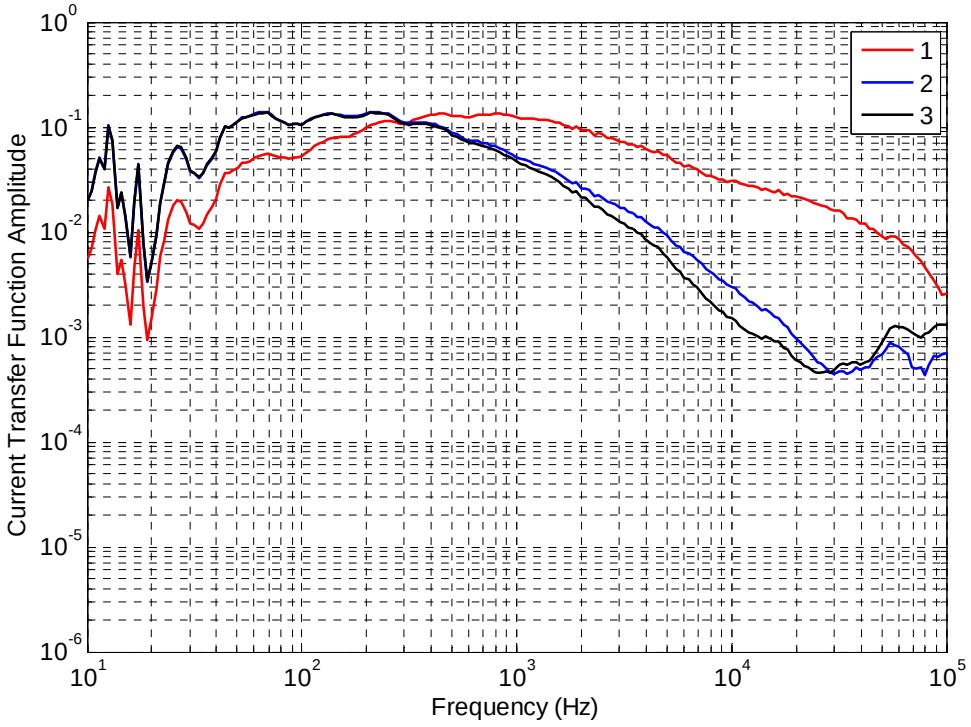

Figure 10-14 Direct Drive Current Transfer Function of Power Cable Shield with a Fence Ground.

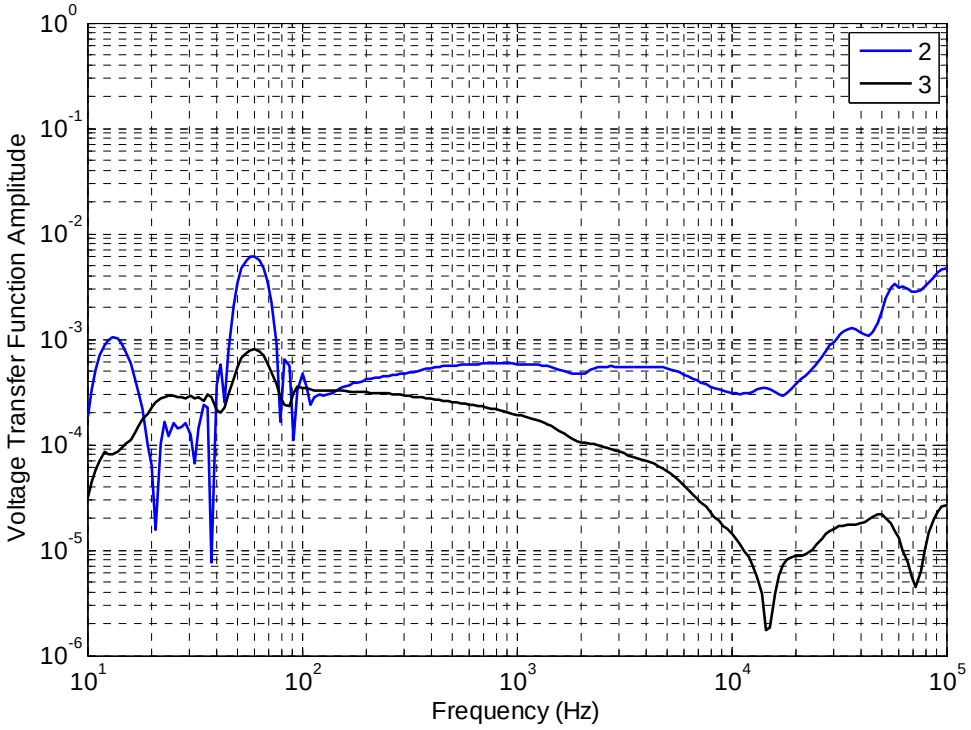

Figure 10-15 Direct Drive Voltage Transfer Function of Rail Structure with a Local Ground.

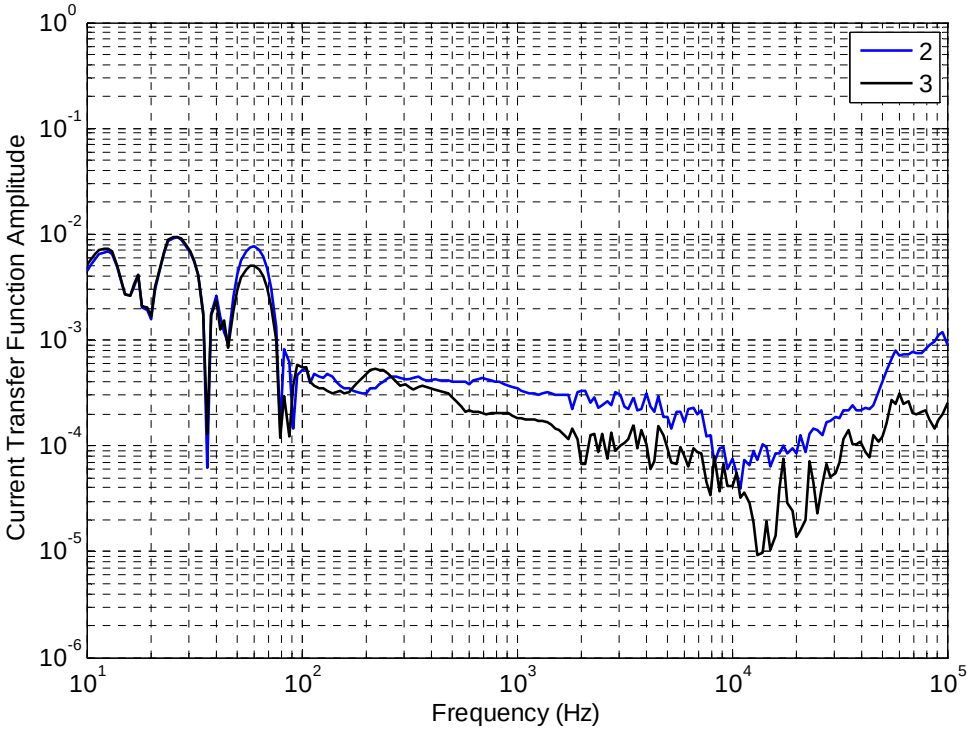

Figure 10-16 Direct Drive Current Transfer Function of Rail Structure with a Local Ground.

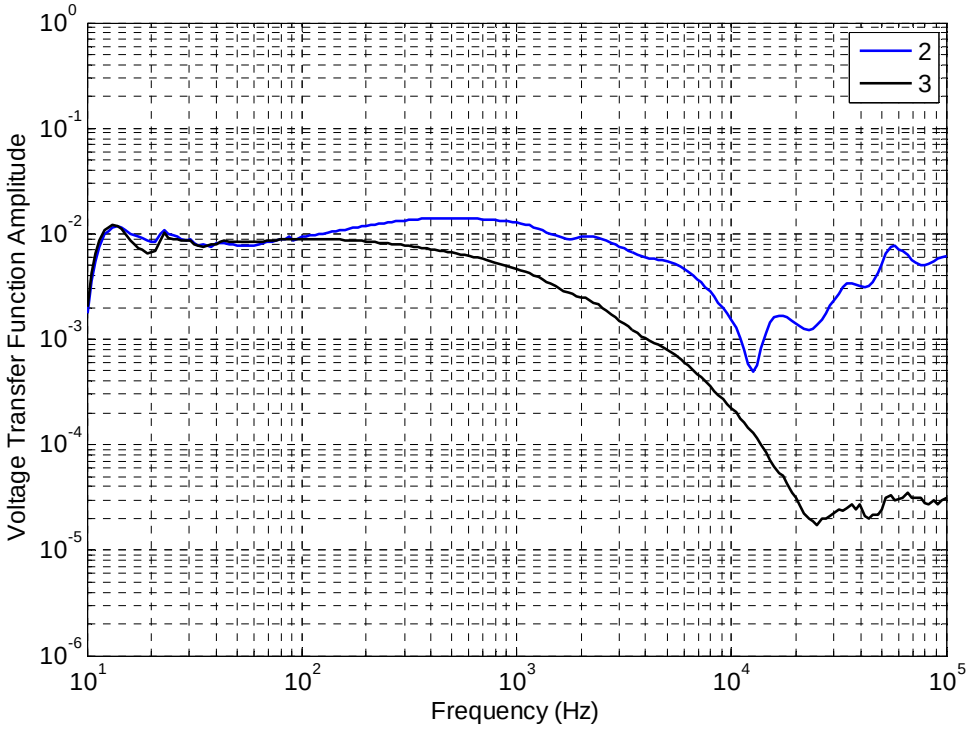

Figure 10-17 Direct Drive Voltage Transfer Function of Rail Structure with a Fence Ground.

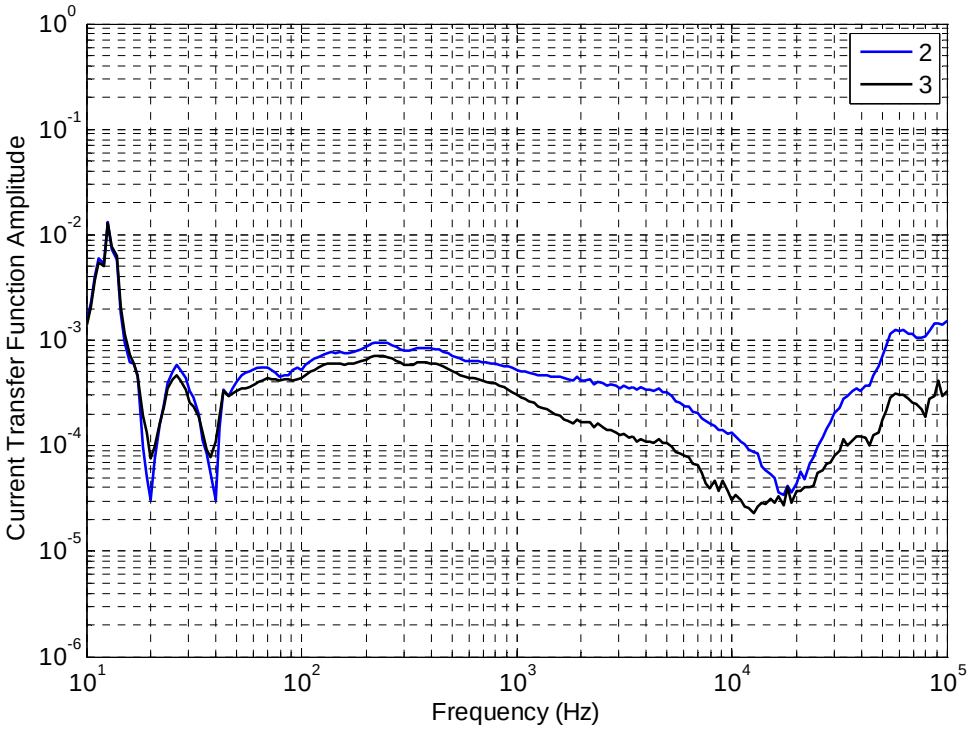

Figure 10-18 Direct Drive Current Transfer Function of Rail Structure with a Fence Ground.

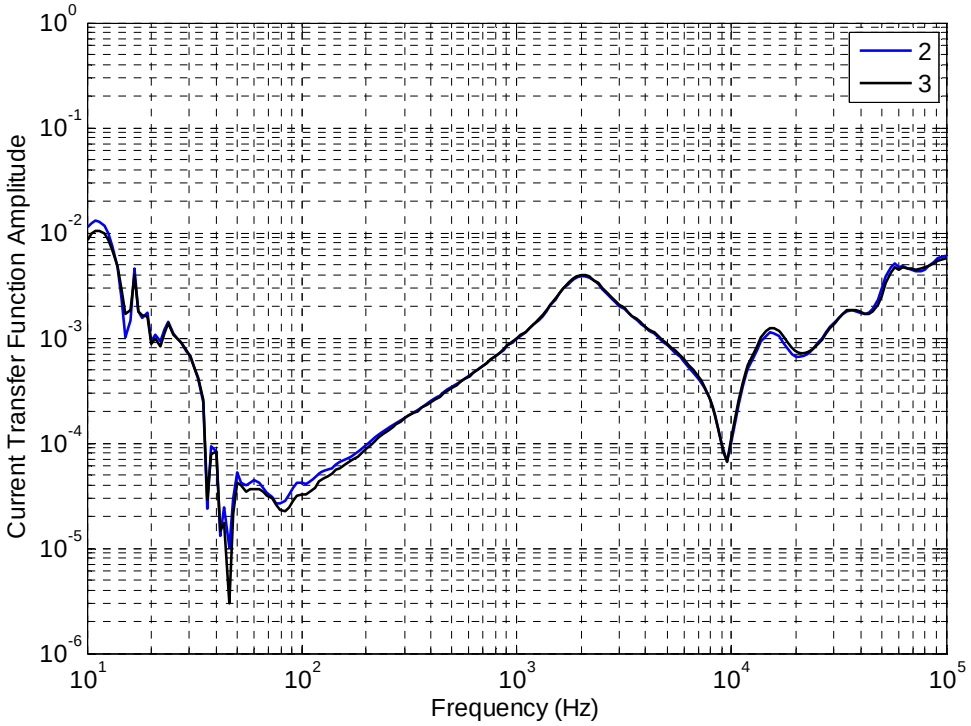

Figure 10-19 Direct Drive Current Transfer Function of Trolley Communication Line with a Local Ground.

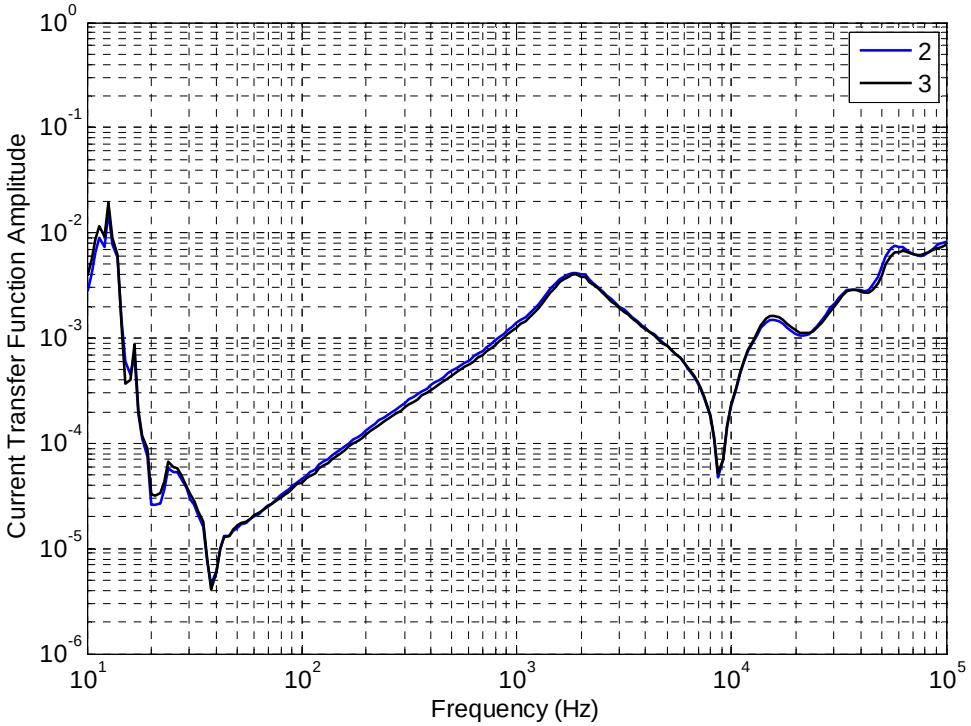

Figure 10-20 Direct Drive Current Transfer Function of Trolley Communication Line with a Fence Ground.

Indirect Drive Transfer Function Data: Surface current drive in the P-direction

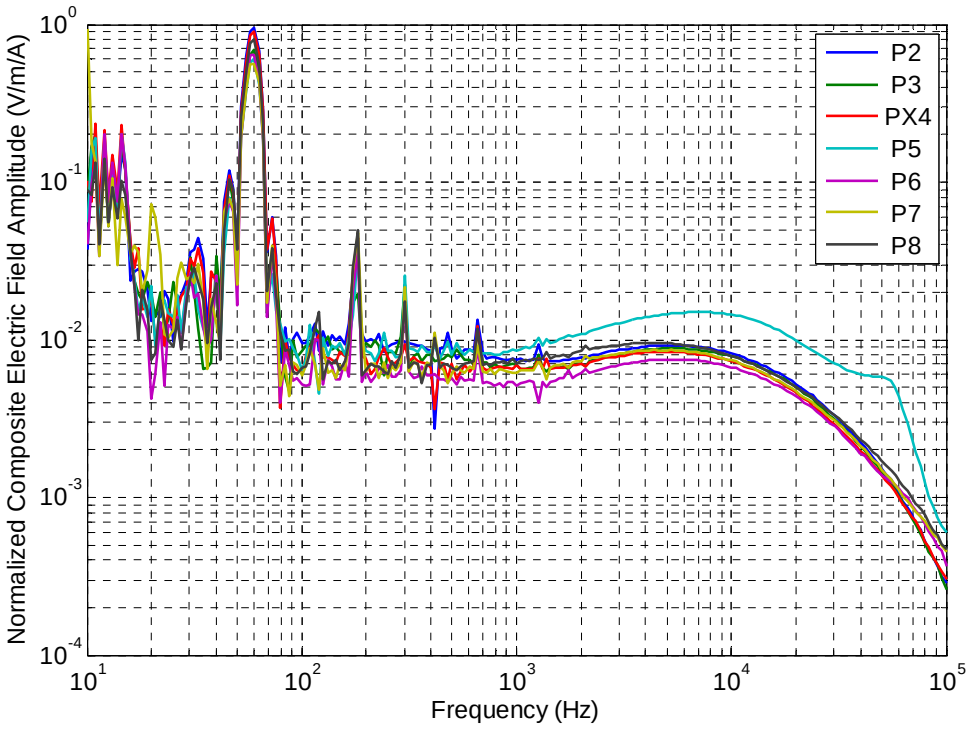

Figure 10-21 Normalized Composite Electric Field for P-Directed Surface Current Drive at Positions from P2 to P8.

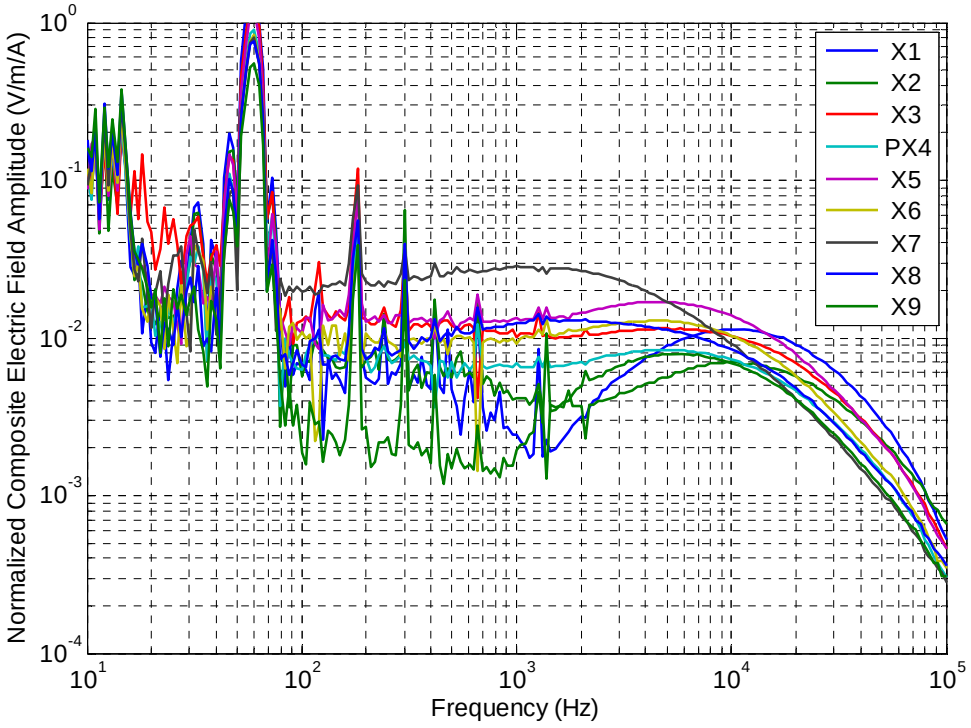

Figure 10-22 Normalized Composite Electric Field for P-Directed Surface Current Drive at Positions from X1 to X9.

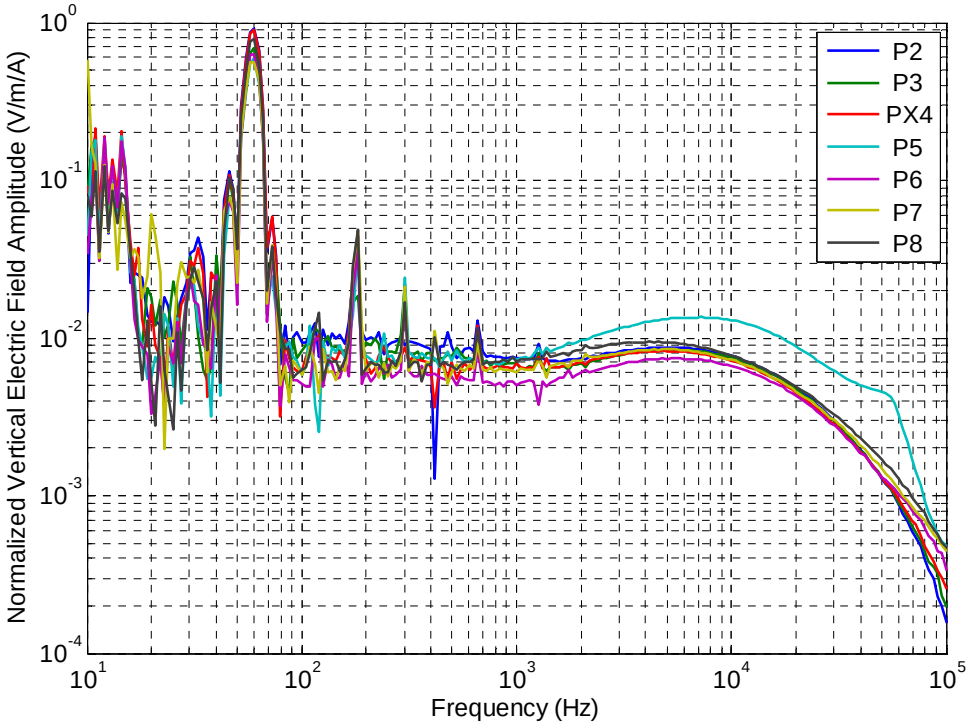

Figure 10-23 Normalized Vertical Electric Field for P-Directed Surface Current Drive at Positions from P2 to P8.

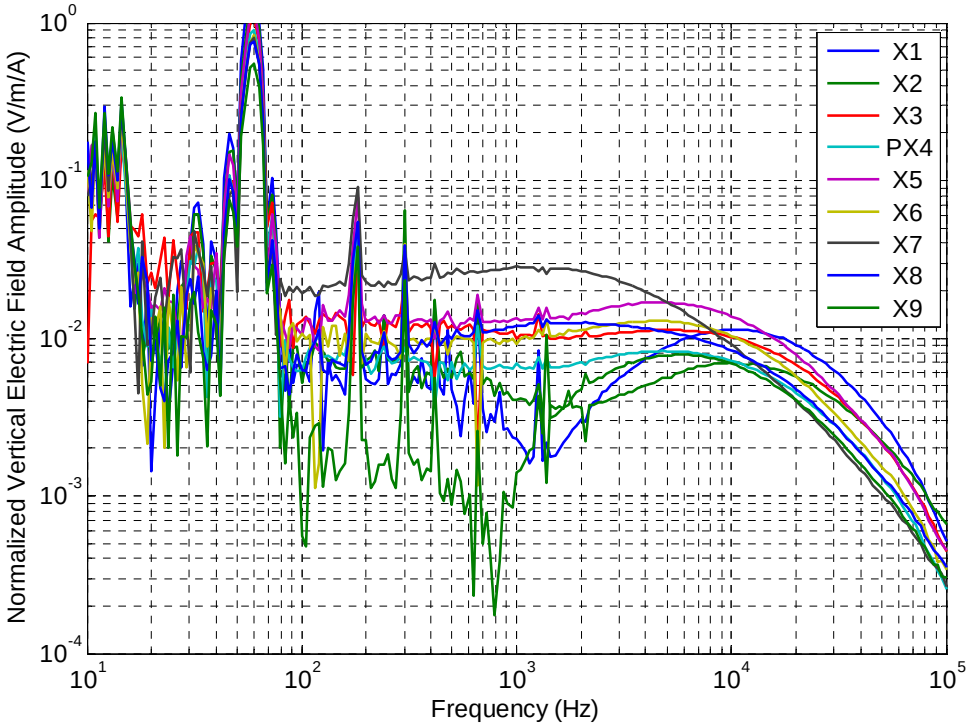

Figure 10-24 Normalized Vertical Electric Field for P-Directed Surface Current Drive at Positions from X1 to X9.

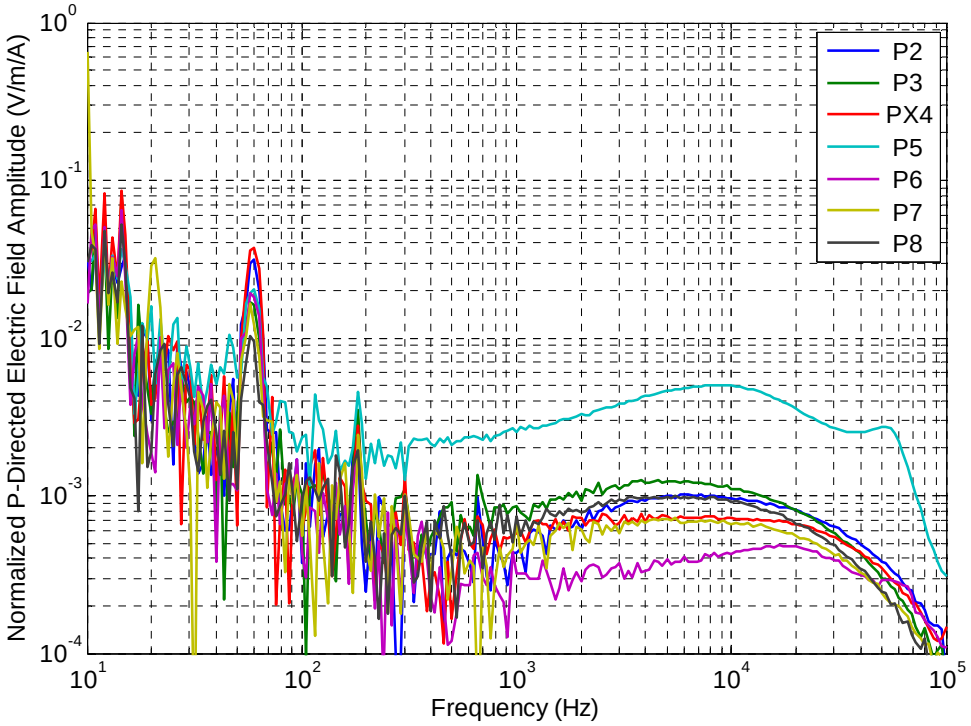

Figure 10-25 Normalized P-Directed Electric Field for P-Directed Surface Current Drive at Positions from P2 to P8.

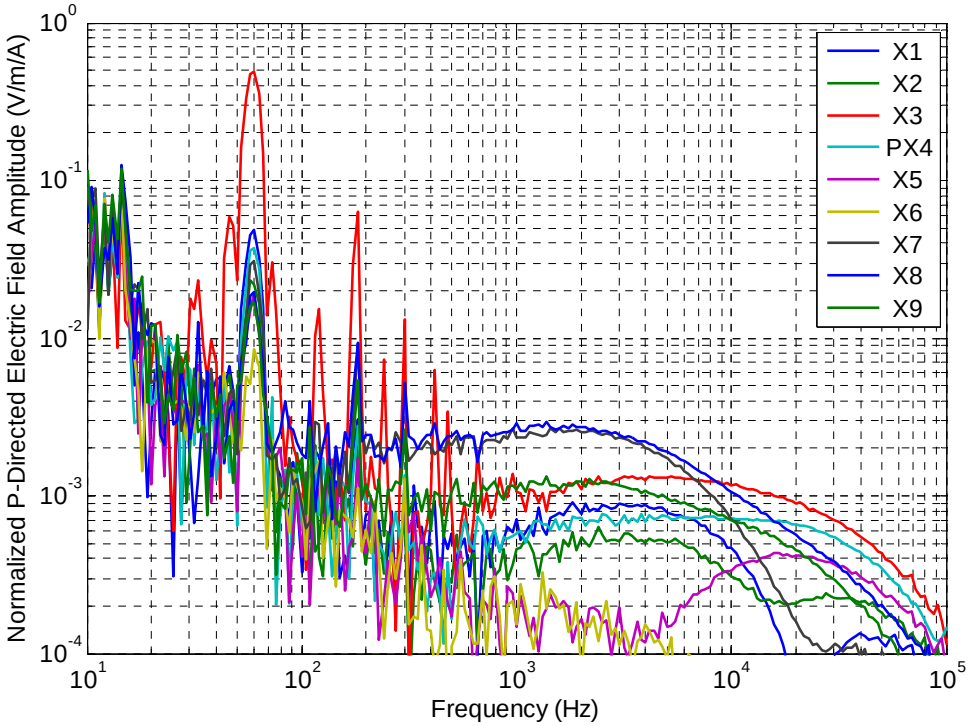

Figure 10-26 Normalized P-Directed Electric Field for P-Directed Surface Current Drive at Positions from X1 to X9.

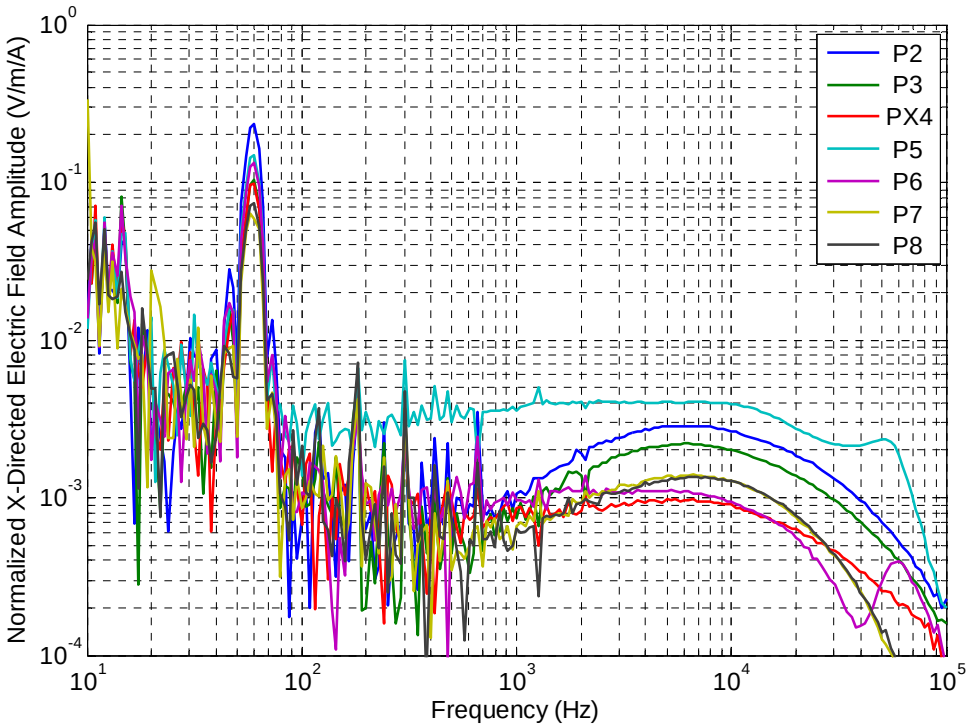

Figure 10-27 Normalized X-Directed Electric Field for P-Directed Surface Current Drive at Positions from P2 to P8.

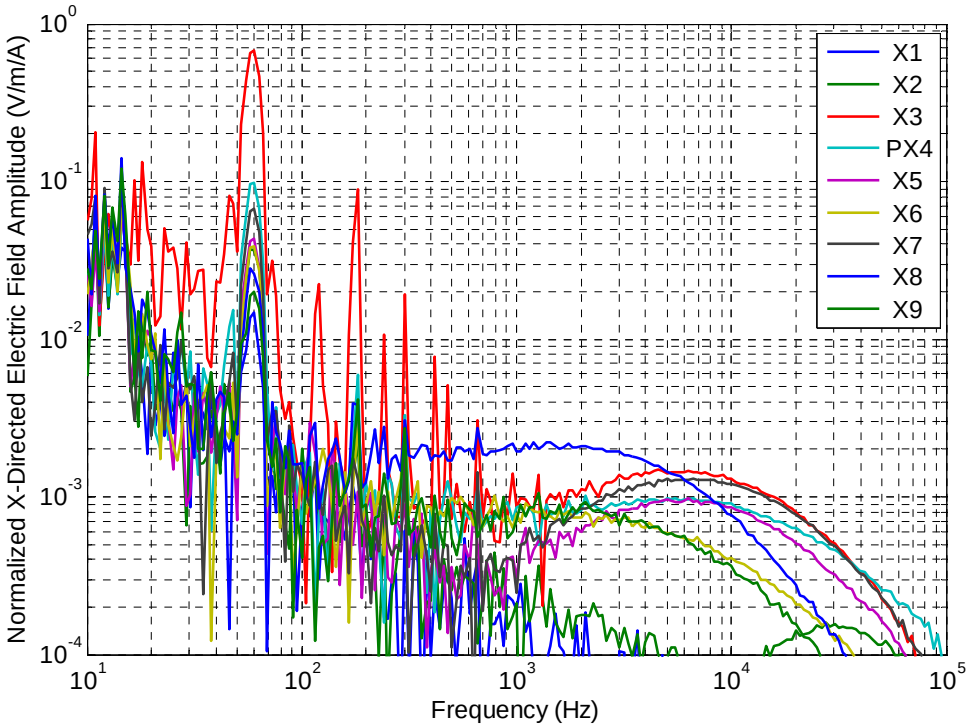

Figure 10-28 Normalized P-Directed Electric Field for P-Directed Surface Current Drive at Positions from X1 to X9.

Indirect Drive Transfer Function Data: Surface current drive in the X-direction

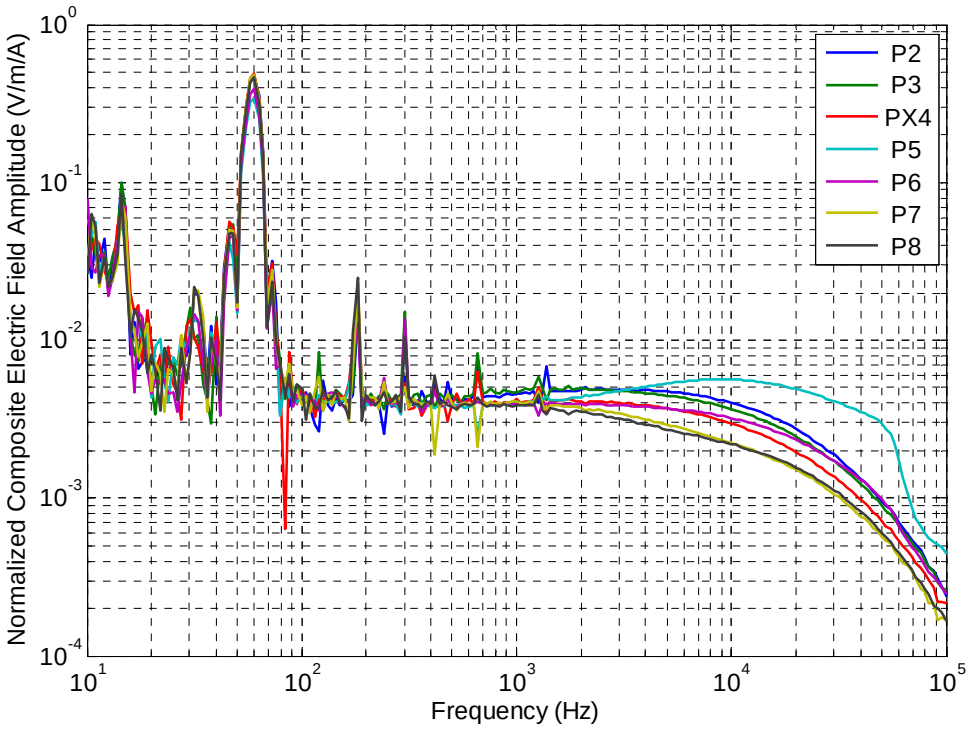

Figure 10-29 Normalized Composite Electric Field for X-Directed Surface Current Drive at Positions from P2 to P8.

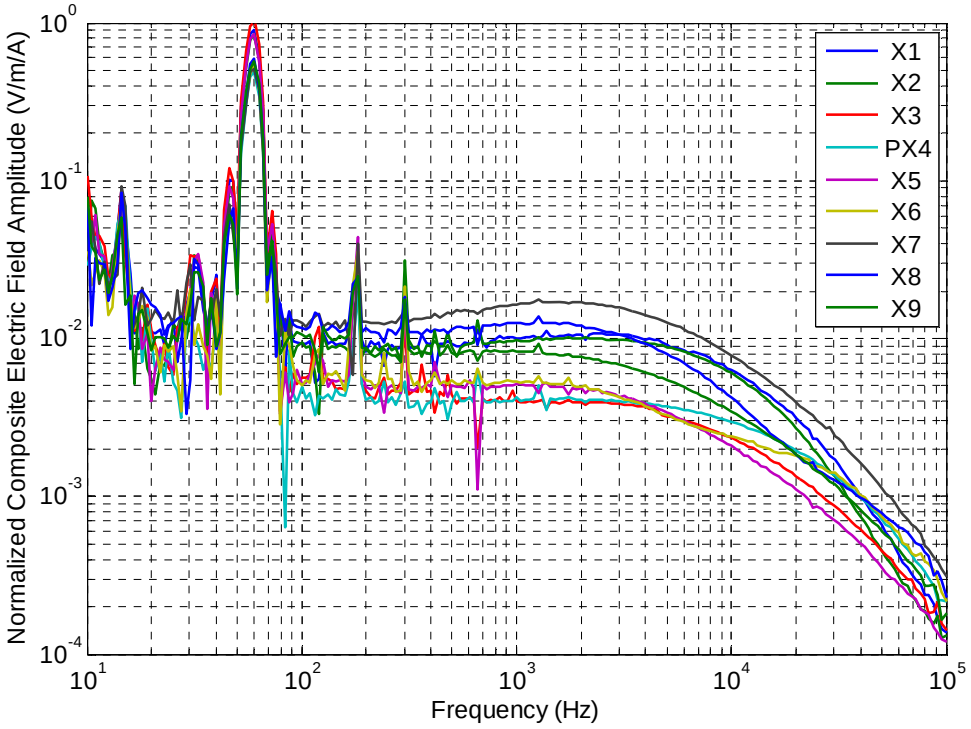

Figure 10-30 Normalized Composite Electric Field for X-Directed Surface Current Drive at Positions from X1 to X9.

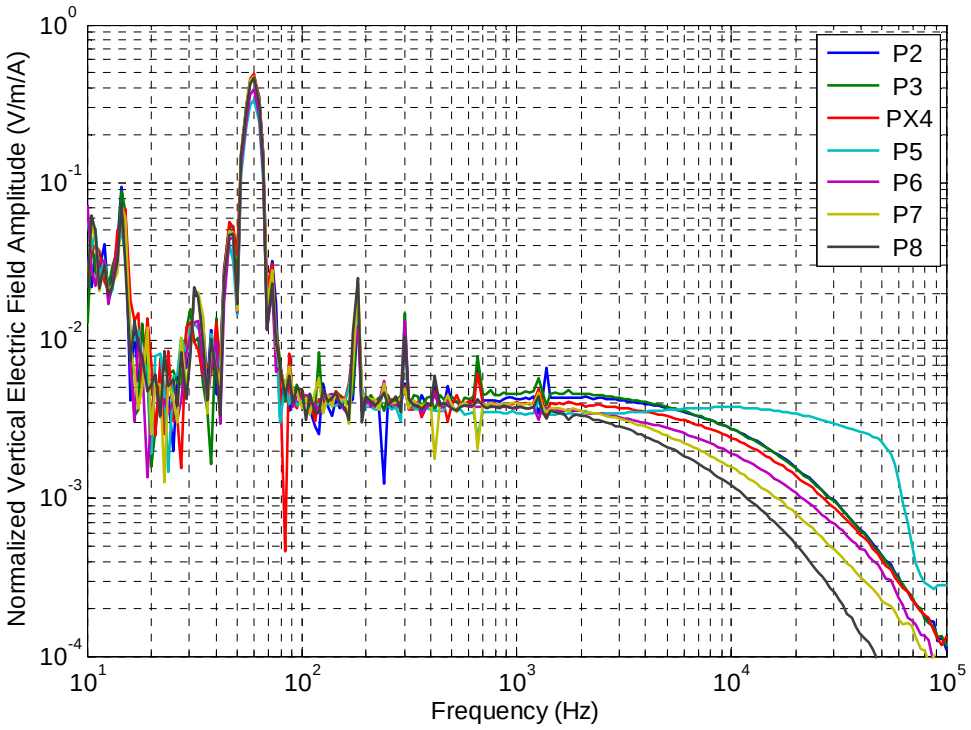

Figure 10-31 Normalized Vertical Electric Field for X-Directed Surface Current Drive at Positions from P2 to P8.

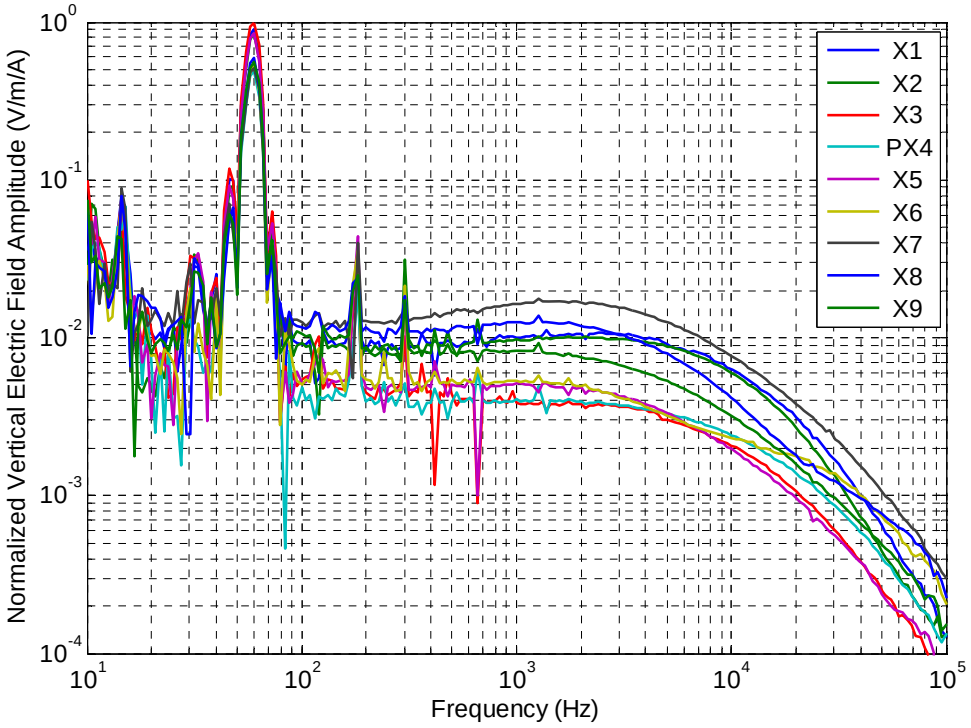

Figure 10-32 Normalized Vertical Electric Field for X-Directed Surface Current Drive at Positions from X1 to X9.

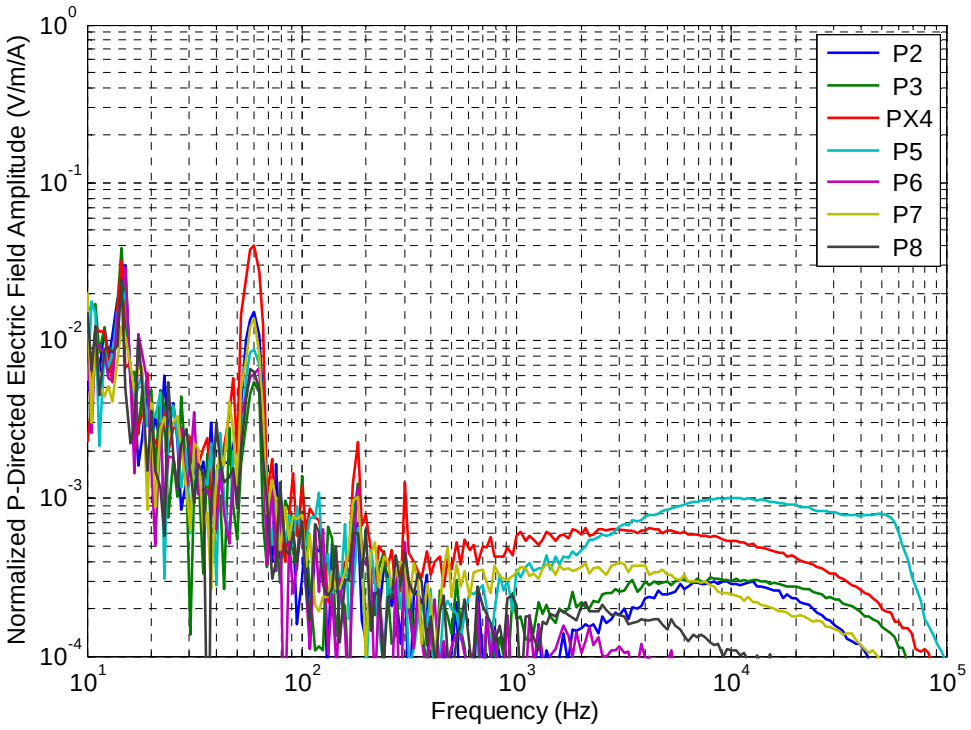

Figure 10-33 Normalized P-Directed Electric Field for X-Directed Surface Current Drive at Positions from P2 to P8.

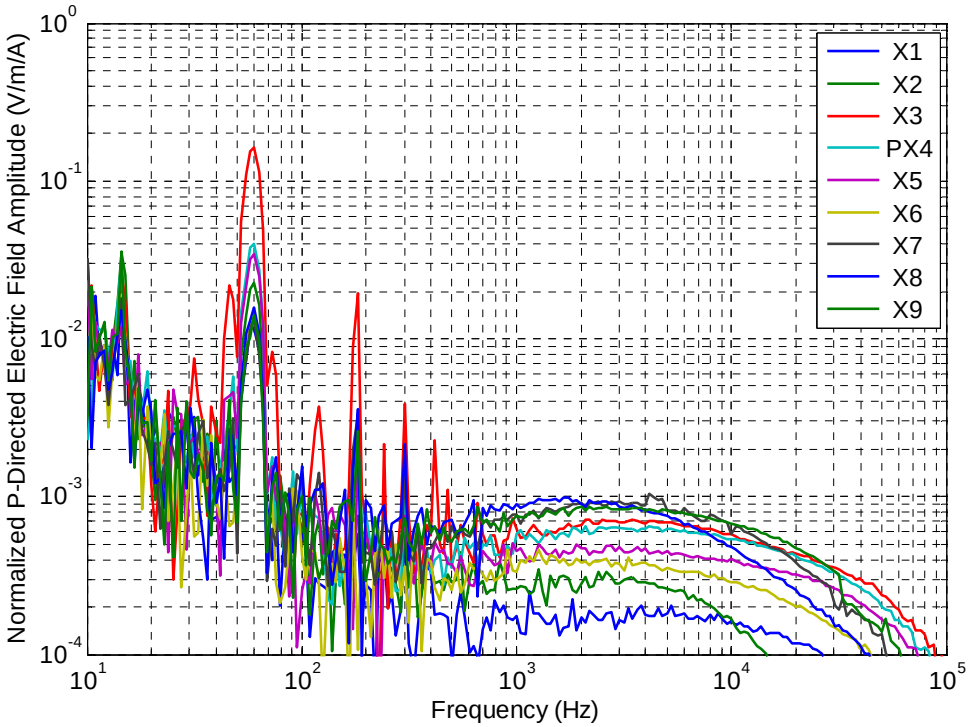

Figure 10-34 Normalized P-Directed Electric Field for X-Directed Surface Current Drive at Positions from X1 to X9.

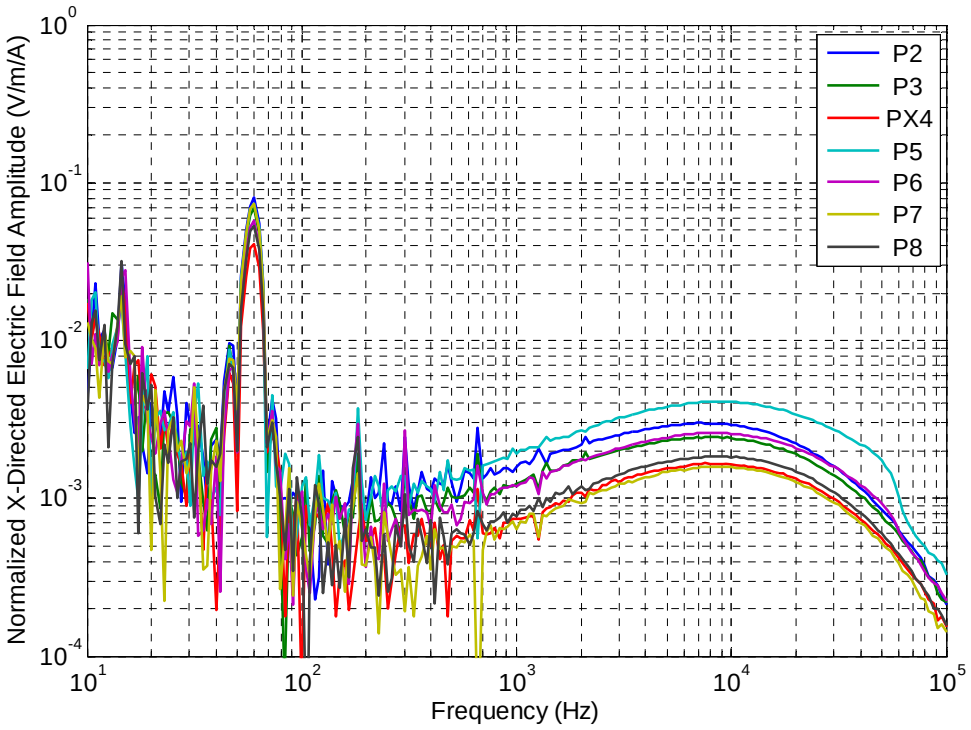

Figure 10-35 Normalized X-Directed Electric Field for X-Directed Surface Current Drive at Positions from P2 to P8.

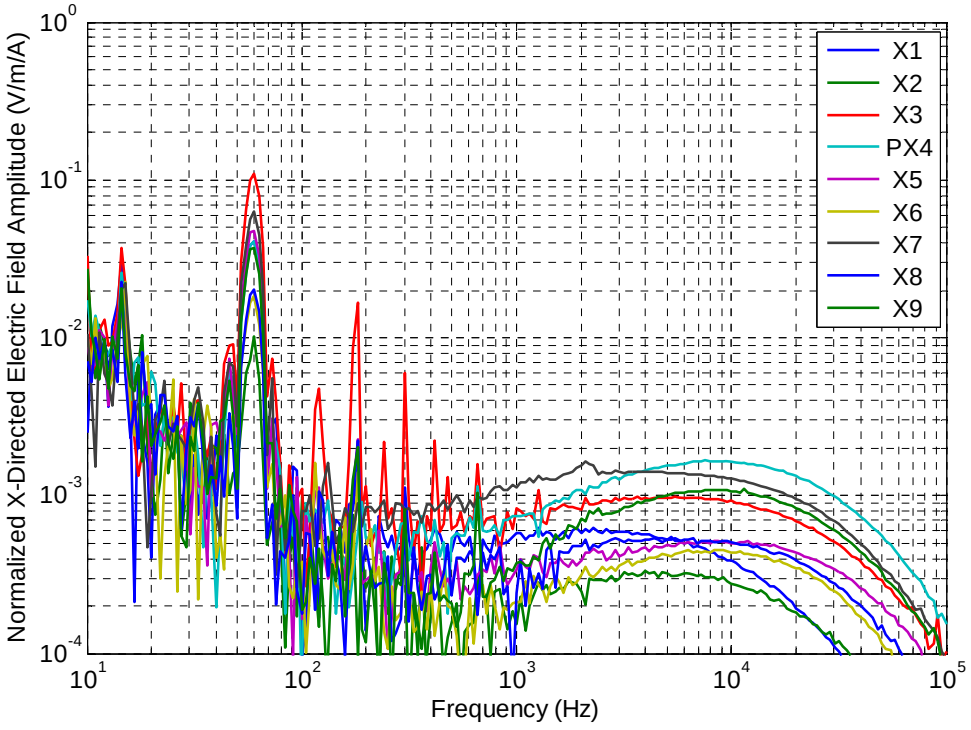

Figure 10-36 Normalized X-Directed Electric Field for X-Directed Surface Current Drive at Positions from X1 to X9.

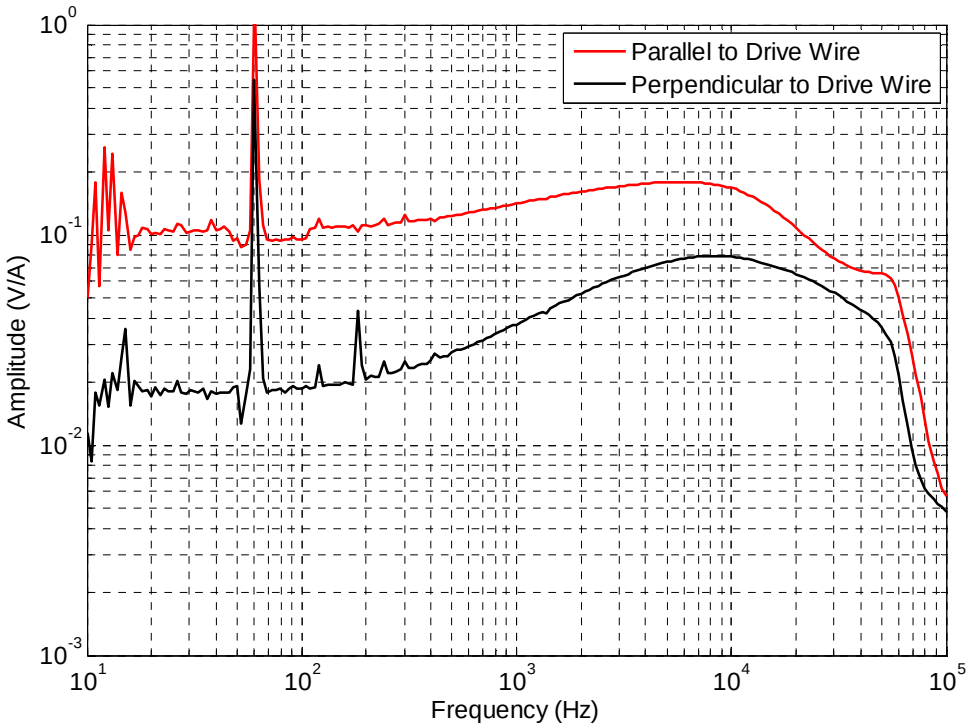

Figure 10-37 Induced Voltage on Pump Cable (~300 m long) due to Wire Current Drives on Surface.

11 Appendix D – List of Underground Sealed Area Coal Mine Explosions Suspected of Lightning Initiation

1. Mary Lee #1 – August 22, 1993, Walker County, AL
2. Oak Grove Mine – April 5, 1994, Jefferson County, AL
3. Gary 50 – Between June 9 and 16, 1995
4. Oak Grove Mine – January 29, 1996, Jefferson County, AL
5. Oasis Contracting Mine # 1 – May 22, 1996, Boone County, WV
6. Oasis Contracting Mine # 1 – June 15, 1996, Boone County, WV
7. Oak Grove Mine – July 9, 1997, Jefferson County, AL
8. Soldier Canyon Mine – July, 2001, Wellington, UT
9. Pinnacle Mine – September 1, 2003, Wyoming County, WV
10. Pinnacle Mine – August 30, 2005, WV, Wyoming County, WV
11. Sago Mine – January 2, 2006, Tallmansville, WV

12 Appendix E – Memorandum from Dr. Krider

Department of Atmospheric Sciences
Institute of Atmospheric Physics

THE UNIVERSITY OF ARIZONA®
TUCSON ARIZONA

PO Box 210081, Room 542
Tucson, AZ 85721-0081
Telephone: (520) 621-6831
FAX: (520) 621-6833
atmosci@atmo.arizona.edu

MEMORANDUM

Date: 17 April 2007

TO: Matthew B. Higgins
Sandia National Laboratories

From: E. Philip Krider, Ph.D.
Professor and Consultant

On 2 January 2006, an explosion occurred at the Sago coal mine in West Virginia. The NLDN lightning detection network reported two large, positive cloud-to-ground (CG) strokes within 5.5 km of the sealed area of the Sago mine about the time of the explosion.

The data provided by the NLDN show that:

-The first stroke occurred at 06:26:35.523 EST and had an estimated peak current of about +39 kA.

-The estimated uncertainty in the location (50% confidence) was better than 400 meters, and the 99% location uncertainty was better than 1.1 km.

-The second stroke occurred at 6:26:35.680 EST and had an estimated peak current of about +101 kA, with the same location uncertainty as the first stroke.

Further examination of the individual NLDN sensor reports showed no evidence of any other cloud-to-ground strokes during the time-window of interest in proximity to the sealed area of the Sago mine.

There are some limitations in the NLDN lightning detection system. Upward, ground-to-ground discharges, such as are frequently initiated by tall vertical structures, will not be detected by the NLDN if the initial, continuous current phase is not followed by at least one leader-return stroke sequence. Also, the NLDN will not report most intracloud or cloud-to-air discharges, and such flashes often have extensive horizontal development.

Distribution

Internal:

5	MS1152	M. B. Higgins, 1653
2	MS1152	M. E. Morris, 1652
2	MS1182	L. X. Schneider, 1650
3	MS1152	M. Caldwell, 1653
1	MS1152	D. R. Charley, 1653
1	MS1152	L. Martinez, 1653
2	MS9018	Central Technical Files, 08944
2	MS0899	Technical Library, 04536

External:

20 William Helfrich
Mine Safety & Health Administration
Pittsburgh Safety & Health Technology Center
P.O. Box 18233
626 Cochrans Mill Road – Bldg. 151
Pittsburgh, PA 15236

1 E. Philip Krider
Institute of Atmospheric Physics
The University of Arizona
P.O. Box 210081, Rm. 542
1118 E. 4th Street
Tucson, AZ 85721-0081

1 Martin A.Uman
Department of Electrical and Computer Engineering
University of Florida
P.O. Box 116200
311 Larsen Hall
Gainesville, FL 32611